Report Title: Recovery Act: Innovative CO_2 Sequestration from Flue Gas Using Industrial Sources and Innovative Concept for Beneficial CO_2 Use

Type of Report: FINAL SCIENTIFIC/TECHNICAL REPORT

Reporting Period Start Date: Jan 1, 2011 through

Reporting Period End Date: August 10, 2012

Principal Authors: Neal Dando, Mike Gershenzon, Rajat Ghosh

Date Report as Issued: July 2012

Award Number: DE-FE0002415

Submitting Organization: Alcoa Inc., 100 Technical Drive, Alcoa Center, PA 15069

Working Partners: Codexis/CO2 Solutions, NELS, Richard Lunt (SSI), CMU, EERC

Cost-Sharing Partners: Alcoa Inc. and DOE – NETL

Contacts:

Recipient Project Director
Rajat Ghosh
Alcoa, Inc.
Phone: 724-337-2148
E-mail: rajat.ghosh@alcoa.com

Recipient Business Officer
Sheree L. Haus
Alcoa, Inc.
Phone: 724.337.5367
E-mail: sheree.haus@alcoa.com

Abstract

The overall goal of this DOE Phase 2 project was to further develop and conduct pilot-scale and field testing of a biomimetic in-duct scrubbing system for the capture of gaseous CO_2 coupled with sequestration of captured carbon by carbonation of alkaline industrial wastes. The Phase 2 project, reported on here, combined efforts in enzyme development, scrubber optimization, and sequestrant evaluations to perform an economic feasibility study of technology deployment.

The optimization of carbonic anhydrase (CA) enzyme reactivity and stability are critical steps in deployment of this technology. A variety of CA enzyme variants were evaluated for reactivity and stability in both bench scale and in laboratory pilot scale testing to determine current limits in enzyme performance.

Optimization of scrubber design allowed for improved process economics while maintaining desired capture efficiencies. A range of configurations, materials, and operating conditions were examined at the Alcoa Technical Center on a pilot scale scrubber. This work indicated that a cross current flow utilizing a specialized gas-liquid contactor offered the lowest system operating energy.

Various industrial waste materials were evaluated as sources of alkalinity for the scrubber feed solution and as sources of calcium for precipitation of carbonate. Solids were mixed with a simulated sodium bicarbonate scrubber blowdown to comparatively examine reactivity. Supernatant solutions and post-test solids were analyzed to quantify and model the sequestration reactions. The best performing solids were found to sequester between 2.3 and 2.9 moles of CO_2 per kg of dry solid in 1-4 hours of reaction time. These best performing solids were cement kiln dust, circulating dry scrubber ash, and spray dryer absorber ash.

A techno-economic analysis was performed to evaluate the commercial viability of the proposed carbon capture and sequestration process in full-scale at an aluminum smelter and a refinery location. For both cases the in-duct scrubber technology was compared to traditional amine-based capture. Incorporation of the laboratory results showed that for the application at the aluminum smelter, the in-duct scrubber system is more economical than traditional methods. However, the reverse is true for the refinery case, where the bauxite residue is not effective enough as a sequestrant, combined with challenges related to contaminants in the bauxite residue accumulating in and fouling the scrubber absorbent. Sensitivity analyses showed that the critical variables by which process economics could be improved are enzyme concentration, efficiency, and half-life.

At the end of the first part of the Phase 2 project, a gate review (DOE Decision Zero Gate Point) was conducted to decide on the next stages of the project. The original plan was to follow the pre-testing phase with a detailed design for the field testing. Unfavorable process economics, however, resulted in a decision to conclude the project before moving to field testing. It is noted that CO_2 Solutions proposed an initial solution to reduce process costs through more advanced enzyme management, however, DOE program requirements restricting any technology development extending beyond 2014 as commercial deployment timeline did not allow this solution to be undertaken.

Table of Contents

LIST OF TABLES

LIST OF FIGURES

Figure No. **Title** **Page**

1.0 Introduction

1.1 Overview

The overall goal of the second phase of the DOE sponsored carbon capture and sequestration project was to demonstrate Alcoa's in-duct scrubber technology at an operating manufacturing facility to capture CO_2 from flue gas exhaust using an enzymatic capture process followed by sequestration of the captured CO_2 into industrial by-products. The aim of the pilot program was to use innovative and proprietary in-duct scrubber technology to capture CO_2 from plant stack emissions. The sequestration aspect of this technology utilizes and treats a primary byproduct of the aluminum manufacturing process known as alkaline clay, or bauxite residue, as well as other alkaline industrial residuals. The pilot project objective was to develop and evaluate a scrubbing process that combines treated flue gas, enzymes and alkaline clay to create a mineral-rich neutralized product that could be used for environmental reclamation projects.

The Phase 2 project, reported on here, sought to improve upon the in-duct scrubber performance of enzymatic CO_2 capture observed during the Phase 1 concept evaluation. The pilot unit developed for ATC laboratory testing in Phase I has been refined to include an expanded section to test higher volumes of gas at various gas flow velocities using freely dissolved optimized CA enzyme heat purified for superior activity. In addition, cross-linked enzyme aggregate (CLEA) made via cross linking the enzyme was tested for activity and stability in a bench-scale set-up at CO_2 Solution's facility. At the end of this part of the project, a gate review (DOE Decision Zero Gate Point) was conducted to decide on the next stages of the project. The original plan was to follow the pre-testing phase with a detailed design for the field pilot test. Unfavorable process economics, however, combined with challenges related to contaminants in the bauxite residue accumulating in and fouling the scrubber absorbent resulted in a decision to conclude the project before moving to the pilot testing. It is noted that CO_2 Solutions proposed an initial solution to reduce process costs through more advanced enzyme management, however, DOE program requirements restricting any technology development extending beyond 2014 as commercial deployment timeline did not allow this solution to be undertaken.

For additional information regarding overall program goals, technical merit, and strategy the reader is referred to the Project Narrative File for DOE FOA No. DE-FOA-0000015.

1.2 Objectives

The overall objectives required to accomplish the Phase 2 project scope were:

1) Efficient capture and conversion of flue gas CO_2 to bi-carbonates using a novel in-duct scrubber with the use of catalyst (CA) in a field pilot setting.
2) Mineral sequestration of the bi-carbonates and carbonates using Alcoa alkaline clay product as well as other industrial alkaline waste media thereby converting this industrial by-product from a land-impounded waste material into a beneficial re-use product for soil amendment applications.
3) Determination of mass balances and process conditions required to implement this system as a continuous, zero waste process.

4) Estimation of CO_2 consumption/production to define net (direct and indirect) CO_2 balance of proposed process.

The scrubber pre-testing phase also had additional objectives to facilitate the design and engineering of the pilot unit for subsequent field testing in 2013. These objectives were:

1) Demonstrate potential for activity stability equivalent of the CA enzyme to a half-life of several months or more under mechanical (e.g., shear) and chemical (e.g., pH, solution strength, defoamer, temperature, co-contaminants) conditions expected in In-Duct scrubber.
2) Demonstrate ~25% CO_2 capture in an In-Duct Scrubber with a single spray bank at a practical L/G (≤~30 gals/1,000 acf) and gas velocity (>8 fps) using either soluble enzyme or CLEA with defoamer as required.
3) Validate enzyme bench-scale stability projections in tests with a single batch of CA lasting a minimum of 100 operating hours.
4) Assess capacity for CO_2 sequestration with simulated sodium carbonate/bi-carbonate chemistry and a variety of alkaline industrial waste media, including, bauxite residue (screen for most promising sequestration agents, based on capacity and availability).

1.3 Approach

In the first part of the Phase 2 project, from June to December 2011 , project efforts focused on:

1) Lab testing of enzyme enhanced carbon capture in the In-Duct Scrubber
2) Lab testing of alkaline waste residuals as sources of alkalinity for the CO_2 scrubber solution
3) Techno-economic evaluation of a large-scale CCS system for smelter and refinery applications
4) CO_2 lifecycle assessments for smelter and refinery applications of the Alcoa CCS process

2.0 Enzyme enhanced carbon capture

2.1 Enzyme development

2.1.1 Enzyme activity and stability testing

2.1.1.1 Stirred-Cell Reactor (SCR) Test

Catalytic activity of carbonic anhydrase solution samples were assessed by running a stirred cell reactor assay similar to the one described by Kucka et al.[1] The experimental setup is shown in Figure 1, and consists of 500 mL jacketed glass reaction vessel and a stainless steel flange with an air-tight seal. Both gas- and liquid-phase is stirred with separate impellers. The solution activity assay is performed by adding 100 mL of CA solution in the reactor, evacuating air from the head-space and adding CO_2 gas into the system. The rate of CO_2 uptake into enzyme-laden solution is monitored using a digital pressure transducer. The kinetics of CO_2 uptake is used to infer enzyme catalytic efficiency.[1]

Figure 1: Stirred-cell reactor experimental setup.

2.1.1.2 Wilbur-Anderson Test

In addition to the stirred-cell reactor assay method noted above, the activity of carbonic anhydrase was measured using an electrometric method (Wilbur-Anderson assay).[2] Following the procedure described in Bhattacharya et al.,[2] 25 mL of CA solution was diluted to 25 mL 20 mM TEA (Triethanolamine) buffer, pH = 8.1. The mixture was stirred and maintained at room temperature (22 C) for several minutes. The assay was initiated by the addition of 10 mL of CO_2-saturated water into the reaction vessel. The change in pH from 8.1 to < 6.9 at 22°C was monitored using a bench-top pH meter and a combination electrode. For comparative purposes, TEA buffer solution with no enzyme was also tested following the procedure outlined above. The typical time for pH drop from 8.1 to 6.9 was ~ 20 sec and ~70 sec in the case of enzyme and TEA solution, respectively.

2.1.1.3 Enzyme Stability Testing

In order to evaluate the effect of pressure and shear-force on enzyme stability in the process of liquid aspiration through high-pressure nozzles, a lab-scale liquid recirculation rig was constructed by NELS Consulting and installed at Codexis, Inc. The recirculation setup is shown schematically in Figure 2. In this setup, liquid solution (typically 0.5 g/L CA enzyme) is pumped through a high-pressure hollow-cone nozzle and is allowed to fall freely through a 12-inch section of Q-PAC contactor. The liquid is accumulated at the bottom of the reservoir and is continuously re-circulated through the nozzle by a gear pump. During the course of the experiment, liquid samples (~100 mL) were collected through a sampling port on the bottom of the reservoir and submitted for enzyme activity testing by SCR and/or W-A assay methods (see above). The walls of the setup are made of Plexiglas, so that solution foaming could be observed under varying process conditions (enzyme strain, enzyme concentration, use of anti-foam, etc.). All tests were performed at 45 psi liquid pressure.

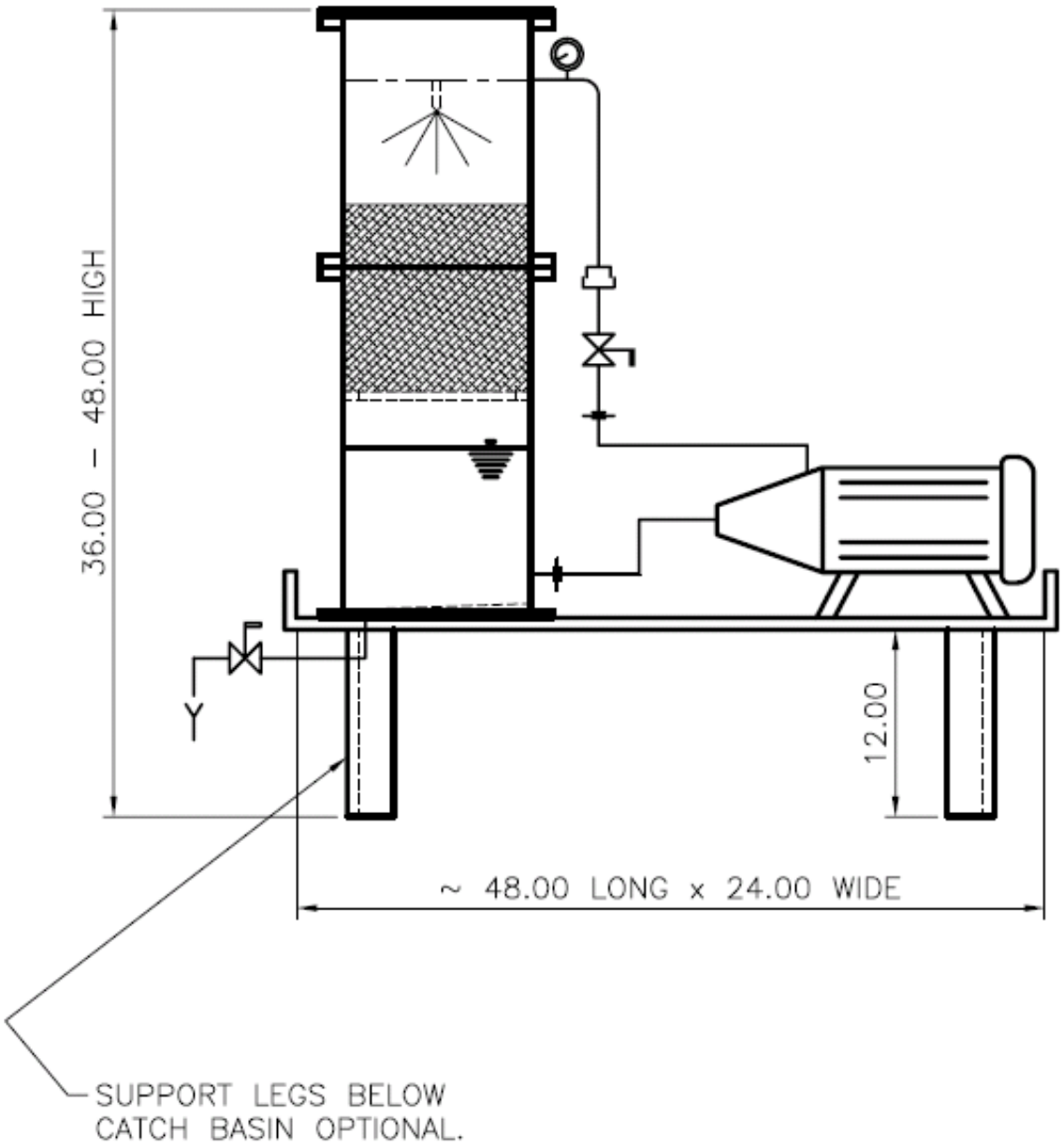

Figure 2: Schematic diagram of recirculation setup used for testing the effect of shear force on enzyme stability.

2.1.1.4 Results

Twelve variants of carbonic anhydrase enzyme (CA00 – CA11) were produced by Codexis and tested with regard to their catalytic activity using the stirred-cell reactor (SCR) assay.[1] In this assay, 100 mL of CA solution is added into a 500 mL temperature-stabilized reactor. The air from reactor head-space is evacuated, and CO_2 gas is added into the system. The rate of CO_2 absorption into enzyme-laden solution is monitored, and catalytic efficiency of enzyme is derived from CO_2 uptake rate.

Comparative SCR activity testing results are shown in Figure 3. The assays were performed at an enzyme concentration of [CA] = 1 g/L. In Figure 1, catalytic activity of different strains of enzyme (CA00 – CA11) is presented in terms of the measured pseudo-first order reaction rate constant of CO_2 hydrolysis (kov, right-hand side axis) and as acceleration factor relative to the rate of CO_2 absorption rate into a 0.3 M Na_2CO_3 solution (without CA) at 30 C. All assay tests were performed 3 times, and error bars in Figure 1 represent one standard deviation for each 3-point data set. As can be seen from Figure 3, enzyme variants CA02, CA04, and CA05 demonstrate the highest CO_2 hydrolysis activity, with acceleration factors between 30 and 40 relative to non-catalyzed rate of CO_2 uptake. Based on these results, CA05 strain was selected as the primary candidate for pilot scale testing at ATC, and all subsequent testing was performed using CA05 enzyme variant.

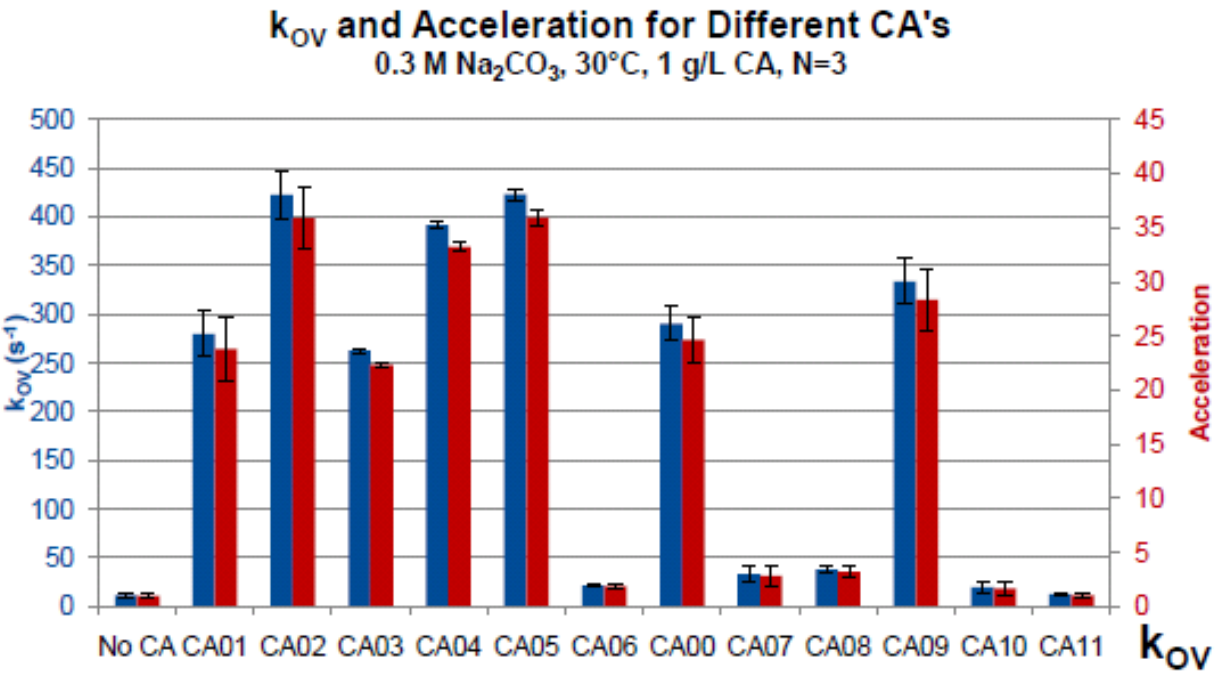

Figure 3: Comparative results of CA screening using stirred-cell reactor assay.

Temporal stability of CA05 enzyme was evaluated by incubating neat solutions of 0.25 and 0.5 g/L CA05 in 0.3 M Na_2CO_3 for 24 hours at T = 30 C, and measuring enzymatic activity using the Wilbur-Anderson method[2] for freshly made solutions (t = 0) and after 1, 2.5 and 22 hr of incubation. The results of enzyme stability testing are shown in Figure 4. As can be seen

from Figure 4, quiescent solutions of CA05 appear to be sufficiently stable, losing approximately 15% of activity after 22 hours of incubation.

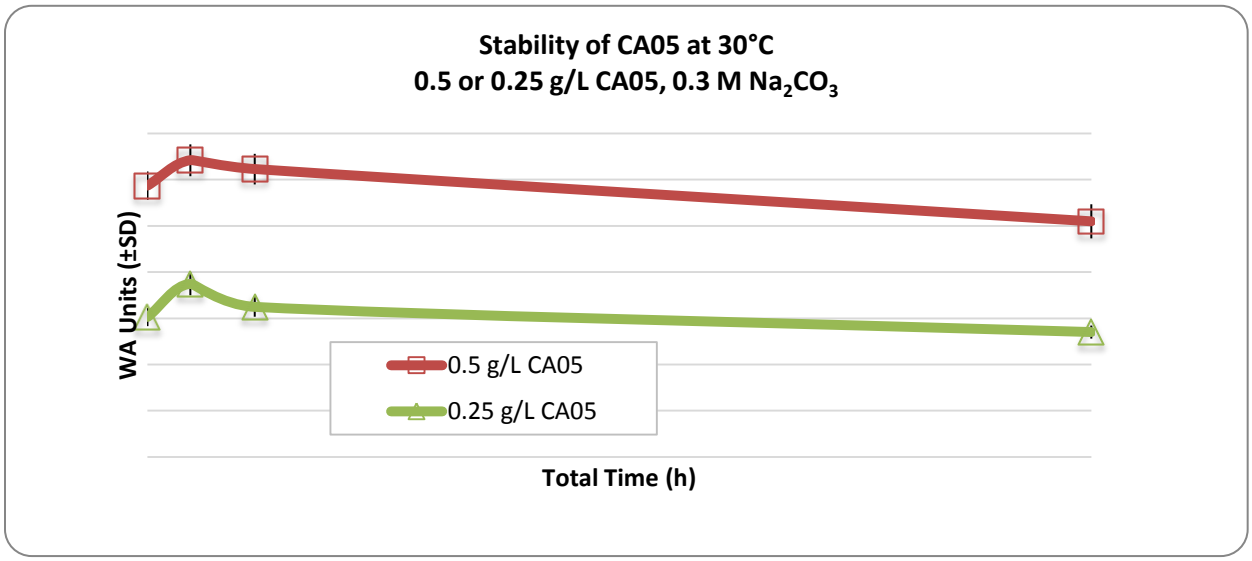

Figure 4: Stability of neat solutions of 0.25 and 0.5 g/L CA05 at 30 C.

The effect of pressure and shear force on enzyme activity was tested by pumping a solution containing 0.5 g/L CA05 and 0.3 M Na_2CO_3 through a high pressure nozzle in a specially designed lab-scale stress test rig, and measuring enzyme activity, using the SCR assay, as a function of re-circulation time. In addition, foam head height was measured in the course of the experiment, and the effect of antifoam was tested by introducing 100 ppm of Sigma Aldrich AF-204 antifoam agent after 1 hr of recirculation. The results of this test are presented in Figure 5.

As can be seen from Figure 5A, the CA05 solution appears to lose ~25% of its original activity after 2 hr of circulation time. As shown in Figure 5C, solution activity loss is accompanied by extensive foaming. Foam height increases with time reaching the top lid of the rig (18 cm) after ~40 min of circulation time. Addition of 100 ppm of AF-204 antifoam after 1 hr of circulation time resulted in complete elimination of the foam head. These observations suggest that an antifoam agent can be used to effectively control the foaming issue. As can be seen from Figures 3 A) and 3 D), CA05 enzyme retains ~75% of initial activity in spite of a ~18 C solution temperature increase.

For pilot-scale scrubber testing, 5 kg of CA05 enzyme was manufactured by Codexis and shipped to Alcoa Technical Center. Produced enzyme was characterized with regard to purity and enzymatic activity. The results of enzyme characterization are shown in Figures 4 and 5. Figure 6 shows the results of SDS page gel analysis of powder produced in lab-scale (control 1, control 2, and Lac200L) and large scale (Alcoa CA) reactors. As can be seen from Figure 6, the manufactured batch is composed of ~65% of CA05 enzyme, 24% extraneous protein, and 9% salts.

Figure 7 shows the results of enzyme activity characterization using the stirred cell reactor method. In Figure 5, the measured CO_2 hydration rate constant is plotted as a function of enzyme (powder) loading of the solution. As can be seen from Figure 7, a rate constant as high as ~1000 s-1 can be achieved at 2 g/L solution loading. This batch of enzyme powder corresponded to that tested in the pilot scrubber system at ATC.

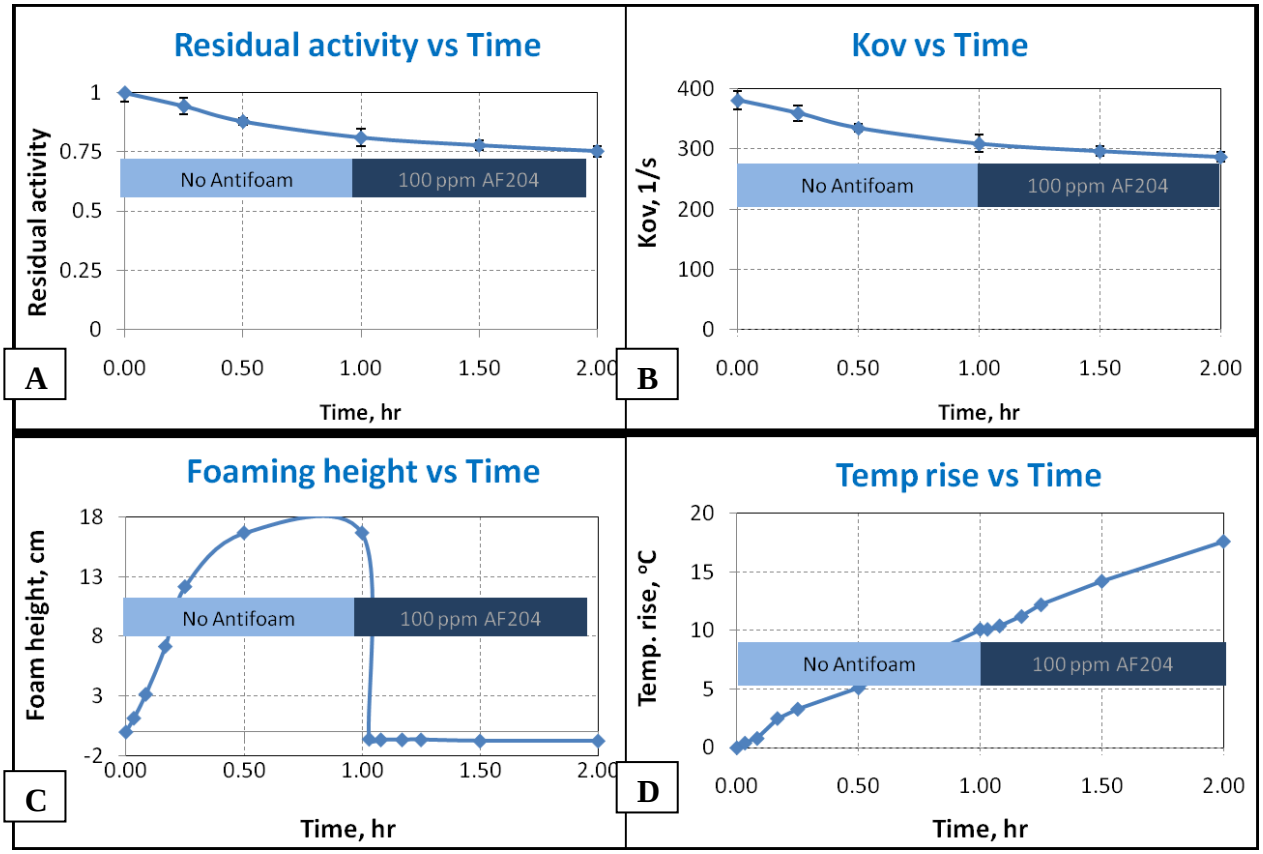

Figure 5: Summary of enzyme stress- and foaming- test results as a function of solution recirculation time in the stress rig. A) Residual (relative) activity of CA05 solution, B) Measured CO_2 hydration rate constant, kov, C) Measured foam height, and D) Measured temperature rise of the solution (degree C over initial T = 22 C).

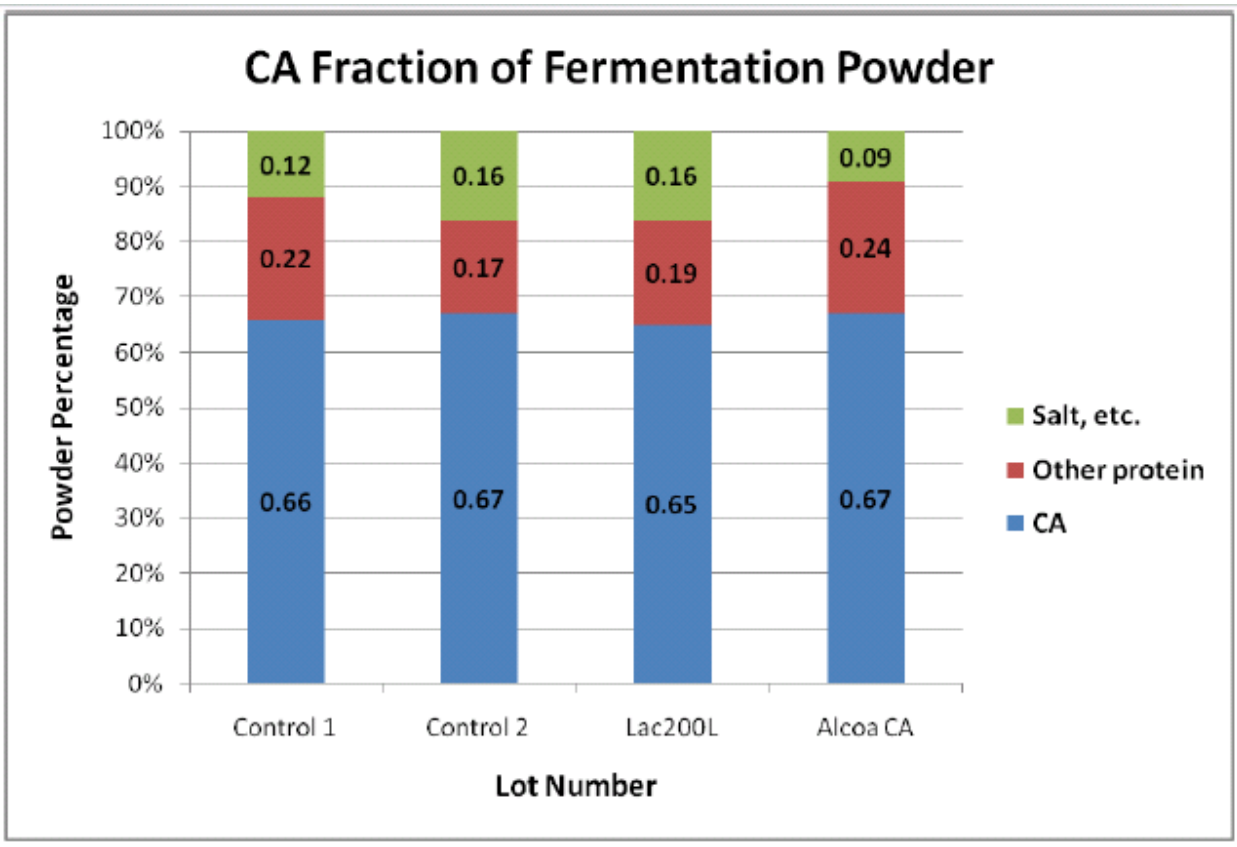

Figure 6: Results of SDS page gel analysis of enzyme powder produced in lab-scale (control 1, control 2, and Lac200L) and large scale (Alcoa CA) reactors.

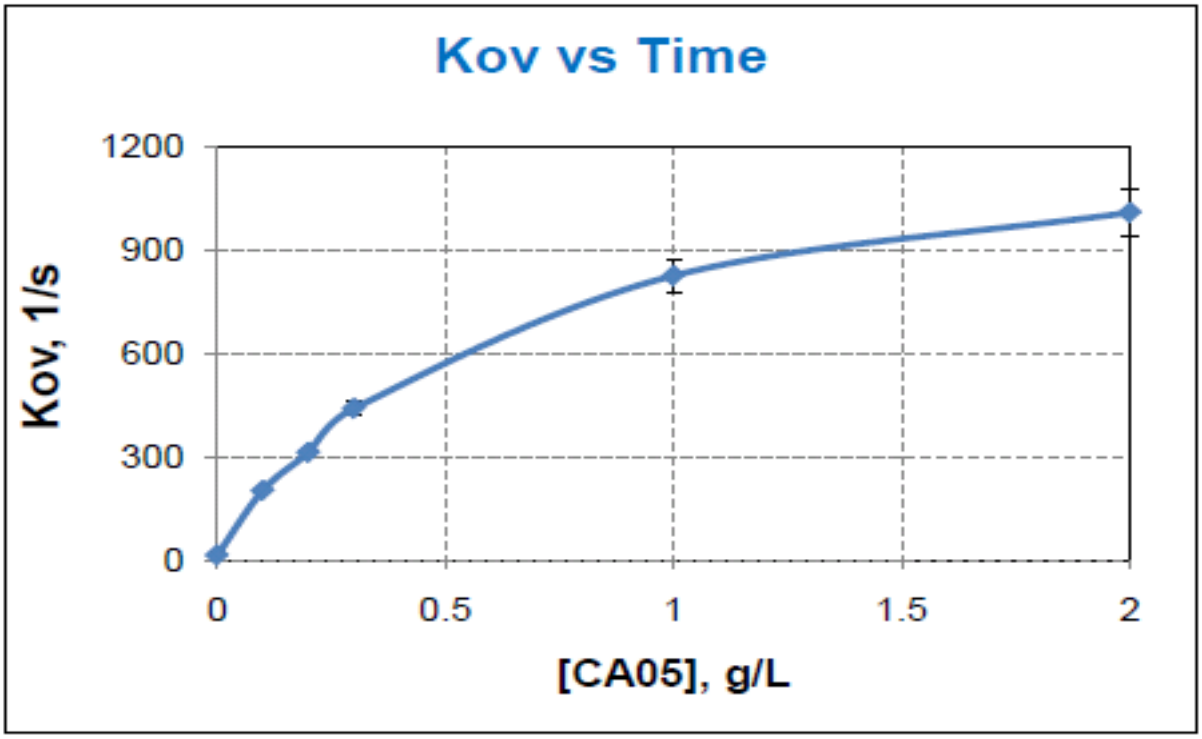

Figure 7: Measured CO_2-hydration rate constant as a function of enzyme (CA05) loading of the solution.

2.1.2 Enzyme performance evaluations

Efficacy experiments for the CA-05 batch of carbonic anhydrase were performed in 0.3M sodium carbonate solution at a nominal pH of 11 to generate information on enzyme performance and durability. Testing of the enzyme at a 0.9 g/L level with 10 ppm defoamer is shown in Figure 8 and indicates that the enzyme provides a four- to fivefold enhancement in scrubbing efficiency over a baseline condition with the same 0.3M sodium carbonate solution (without CA).

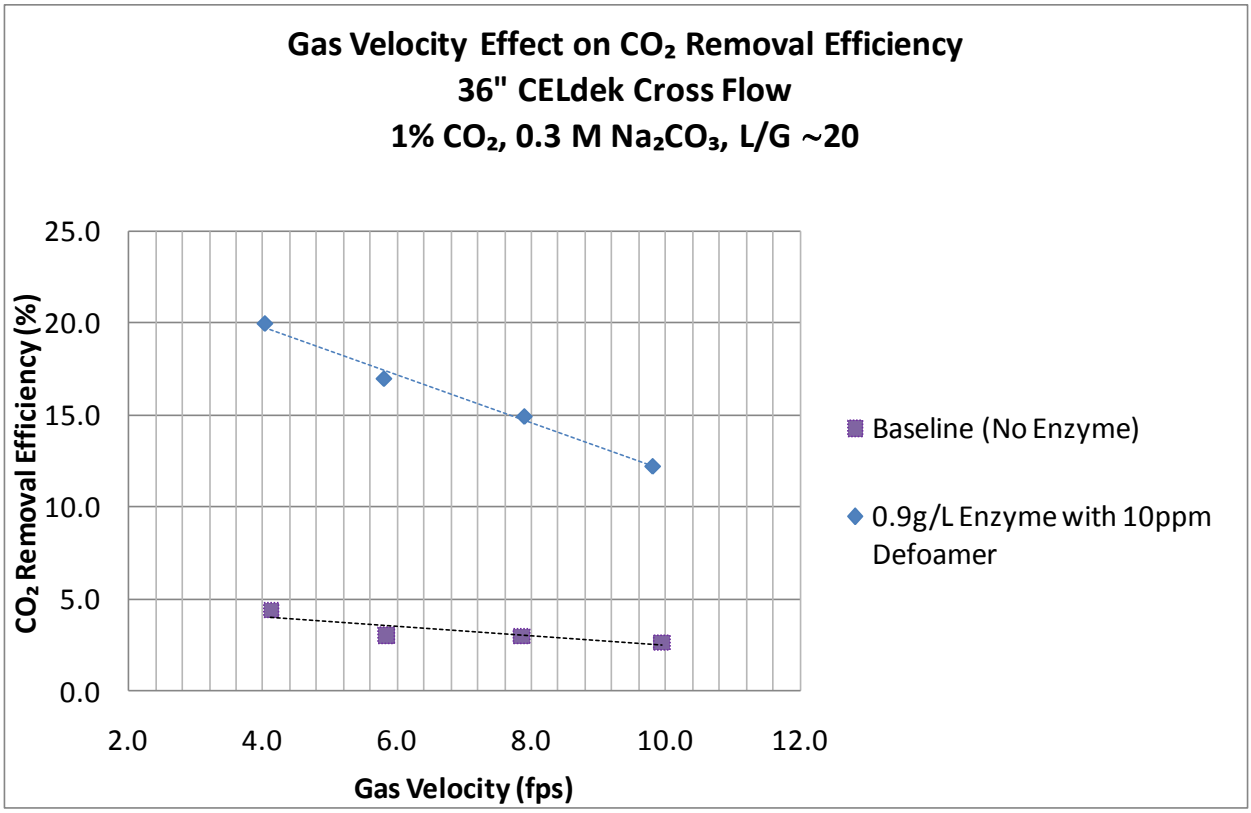

Figure 8: Scrubbing Enhancement for Enzyme in 0.3M Sodium Carbonate.

A series of experiments were performed to assess performance enhancement by the enzyme at concentrations ranging from 0.15 to 0.9 g/L and with different contactors as shown in Figure 9. Successful scrubbing enhancement was obtained with both contactor types and in the absence of defoamer at the relatively low enzyme concentration of 0.15 g/L. Increasing efficiency was observed as enzyme concentration increased. For all enzyme concentrations, the efficiency exceeded that for the baseline condition shown in Figure 8, but did fall short of matching the highest efficiencies obtainable at pH =13.5 (0.6M NaOH, no CA) and high L/G for both contactor types.

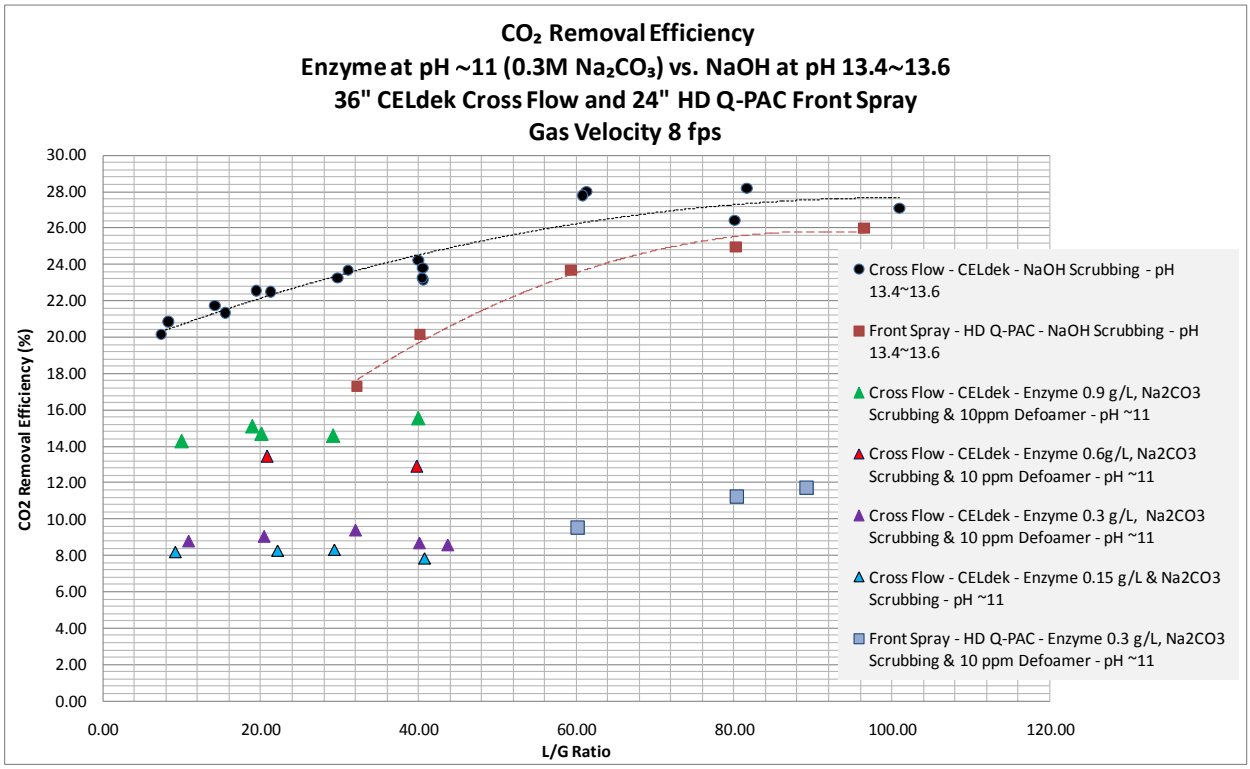

Figure 9: Scrubbing Efficiency with Varying Enzyme Concentrations and L/G Ratios.

In Figure 10, a comparison of enzyme scrubbing efficiency for 1% and 8% CO_2 feed streams is provided for the above range of enzyme concentrations, with and without the defoamer. As can be seen from Figure 10, CO_2 removal efficiency is slightly (~25%) lower for the 8% CO_2 gas stream than for the 1% CO_2 concentration.

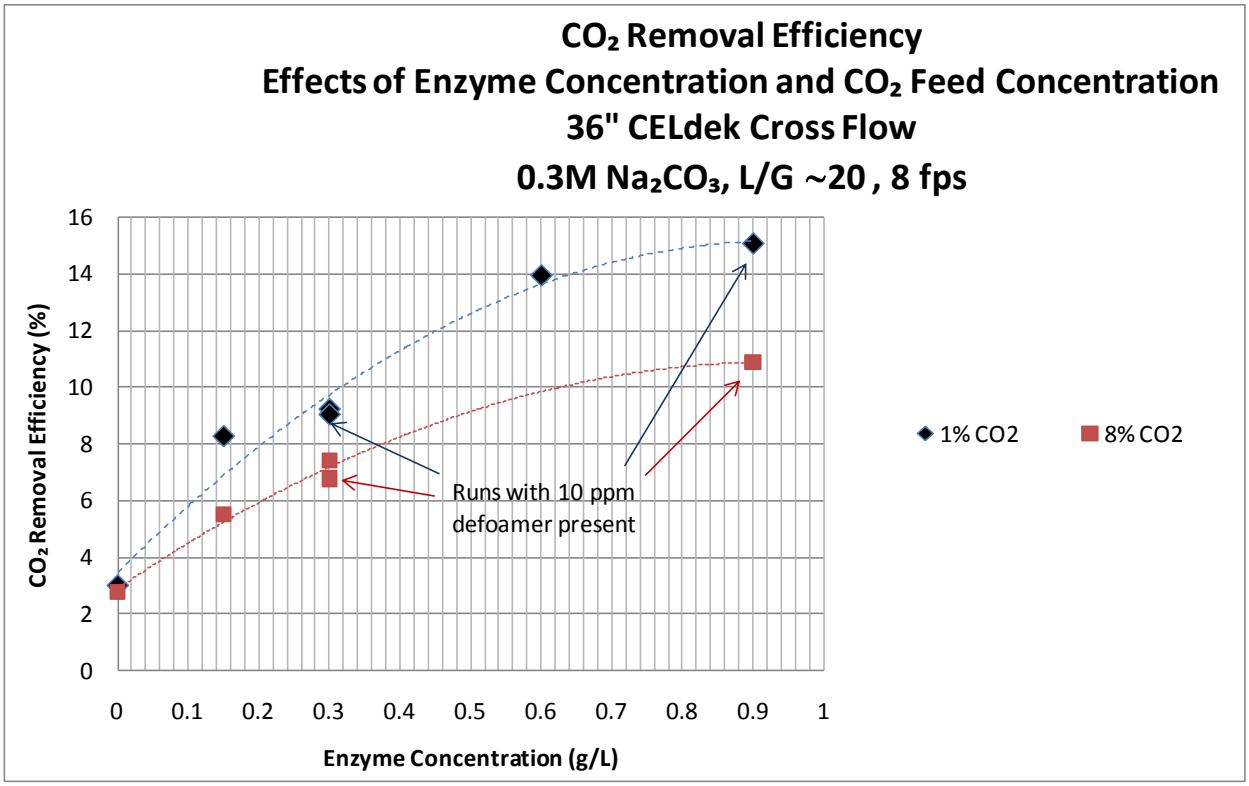

Figure 10: Relative Scrubbing Performance of Enzyme at Different Feed CO_2 Levels.

The performance of the enzyme was evaluated over a range of pH values. Unlike the earlier (Phase 1) work, where a decrease in pH from the initial13.4~13.6 value for 0.6M sodium hydroxide was monitored, these experiments commenced with 0.3M sodium carbonate at pH ~11 and sodium hydroxide was metered in at a rate that overcame the natural pH reduction as CO_2 scrubbing occurred. The resulting plots, Figure 11, compare the scrubbing efficiency of the enzyme at three concentrations as pH was raised. In general, efficiency remained relatively constant as pH increased to about 12.5, where a reduction began to occur resulting presumably from enzyme denaturation. This was followed by an increase in efficacy as the effect of high pH took over.

A follow-up experiment was performed in which the scrubbing efficiency of the enzyme solutions was monitored as pH was increased to about 13.5 and then reduced gradually as scrubbing occurred. The results indicate the denaturing of the enzyme was irreversible, such that the scrubbing efficiency at pH values under 12.5 was not enhanced over the baseline case with no enzyme present. This is shown in Figure 12.

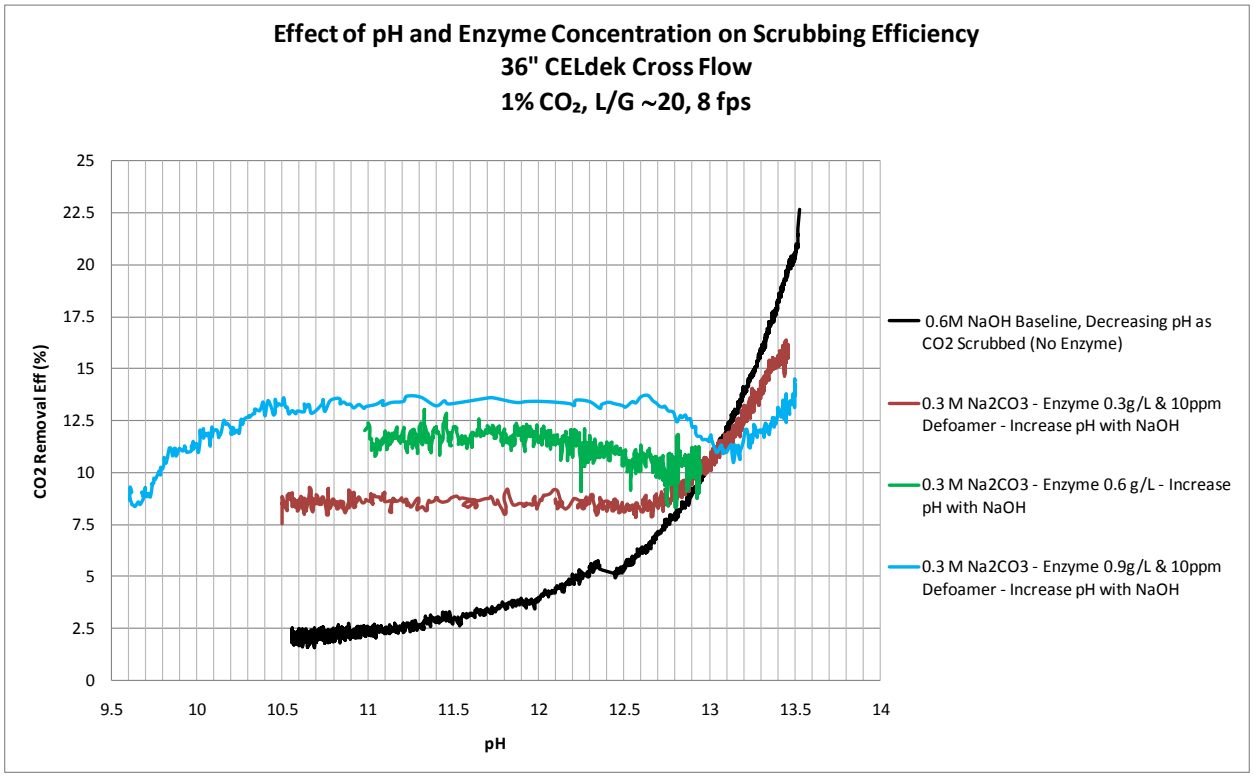

Figure 11: Enzyme Scrubbing Efficiency as a Function of pH.

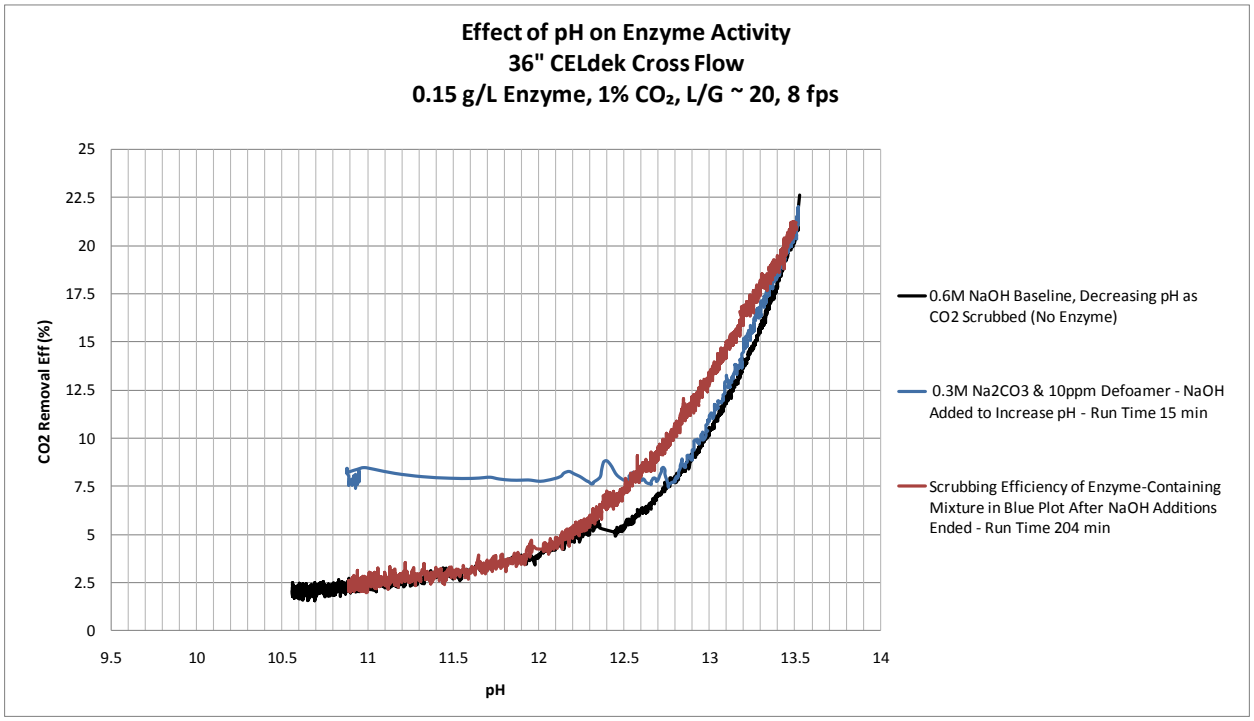

Figure 12: CO_2 Removal Efficiency Before (blue curve) and After (red curve) Enzyme Denaturation due to the pH Effect.

A series of experiments were performed to assess the lifetime of the CA enzyme in 0.3M sodium carbonate solution under different shear conditions. In Figure 13, runs were performed at relatively constant pH by limiting the CO_2 level to that in ambient air between measurements and raising pH as needed with sodium hydroxide. The results in Figure 13 suggest at most a limited reduction in efficiency (ca. 15%) in the course of 8 hours run time at L/G of 60, where the full system volume is recirculated in slightly over 2 minutes.

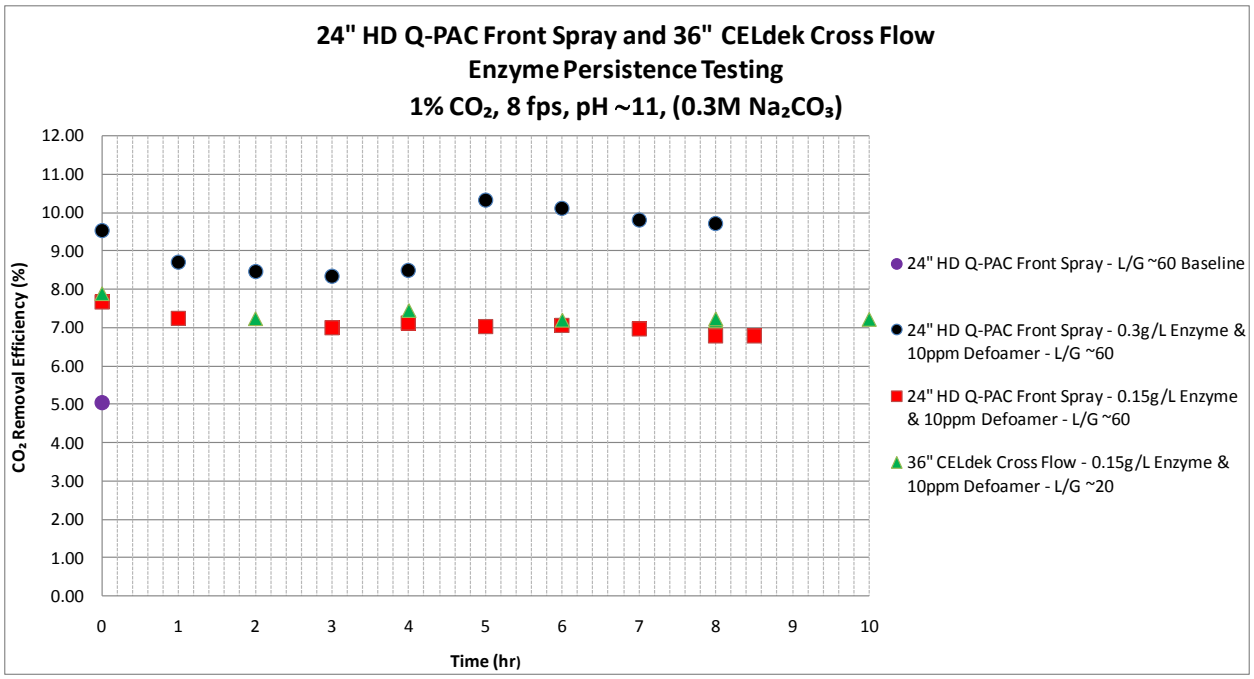

Figure 13: Enzyme Stability Testing at pH ~11.

One enzyme stability test, as shown in Figure 14, was run with pumping and spraying for a total of 24 hrs over the course of three operating days in a five-day span, again at relatively constant pH. The total efficency decrease was from 7.9% to 5.0%, a 37% reduction, with the majority of that occurring during the final day of operation.

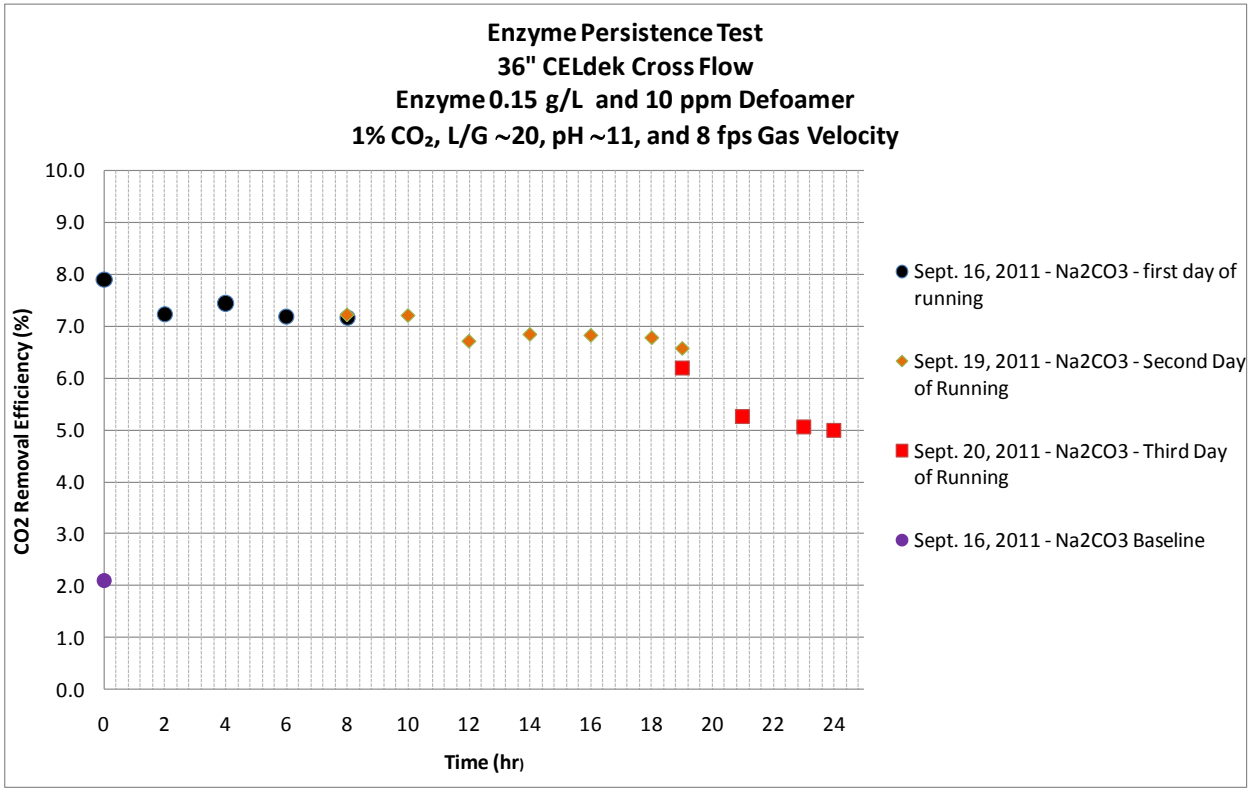

Figure 14: Long-Term Enzyme Stability Test Results.

Additional tests were run to assess the potential impact of the defoamer on scrubbing efficiency and on pressure drop across the contactors. In Figure 15, the effect of 10 ppm of defoamer on scrubbing efficiency of a 0.3 g/L enzyme solution is shown over a range of L/G ratios. The data suggest little if any impact of the defoamer on scrubing efficiency at this level.

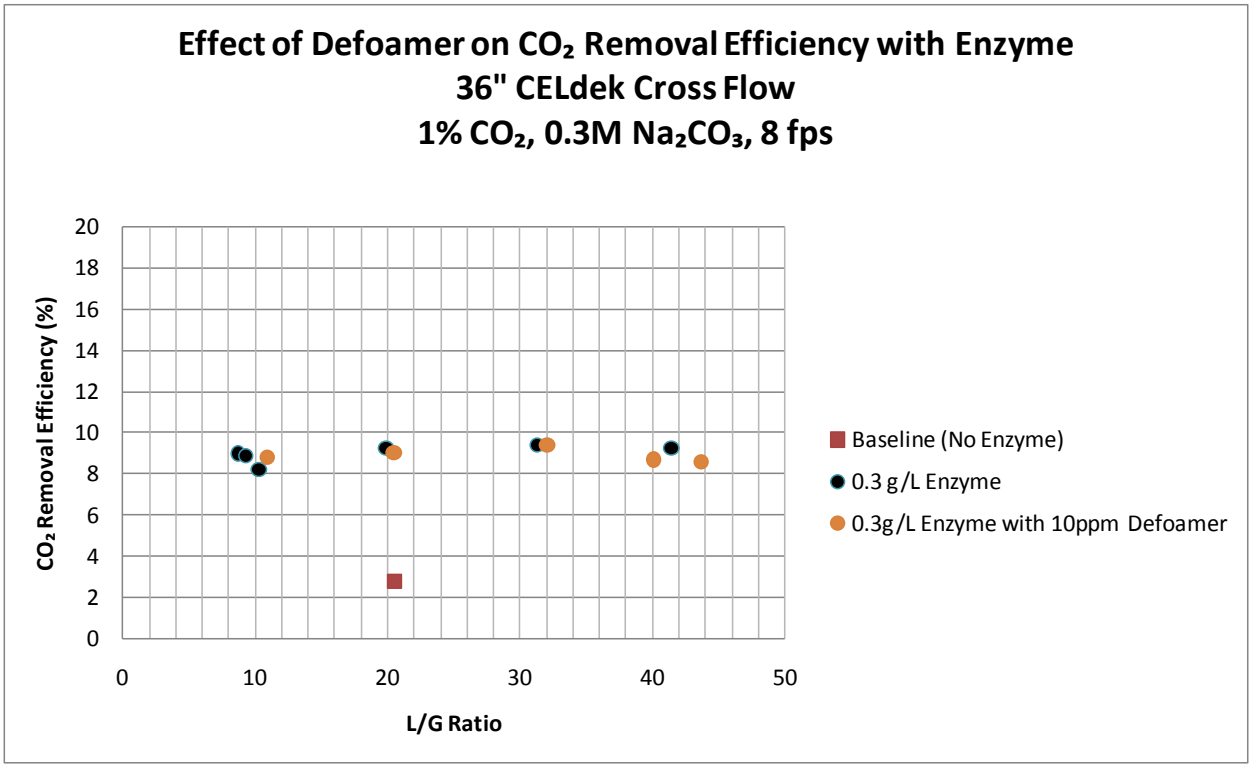

Figure 15: Assessment of Potential Impact of Defoamer on Scrubbing Efficiency.

In Figure 16, the impact of defoamer on pressure loss across the contactor is shown, with the defoamer showing benefit in reducing the pressure loss for a 0.3 g/L enzyme concentration, which is sufficient to generate substantial foam under these operating conditions. Presumably, by minimizing the foam intensity, the impact of foam on gas flow through the channels in the contactor is reduced. Based on these results, and the expectation of significantly reduced energy requirements for the system blower with antifoam, its use is supported.

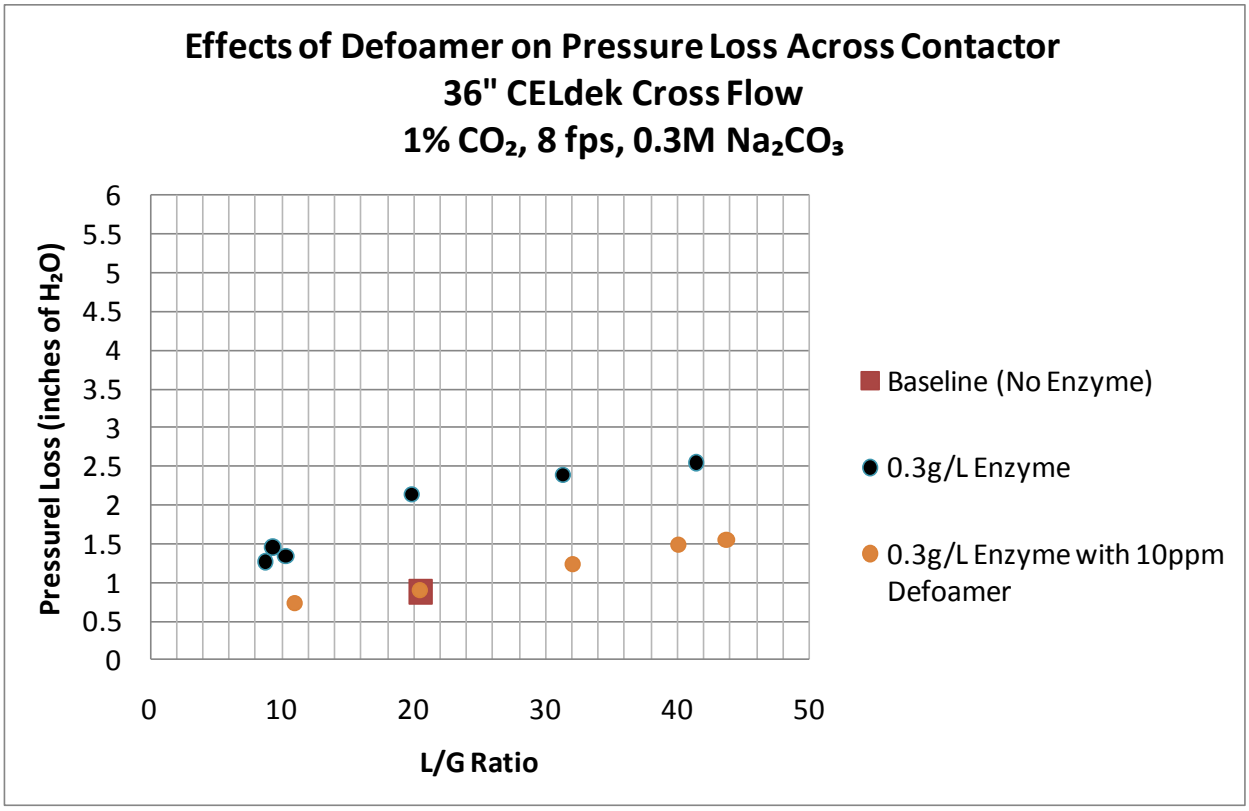

Figure 16: Impact of Defoamer on Pressure Drop Across CELdek Contactor.

In summary, CO_2 uptake enhancement by a factor of ~5 was observed at an enzyme concentration of 0.9 g/L and 1% CO_2 gas concentration. The enzyme maintains its activity during long term scrubber operation (~63% of initial activity in 5 days of testing), with the antifoam providing the benefits of minimal foaming and reducing pressure drop across the contactor with little if any negative impact on scrubbing performance at the 10 ppm level.

2.2 ATC scrubber design, refinement, and testing

The horizontal induct scrubber design was refined to a process-scalable 27 inch by 27 inch by 36 foot long single spray bank design for deployment at Alcoa Technical Center. This design was developed to minimize the impact of wall effects on the gaseous carbon dioxide absorption into the scrubber liquor sprayed into the gas stream. The clear acrylic scrubber construction material was fabricated to include a modified gaseous carbon dioxide injection manifold, a three by three nozzle array spray bank, bulk entrainment separator, a four pass mist eliminator, a larger capacity blower and a brand new exhaust stack.

Key tasks completed during this period are as follows:

- Design of the larger ATC pilot scrubber to the 27 inch by 27 inch size for scaling up to full scale installation;
- Fabrication of the scrubber sections for horizontal spray nozzle configuration;
- Development of the cross flow scrubber design for low scrubbing liquor shear on the enzyme;
- Mass and energy balances for the experimental test protocol were revised to determine maximum ability;
- The scrubber stack was increased in diameter to 22" to accommodate the larger capacity blower;
- Main process equipment was procured including the direct drive, 10,000 CFM Chicago Blower, lower shear centrifugal pump; and
- To appropriately simulate the carbon dioxide concentration of the flue gas, two trailer mounted carbon dioxide supply tanks were procured. The combination of the 15 ton and 20 ton supply trailers will accommodate up to 3200 pounds per hour of carbon dioxide to the scrubber system which will allow variation of CO_2 levels from 1 to 8% v/v.

2.2.1 ATC Pilot Scrubber Design – Operational Flexibility

Two scrubber designs were evaluated – the Alcoa patented induct scrubber with co-current spray array approach and a cross-flow low shear induct scrubber approach. Figure 17 shows the schematic for the original co-current induct design while Figure 18 depicts the cross-flow design.

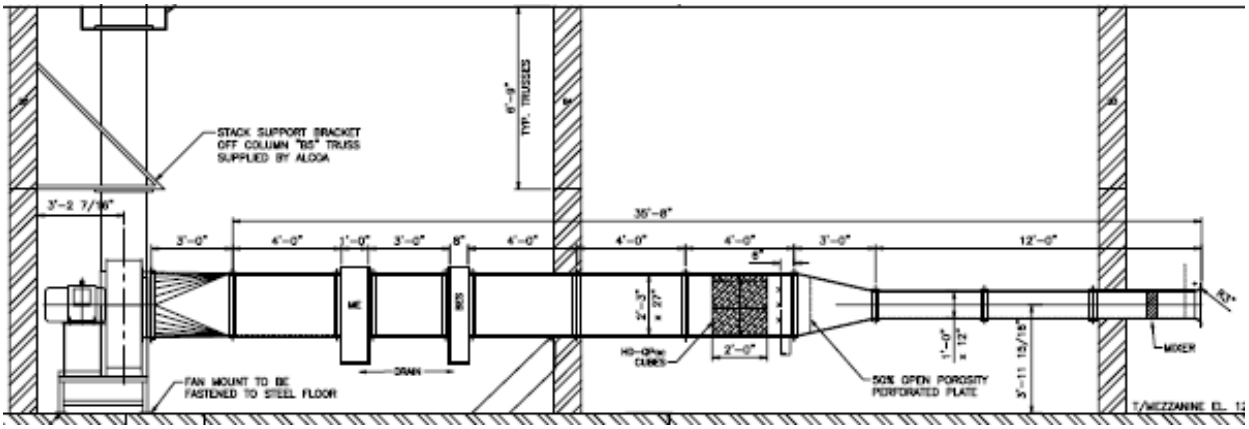

Figure 17: Co-current induct scrubber schematic

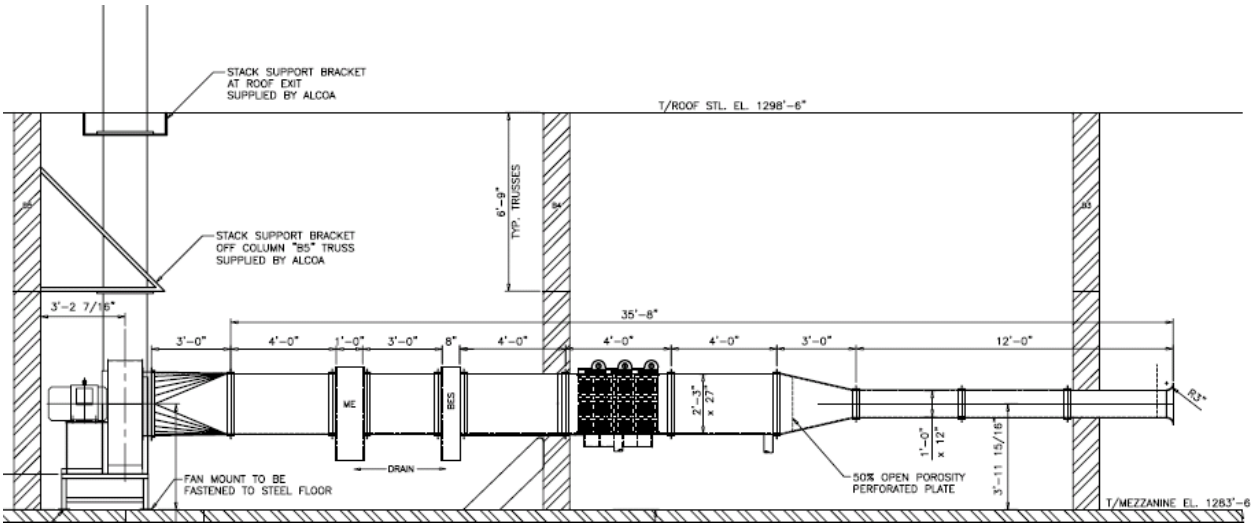

Figure 18: Cross-flow induct scrubber schematic

The modular nature of the scrubber system allows for the section containing the co-current spray nozzle to be removed and replaced with the cross flow scrubber design. The cross flow scrubber design utilizes distribution piping on the upper surface of the scrubber to distribute the scrubber liquor uniformly over a open surface contact media allowing for low shear liquor distribution to preserve the enzyme activity and allowing for a reduced gas side pressure drop. The photos provided (Figures 19 and 20) below show the cross-flow scrubber and co-current scrubber modules respectively, including the liquid – gas contact media.

Figure 19: Cross-flow Scrubber Module.

Figure 20: Co-Current Scrubber Module.

The cross-flow design is also equipped with high surface area contactor media which provides significantly less pressure drop through the scrubber as opposed to a co-current spray using contactor media.

2.2.2 Baseline Testing Results – Co-Current and Crossflow Design

Two different sets of baseline testing were performed, one with 0.6 M NaOH solution and the other with 0.3 M Na_2CO_3 solution. The 0.6 M NaOH solution was chosen to provide the maximum CO_2 removal under practical achievable conditions using Na solution scrubbing and is also used to optimize the scrubber arrangement in terms of maximizing the gas-liquid contact and surface area as well as reducing any potential gas flow mal distribution. The 0.3 M Na_2 CO_3 solution was chosen to represent the baseline condition for enzyme testing.

Figure 21 shows the impact of different contactor types on CO_2 removal efficiency for scrubbing with 0.6 M NaOH solution. As shown in this plot, the cross-flow scrubber with 36 inch of CELdek media offers superior CO_2 removal performance as compared to the frontal spray with HD-QPAC media. Also, consistent with Phase I results, the use of contactors greatly enhances

removal efficiency compared to co-current open spray configuration. Finally, a CO_2 removal efficiency of >25% is reached with a single spray bank at L/G ratio of 40.

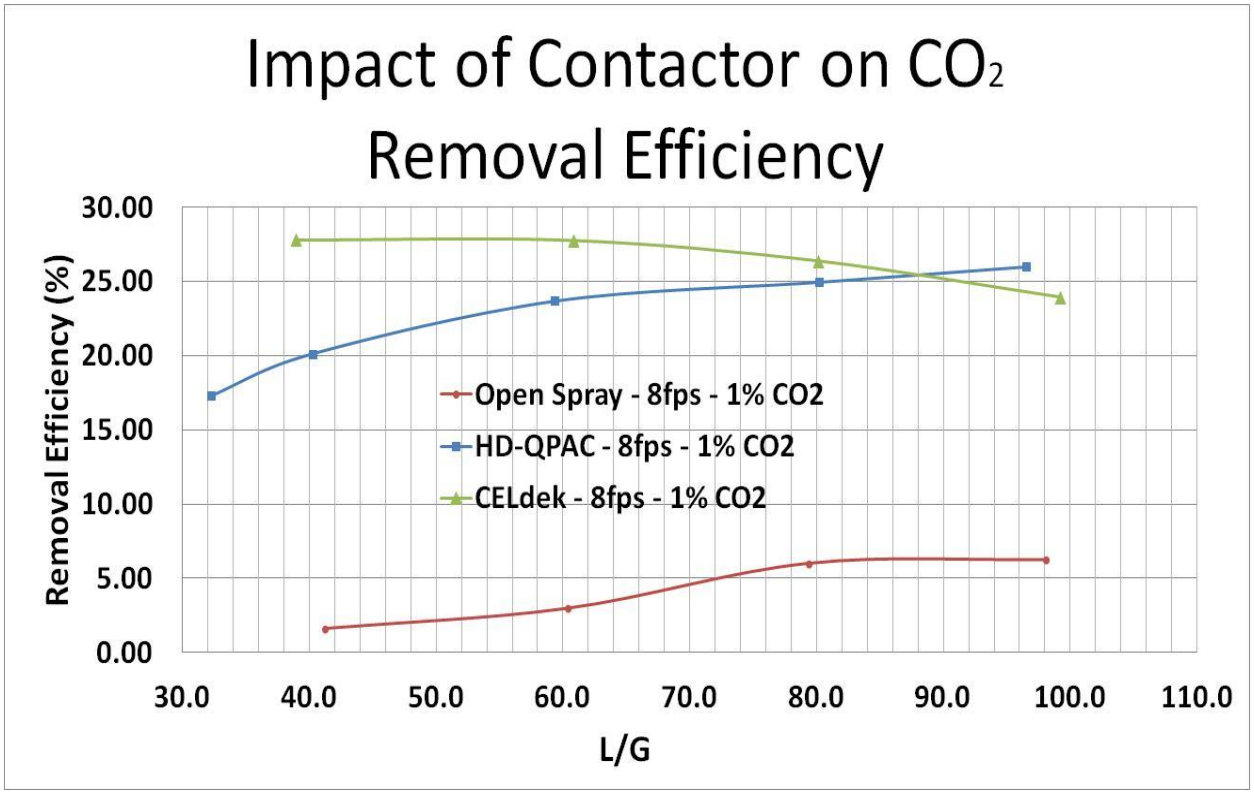

Figure 21: Impact of Contactor on CO_2 Removal Efficiency using 0.6 M NaOH as the scrubbing medium.

The cross-flow scrubber with the CELdek media proved to be the optimal media based on superior performance at a significant lower pressure drop at the contactor and lower liquid delivery pressure as illustrated in Figure 22. The lower pressure drop and superior gas-liquid contact allowed the cross-flow scrubber design with the CELdek media to be the first choice for testing CO_2 removal employing the carbonic anhydrase enzyme dissolved in 0.3 M Na_2CO_3 solution.

2.2.3 Testing with Carbonic Anhydrase Enzyme

Figure 23 shows the performance enhancement in terms of CO_2 removal using three different enzyme concentration levels (0.6 g/L, 0.3 g/L and 0.15 g/L of enzyme solubilized in 0.3 M Na_2CO_3 solution). As shown in Figure 14, a 5X enhancement in CO_2 absorption has resulted from enzyme introduction compared to the baseline with no enzyme. Note, the target removal of 20-25% CO_2 using a single bank of scrubbing media was not achieved. It is important to note that the low pressure drop of the system allows for serial application of multiple scrubber contactor banks to achieve increase CO_2 removal efficiency.

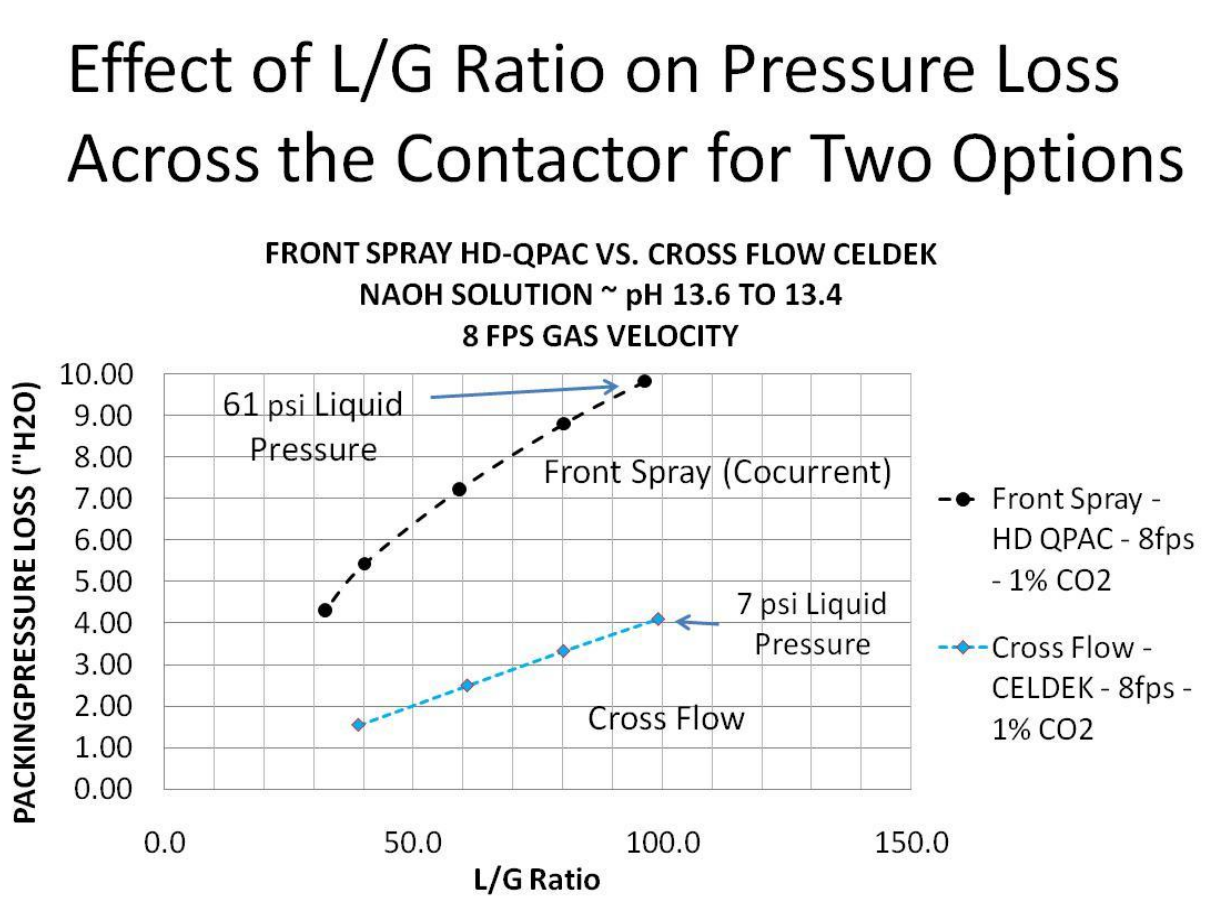

Figure 22: Effect of two different scrubber configurations on pressure drop and L/G ratio.

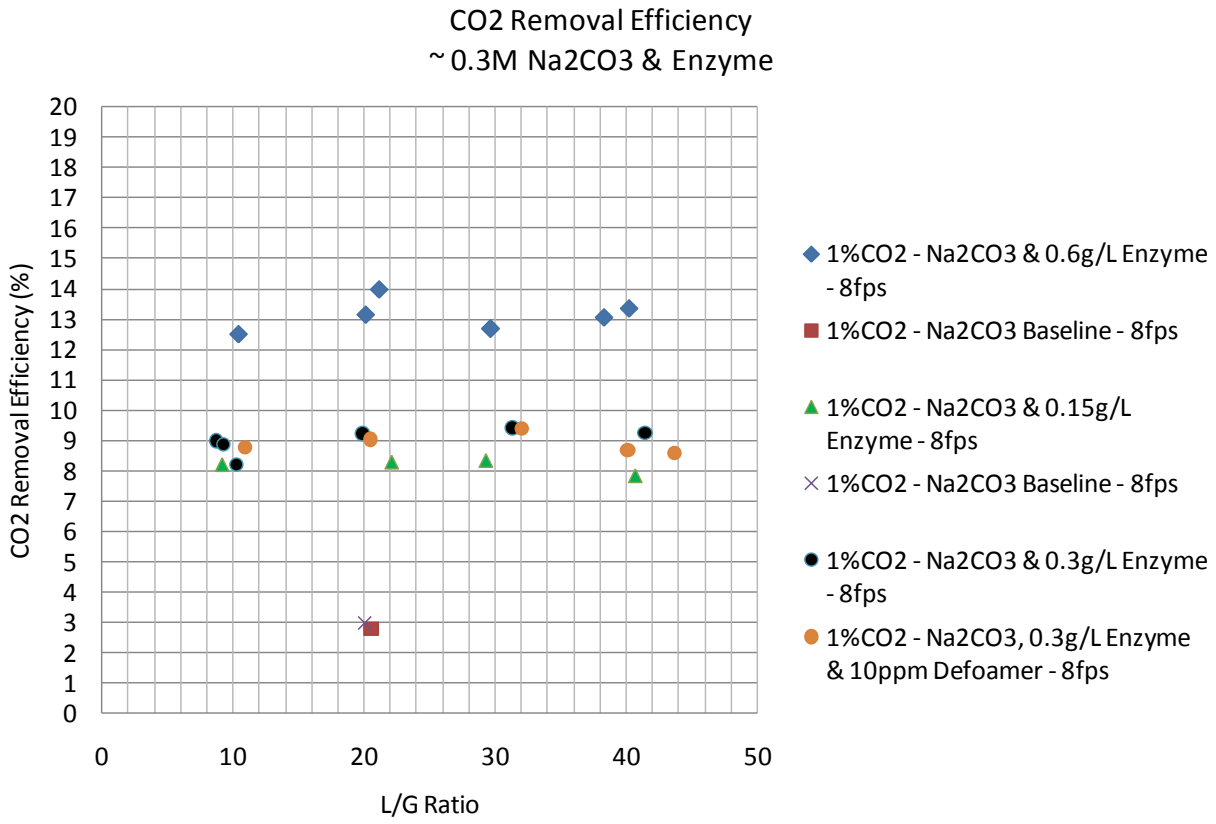

Figure 23: Enzyme Performance as a function of L/G ratio using the Cross-flow scrubbing configuration using the CELdek packing media.

2.2.4 Contactor Performance Assessment

Following equipment performance verification, initial experiments as shown in Figure 24, compared the relative efficiency of CO_2 scrubbing using the 12-nozzle array with and without a 24" thickness of HD Q-PAC media as a contactor. For experimental conditions shown in Figure 24 (0.6M NaOH solution, 1% CO_2 concentration, and 8 fps gas flow velocity), the contactor enabled a roughly fourfold increase in scrubbing efficiency compared to an open spray configuration.

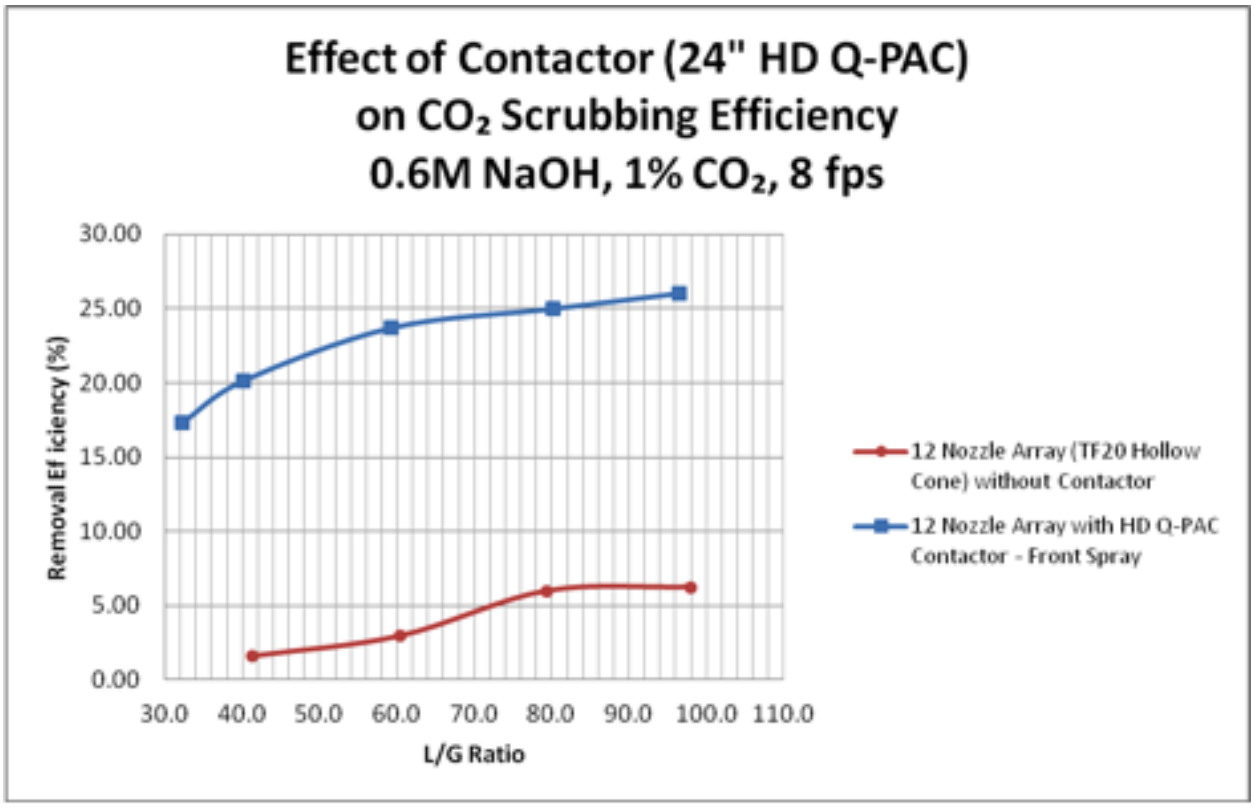

Figure 24: Effect of Contactor (24" HD Q-PAC) on CO_2 Scrubbing Efficiency

As anticipated, scrubbing efficiency is highly pH dependent. Figure 25 shows measured CO_2 scrubbing efficiency (with HD Q-PAC contactor) as a function of solution pH, CO_2 concentrations in the range between 1 and 8 %, and no enzyme added. As can be seen from Figure 25, the difference between CO_2 removal efficiency at 1, 4, and 8% CO_2 levels is not significant. For the one run with defoamer present (blue trace in Figure 25), slightly lower efficiency was observed. This run was in anticipation of future runs with enzyme; however, the high (100 ppm) level of defoamer used may have interfered with CO_2 absorption.

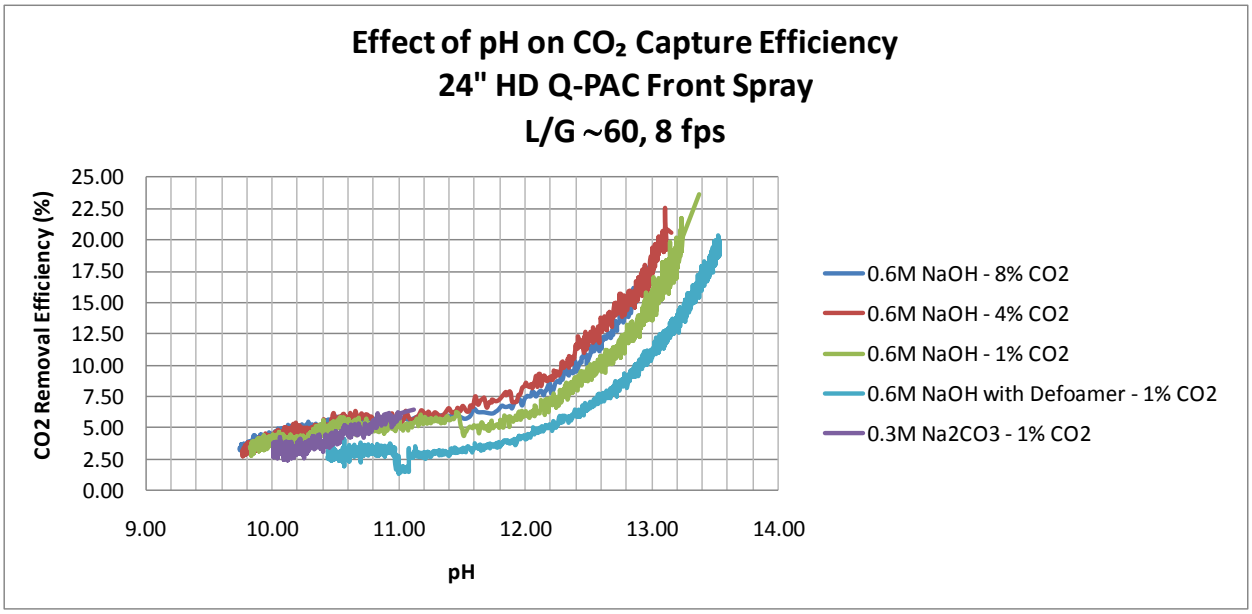

Figure 25: Effect of pH on CO2 Capture Efficiency (no enzyme added).

Figure 26 shows the results of scrubbing solution alkalinity measurements at various pH levels. As shown in Figure 26, the hydroxide alkalinity present at high pH of about 13.5 for the sodium hydroxide solution is converted initially to carbonate alkalinity. As CO_2 scrubbing continues, at a pH of about 11.5, the hydroxide is depleted and bicarbonate alkalinity begins to form. At pH values below about 10, scrubbing efficiency is significantly reduced as is shown in Figure 25.

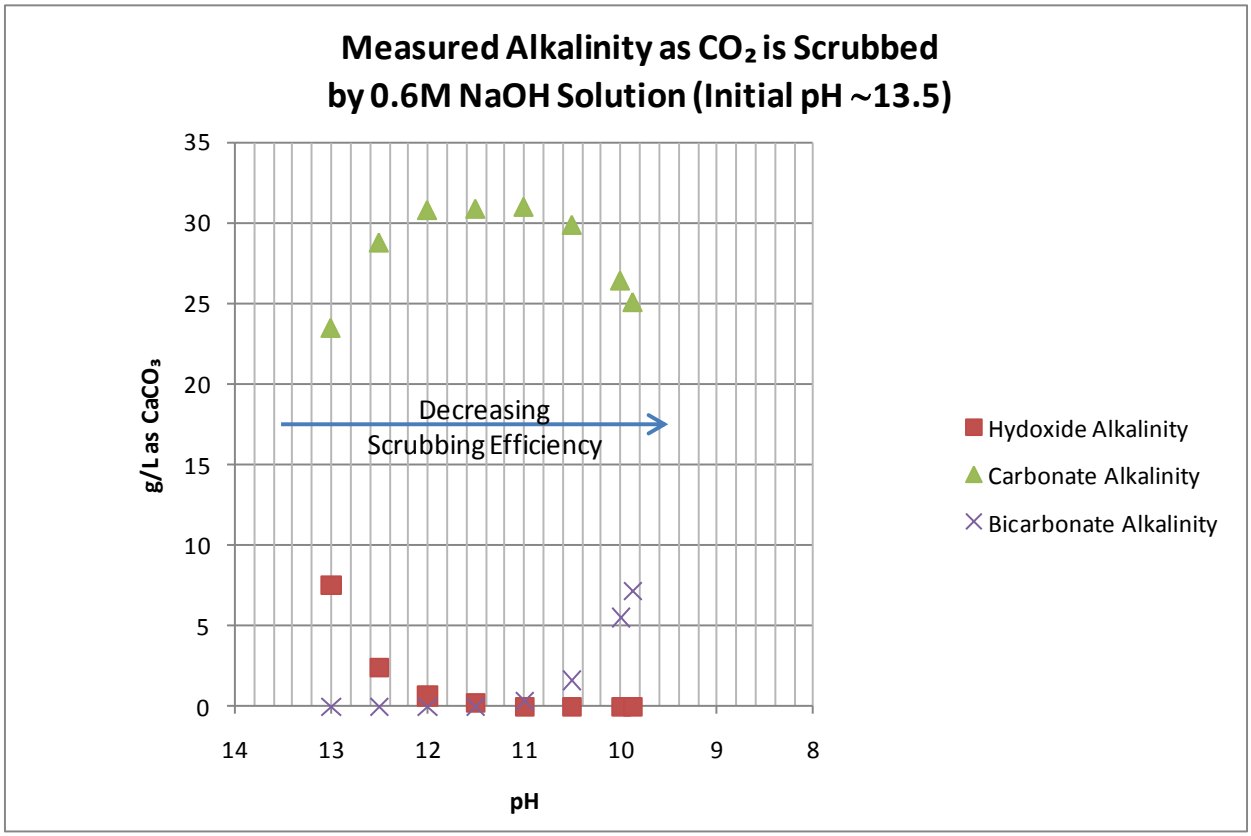

Figure 26: Measured Liquor Alkalinity as a Function of Solution pH.

Figure 27 shows the effect of L/G ratio on CO_2 removal efficiency (using HD Q-PAC contactor) for 0.6 M NaOH and 0.3 M Na_2CO_3 solutions. The four runs with the higher pH of the 0.6M sodium hydroxide solution were clearly much more efficient than that with the lower pH sodium carbonate solution. The run with defoamer did have a slightly lower scrubbing efficiency than the analogous run without defoamer, but the difference was not as great as seen for the runs in Figure 25.

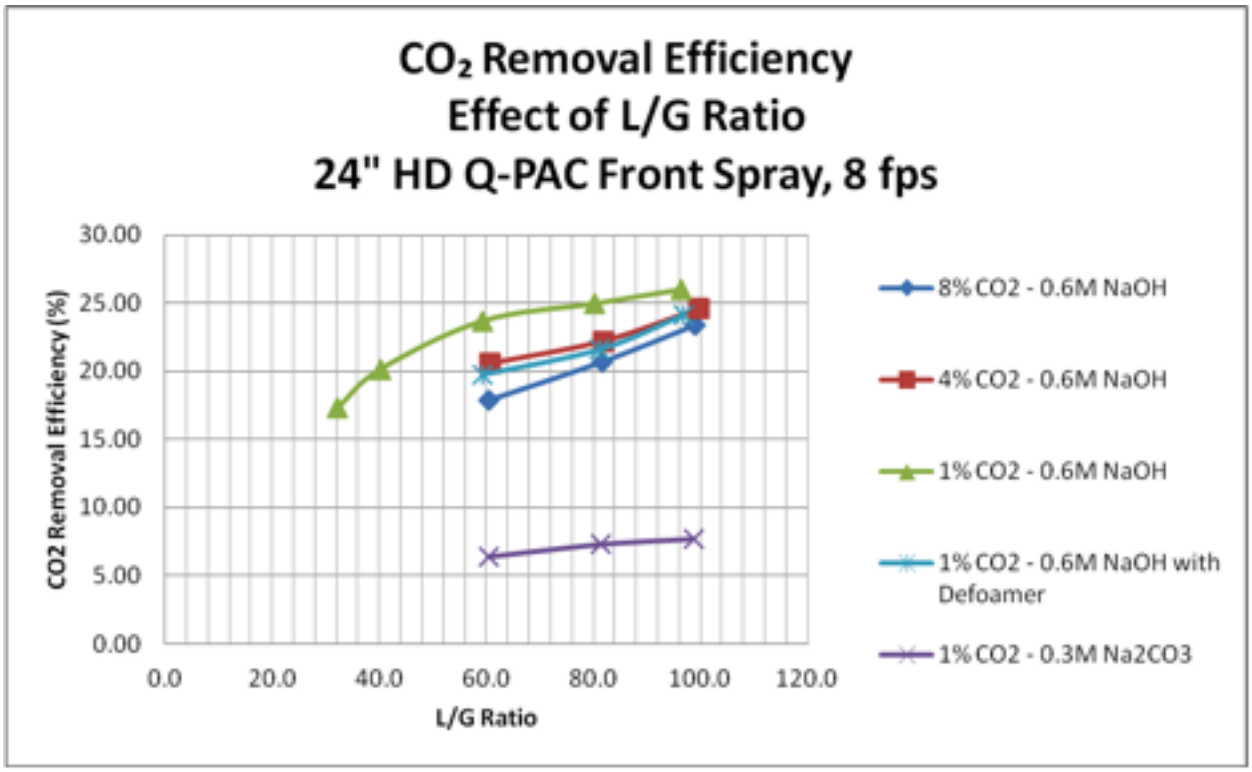

Figure 27: CO2 Removal Efficiency as a Function of L/G Ratio.

An important feature of a contactor medium is the pressure drop across it, since this will influence the energy requirements to operate the system. A study of pressure drop across the HD Q-PAC contactor is shown in Figure 28 for the 8 fps flow rate and a range of L/G ratios between ~32 and ~100. Over this range of liquid flow rates, the ΔP ranged from 4.3 to 9.8 inches of water, suggesting that the higher liquid flow rates increase overall resistance to flow through the contactor.

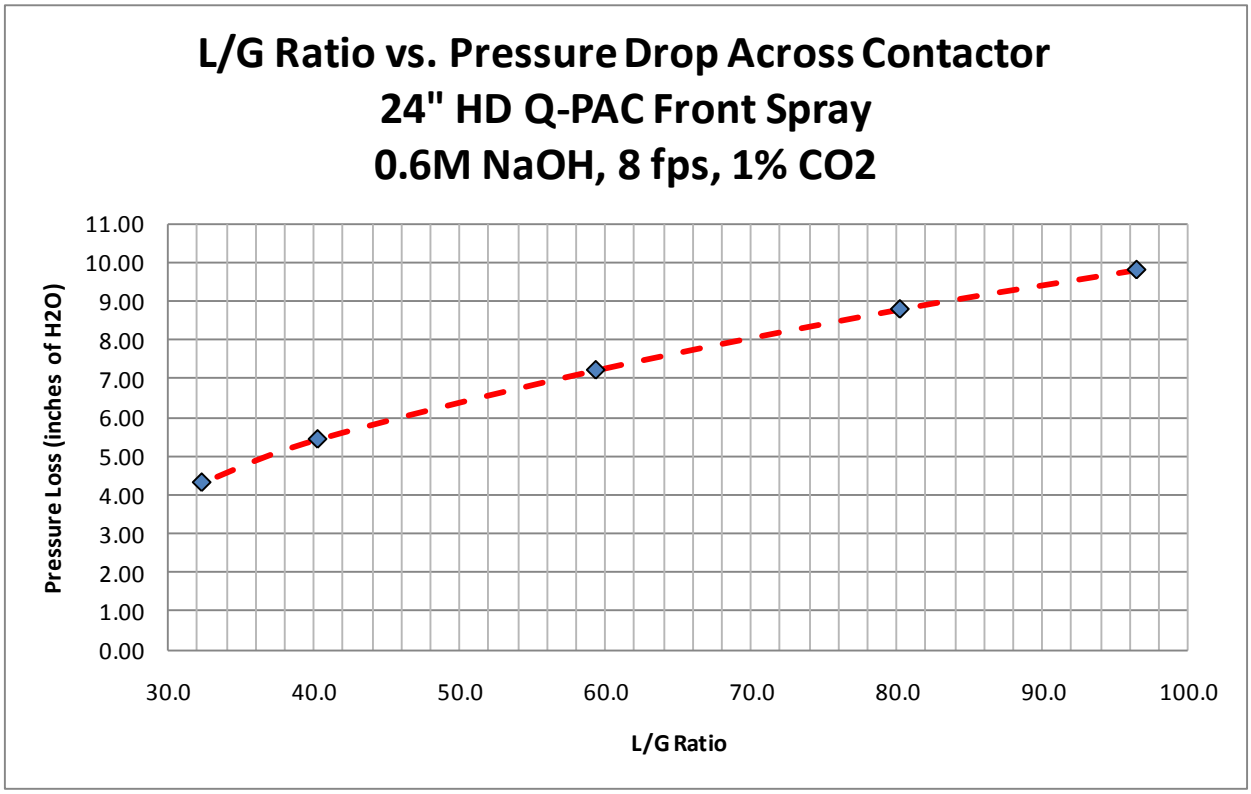

Figure 28: L/G Ratio vs. Pressure Drop Across HDQ-PAC Contactor.

The second contactor used in this study was a 36" thick CELdek, a medium used commonly in combination with water to humidify air streams. In Figure 29, the scrubbing efficiency of this type of contactor in a cross flow configuration (with fluid applied from the top) is shown as a function of L/G ratio. As a reference, the performance of the HD Q-PAC contactor is shown as a black dashed curve in Figure 27.. The CELdek was run both prior to and after the use of defoamer in the system, addressing the question as to whether the defoamer could negatively influence scrubbing efficiency. Such a negative effect was not apparent in this work. As can be seen, scrubbing efficiency for the CELdek is superior to the HD Q-PAC up to the highest of the L/G ratios studied (L/G ~100 gal/1000ft^3).

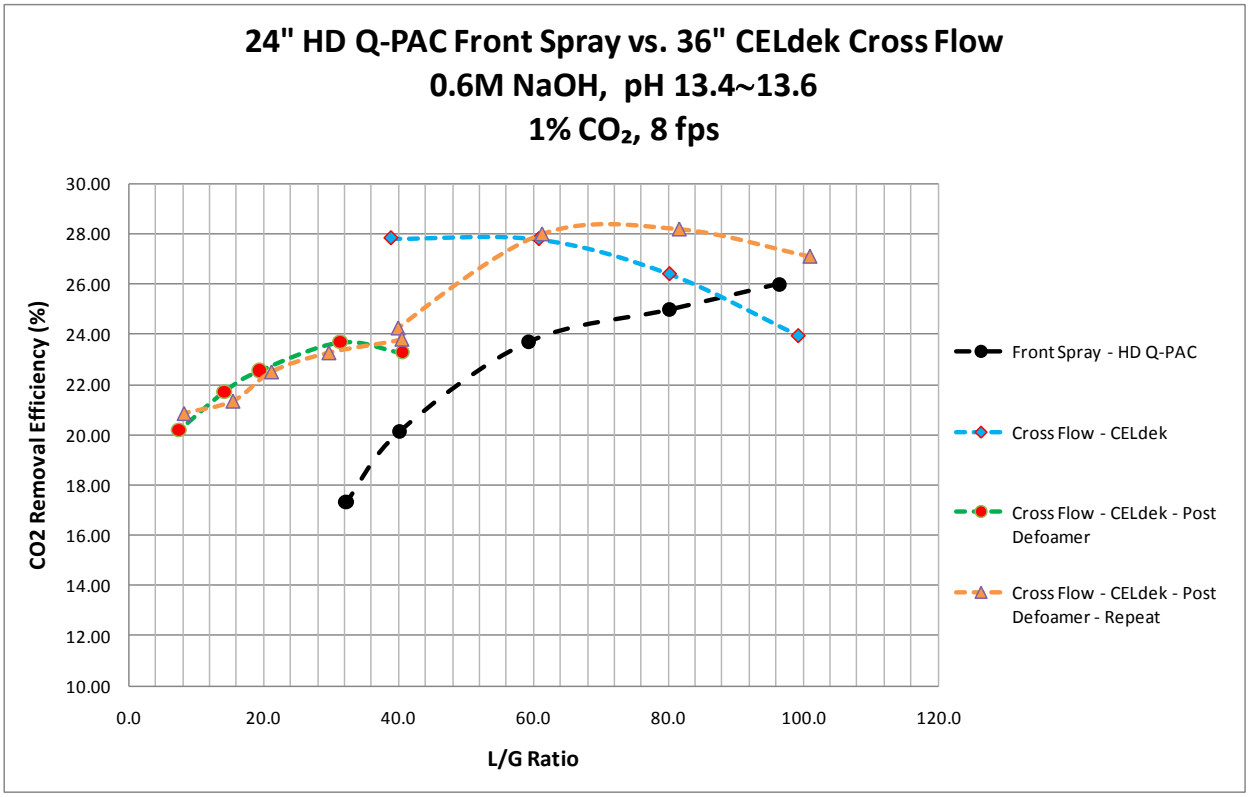

Figure 29: Relative Scrubbing Efficiency of 24" HD Q-PAC Front Spray vs. 36" CELdek Cross Flow.

The second important performance criterion is the ΔP across the contactor under the conditions of the testing. In Figure 30, a comparison of the pressure losses for the two contacting media and 8 fps gas flow velocity is shown for a range of L/G values. As can be seen from Figure 30, the HD Q-PAC, produces considerably higher pressure drop under simple scrubbing at high pH. Additionally, differences are also seen for scrubbing under lower pH conditions with enzyme as discussed below. Such a pressure drop difference becomes significantly more important should a series of contactors be employed for a higher overall system scrubbing efficiency.

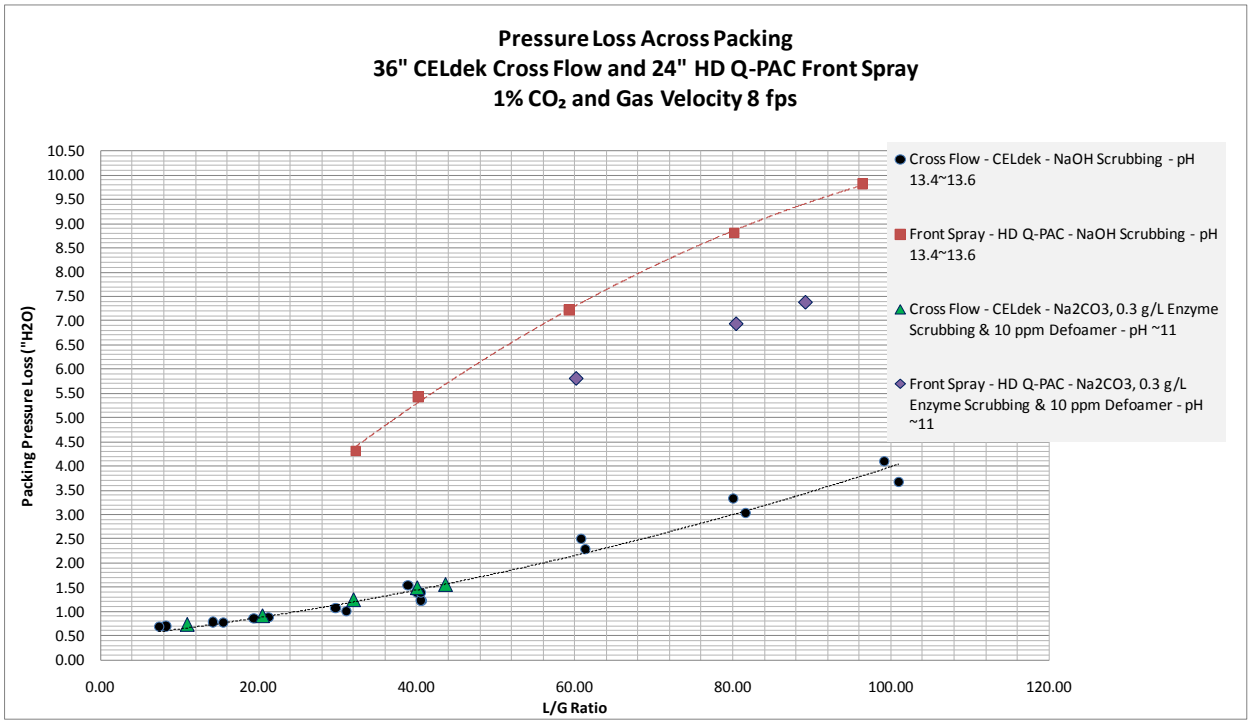

Figure 30: Comparison of Pressure Drop across CELdek and HD Q-PAC Contactors.

Figures 31 through 33 provide information on the performance of the CELdek contactor in the cross flow mode. In Figure 31, the scrubbing efficiency as a function of L/G ratio is shown for a range of CO_2 feed gas concentrations at high scrubbing fluid pH. For these experiments, the efficiency is higher for the lower CO_2 concentrations. For the runs after defoamer had been used in the system, some differences are observed, but no systematic effect on scrubber efficiency is apparent.

In Figure 32, the pressure drop across the CELdek contactor is shown for the same experimental conditions as in Figure 31. Over the range of L/G ratios studied, the pressure drop increases with increasing scrubbing fluid flow at a constant air velocity. The CO_2 content of the gas stream has little if any influence.

The plots in Figure 33 show the reduction in scrubbing efficiency in runs where the 0.6M sodium hydroxide solution is used to scrub gas streams varying from 8 to 1% CO_2 at L/G of 60. The plots follow very similar patterns, with perhaps the largest differences being with the initial scrubbing gas blend, where accurate pH measurements can be more difficult to obtain. The lower efficiency at L/G of 20 is consistent with the observations from Figure 31. The experimentally measured CO_2 removal efficiency using 0.3M sodium carbonate solution at L/G of 20 (light blue line in Figure 33) is comparable to that of sodium hydroxide solutions at pH in the range between 11 and 11.5.

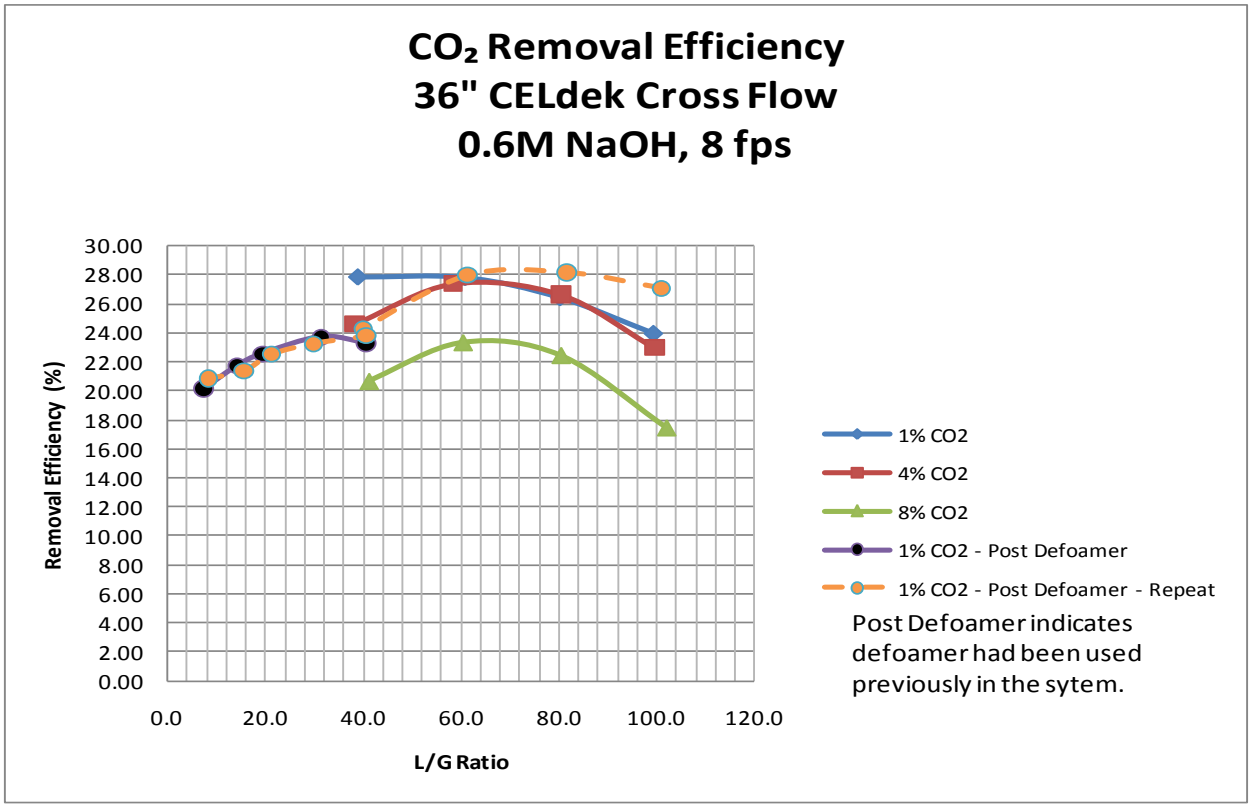

Figure 31: Scrubbing Efficiency of 36" CELdek Contactor in the Cross Flow Configuration.

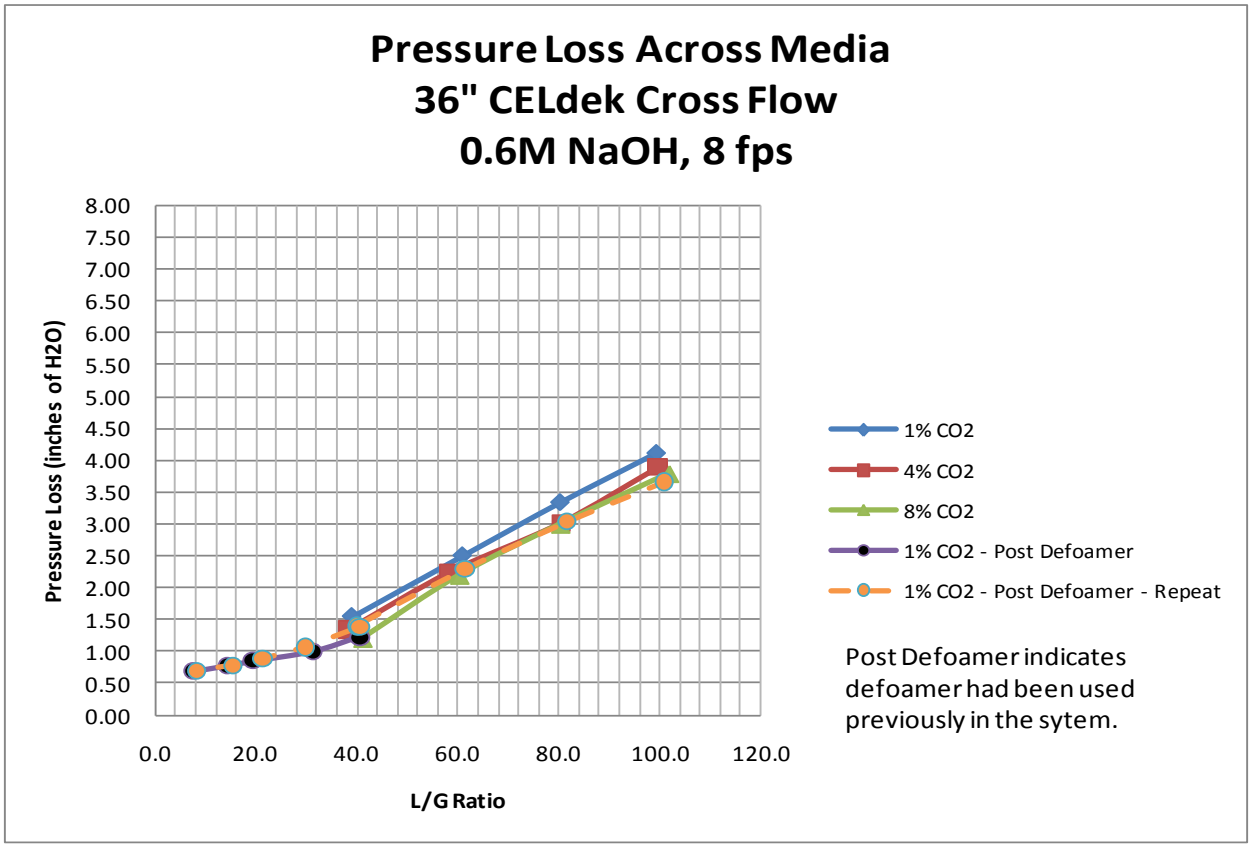

Figure 32: Influence of L/G Ratio and CO_2 Content on Pressure Loss Across CELdek Media.

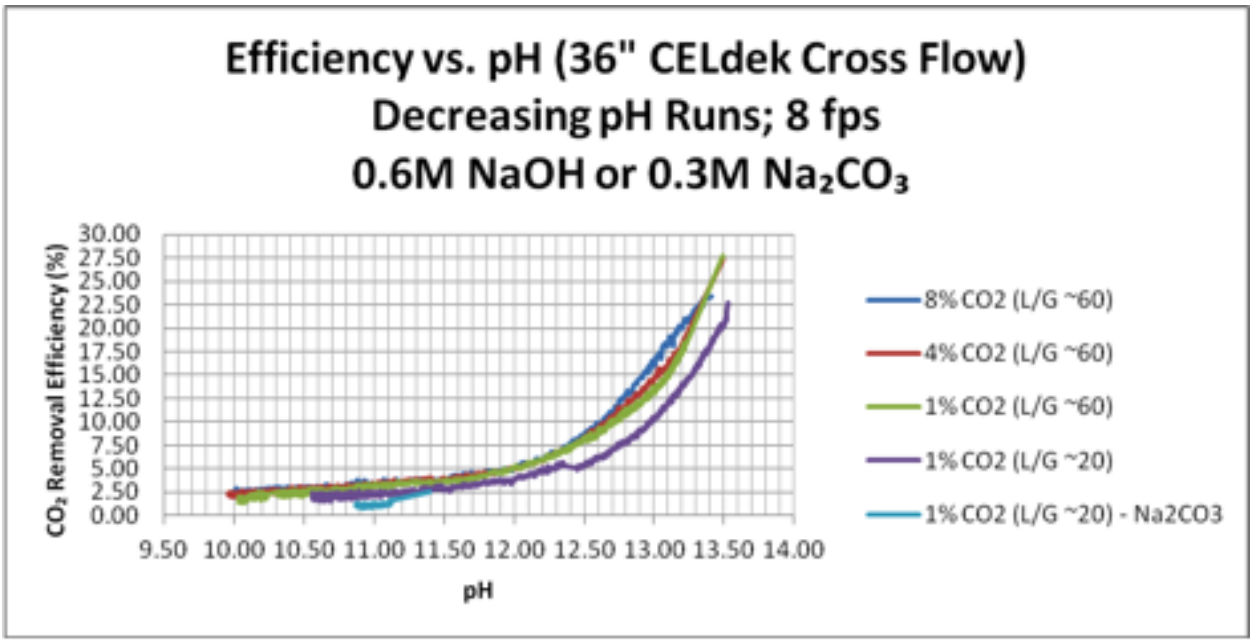

Figure 33: Efficiency of CELdek Cross Flow Scrubbing as a Function of pH.

3.0 Mineral sequestration via alkaline industrial waste carbonation

3.1 Investigation of bauxite residue

3.1.1 Temporal pH Behavior of Partially Neutralized Bauxite Residue Under Simulated Dry Stacking Conditions

All bench scale CO_2 sequestration testing to-date was performed using bauxite residue slurry and supernatant samples taken from the Alcoa Point Comfort alumina refinery, located on the Gulf Coast of Texas. These samples were taken on 2010-02-04 and 02-10 from the 6A washer underflow. This sampling location is the last point in the refinery washer circuit before bauxite residue is pumped to the impoundment lake. These bauxite slurry samples were composed of ~ 50% bauxite residue (dry weight) in water. The initial pH of these samples was pH = 13.

Residue slurry samples were prepared by stirring up slurries in the original 5-gallon shipping containers of thickener underflow samples taken at the Alcoa Pt. Comfort refinery on 2010-02-04 and 02-10. The 50 mL slurry aliquots (~ 75 g) were rapidly collected from the mixture and placed in 150 mL polyethylene bottles. These samples were then transferred to covered beakers for carbon sequestration capacity studies.

All time-dependent simulated blowdown exposure studies detailed in 2010 interim project reports were performed by mixing known volumes of bauxite residue slurry with known volumes of bicarbonate solution, then measuring the supernatant pH as a function of time, as shown in Figure 34. The temporal pH behavior shown in Figure 34 indicates that solution pH increases the first few days of mixing. After one week, however, no further pH change was observed over the duration of the 3-month test periods for any of the mixing ratios evaluated. This data demonstrates that by choosing appropriate mixing ratios, BR slurries could be partially neutralized and stabilized at pH $\leq$ 12, making the dried residue suitable for soil amendment applications and precluding pH-based (>12) hazardous material classifications. It is important to note, however that at no point were the supernatant and solids separated during the temporal pH study shown in Figure 34.

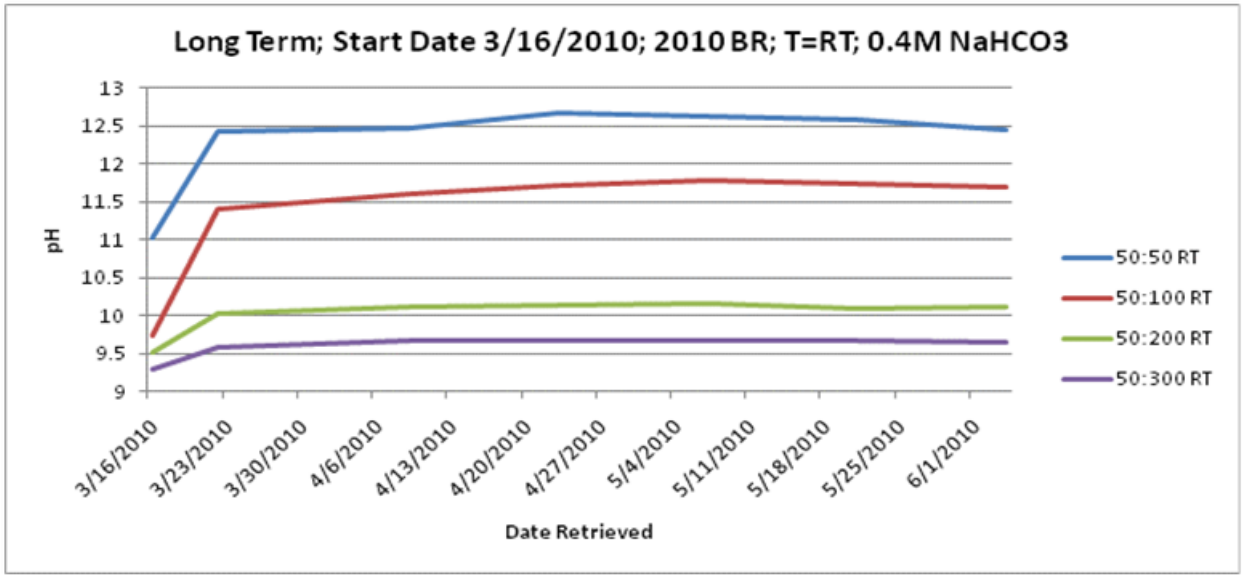

Figure 34: Long term, room temperature pH test of 50 ml BR slurry mixed with 50, 100, 200 and 300 ml of 0.4 M $NaHCO_3$.

At Alcoa refineries, a process known as dry-stacking was developed as a means of allowing more efficient storage of bauxite residue. In this process, bauxite residue slurry from the last stage thickener underflow is pumped to a storage area where the slurry is spread atop a cake of previously dried slurry. Underdrains from the residue storage area pump the supernatant that drains from the drying slurry to a holding pond for return to the refinery liquor circuit. In this process, sodium is reclaimed from the drying residue stack and recausticized for re-use in bauxite digestion.

Assuming that bauxite residue slurry was used for regeneration of carbonate and CO_2 sequestration by reaction with blowdown from a carbonate-based CO_2 scrubber, dry stacking of the residue from this process would effectively remove supernatant and temporal pH rebound would then be determined by residual pore water chemistry.

The test protocol listed in Table 1 was developed in order to evaluate the temporal pH rebound performance of bauxite residue if exposed to bicarbonate-based CO_2 scrubber blowdown under anticipated process conditions (50C) at varying mix ratios (ml residue slurry: ml 0.5 M bicarbonate).

Table 1: Temporal pH Rebound Protocol Under Simulated Dry Stacking Residue Storage.

Mix Time	Temp	Mix Ratio	Bicarb M	Carb M	Replicates	Supernatant separation
15 m	50	1,2,4	0.5	0	1	Vacuum Filter
30 m	50	1,2,4	0.5	0	1	Vacuum Filter
1 hr	50	1,2,4	0.5	0	1	Vacuum Filter
2 hr	50	1,2,4	0.5	0	1	Vacuum Filter
4 hr	50	1,2,4	0.5	0	1	Vacuum Filter
1 hr	50	1,2,4	0.3	0.1	0	Vacuum Filter
2 hr	50	1,2,4	0.3	0.1	0	Vacuum Filter

Where Temp = temperature, bicarb M= sodium bicarbonate molarity, carb= sodium carbonate molarity.

As listed in Table 1, 50 ml samples of bauxite residue slurry were mixed with 50, 100 or 200 ml 0.5 M bicarbonate or mixtures of 0.3 M $NaHCO_3$ and 0.1 M Na_2CO_3 for fixed periods of time, at 50C (typical refinery process temperature), then:

1) mixing is stopped,
2) solution pH are measured,
3) the slurry is vacuum filtered and
4) the filter cake is stored in a polyethylene bottle for future pH evaluation.
5) At later time intervals (1 week, 2 weeks, 1 month, 2 months and 3 months), 5 grams of residue cake is mixed with 20 ml of deionized water for 1 hour, then pH is measured.

Initial data from the test protocol described above are shown in Figure 35. Each of the 8 colored lines in Figure 35 represents pH data for either 1) the slurry pH at the end of specific mix times (as listed in Table 1), or the reconstituted residue slurry pH after one week (for a given initial mix time) as a function of initial mix ratio (ml residue slurry : ml 0.5 M $NaHCO_3$).

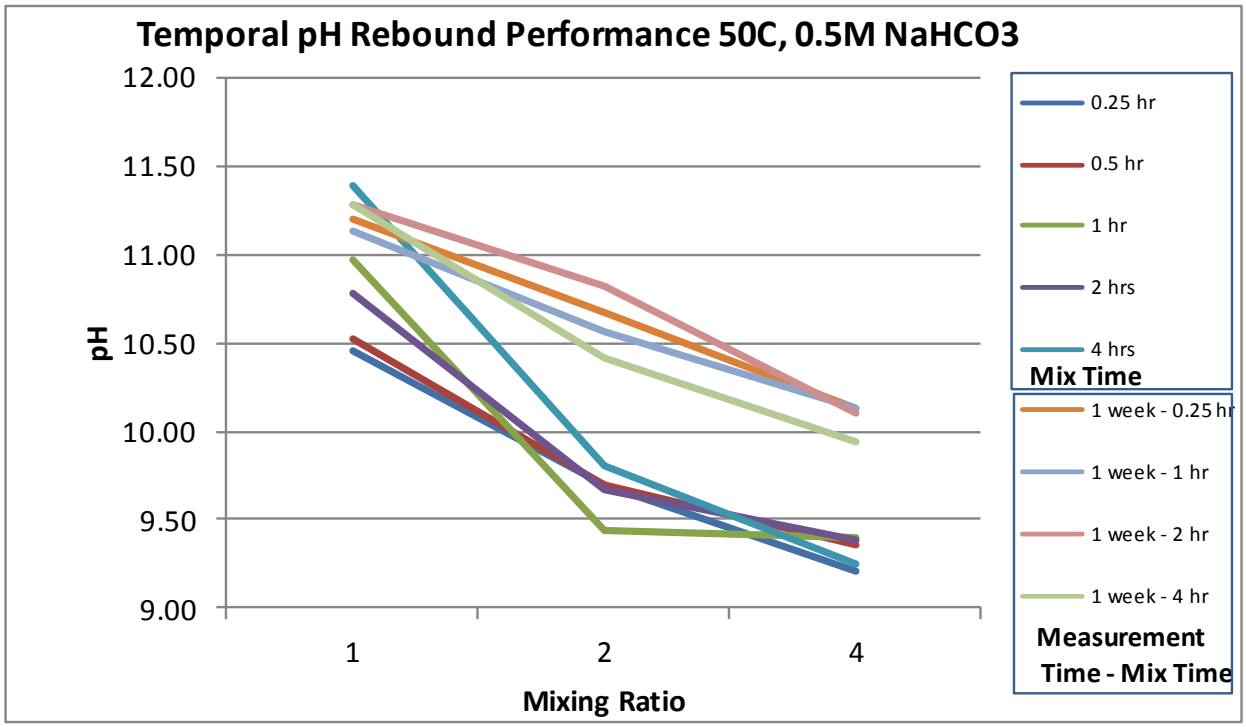

Figure 35: Initial data from long term, room temperature pH test of 50 ml BR slurry mixed with 50, 100, 200 and 300 ml of 0.5 M $NaHCO_3$.

The data shown in Figure 35 supports several initial observations regarding pH springback performance, as listed below.

1) The pH of the residue slurry (both initial and reconstituted) is reduced as mix ratio increases (high amount of bicarbonate to residue).
2) For any given mix ratio, the pH increases (springs back) as a function of time.

Observation #1 is supported by comparing pH data for an given line at different mix ratios (x-axis). Observation #2 is supported by comparing data at any given mix ratio. For example, the one week pH data is higher than the initial pH data at all mix ratios.

A representative subset of the longer term (up to 2 months) pH stability performance of the stored bauxite residue filter cake is shown in Figure 36. This data represents two distinct test populations, where the initial mix solution was either 0.5 M $NaHCO_3$ or a mixture of 0.3 M $NaHCO_3$ plus 0.1 M Na_2CO_3. While both of these mix solutions have the same total sodium value, the latter condition better simulates a blowdown solution from a carbonate-based CO_2 scrubber, where some of the bicarbonate has been converted to carbonate.

The pH stability data shown in Figure 36 evidence a gradual increase in pH over the 2-month test period, however the pH of all solutions remained below 12. It is interesting to note that the pH data segregates into 3 groups, which are delineated by the volumetric mix ratio (1:1, 1:2 and 1:4)

of the initial BR slurry to bicarbonate solution. The partial conversion of bicarbonate to carbonate did not accelerate pH springback over the test period.

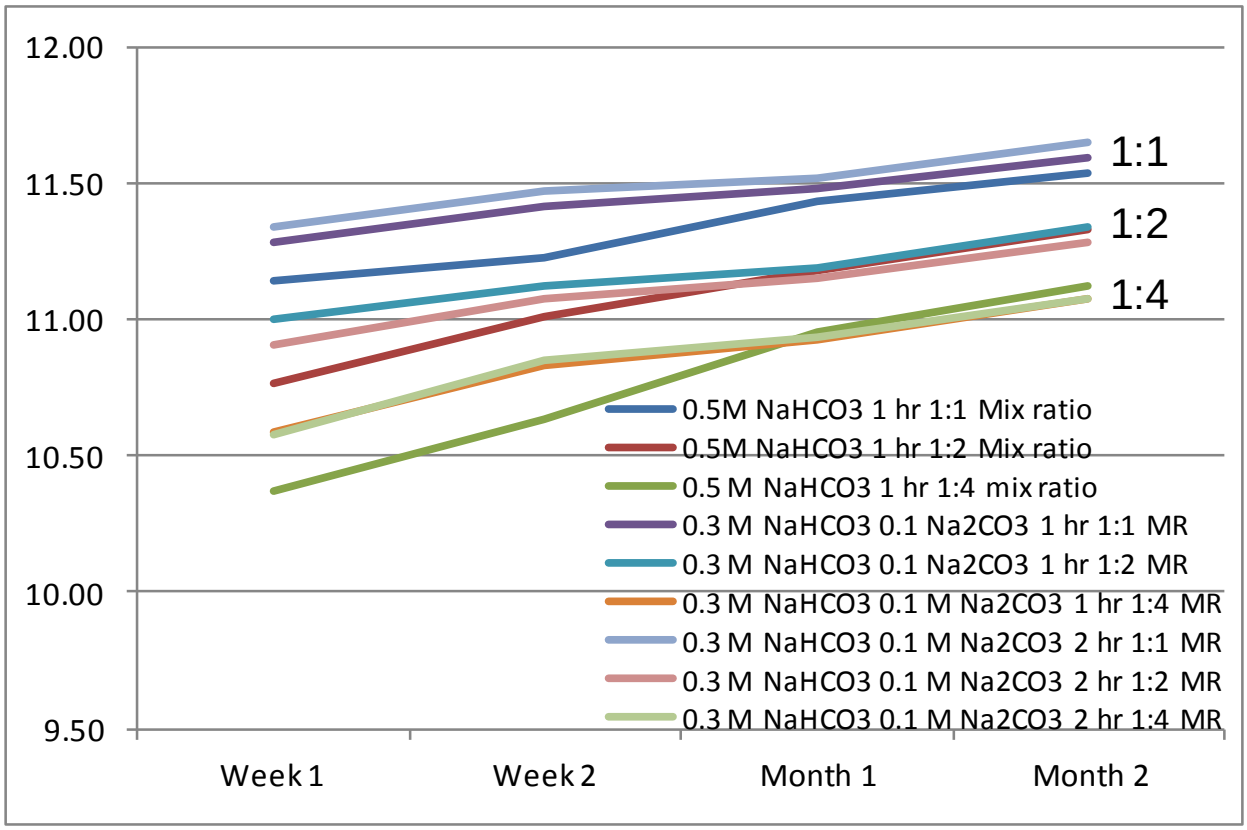

Figure 36: Intermediate term, pH stability data of stored BR solids after mixing with 50, 100, 200 and 300 ml of 0.5 M $NaHCO_3$, or a mixture of 0.3 M $NaHCO_3$ and 0.1 M Na_2CO_3.

As noted above, the primary objective of this temporal pH springback work is to understand residue pH behavior under conditions that more closely simulate expected plant conditions. Identification of a practical process for stabilizing bauxite residue at pH $\leq$ 12 would facilitate beneficial reuse by enabling transportation of partially neutralized residue under a non-hazardous material classification.

3.1.2 Impact of Bauxite Residue on CA Activity

The stability of CA enzyme upon exposure to bauxite residue was evaluated by mixing 25 mL of ca. 0.3 g/L solution of CA in 0.3 M $NaHCO_3$ with varying amounts of BR supernatant. The enzyme activity was measured using the Wibur-Anderson assay at 0 time (immediately after mixing) and 6 hrs after mixing. Experimental results are presented in Figure 37. As can be seen from Figure 37, activity of CA enzyme decreases with increasing mixing ratio of BR supernatant. At mixing ratio of 50% (25 mL of CA solution + 25mL of supernatant) and 6 hrs of contact time, enzyme activity was reduced by ~75%. This observation suggests that enzyme recovery from a bauxite residue slurry-based sequestration reactor may significantly reduce enzyme utilization lifetime, owing to impurities releases by sequestration agents. Additional

work will be required to identify the root causes negatively impacting CA and devise countermeasures for enabling practical recovery and activity conservation of CA from the sequestion reactor. Additionally, regardless of enzyme performance, there was no method as yet idenfified to prevent contaminants in the bauxite residue from entering and fouling the CO_2 absorbent solution in the scrubber, an inherent process design challenge when considering CO_2 sequestration in bauxite residue slurry.

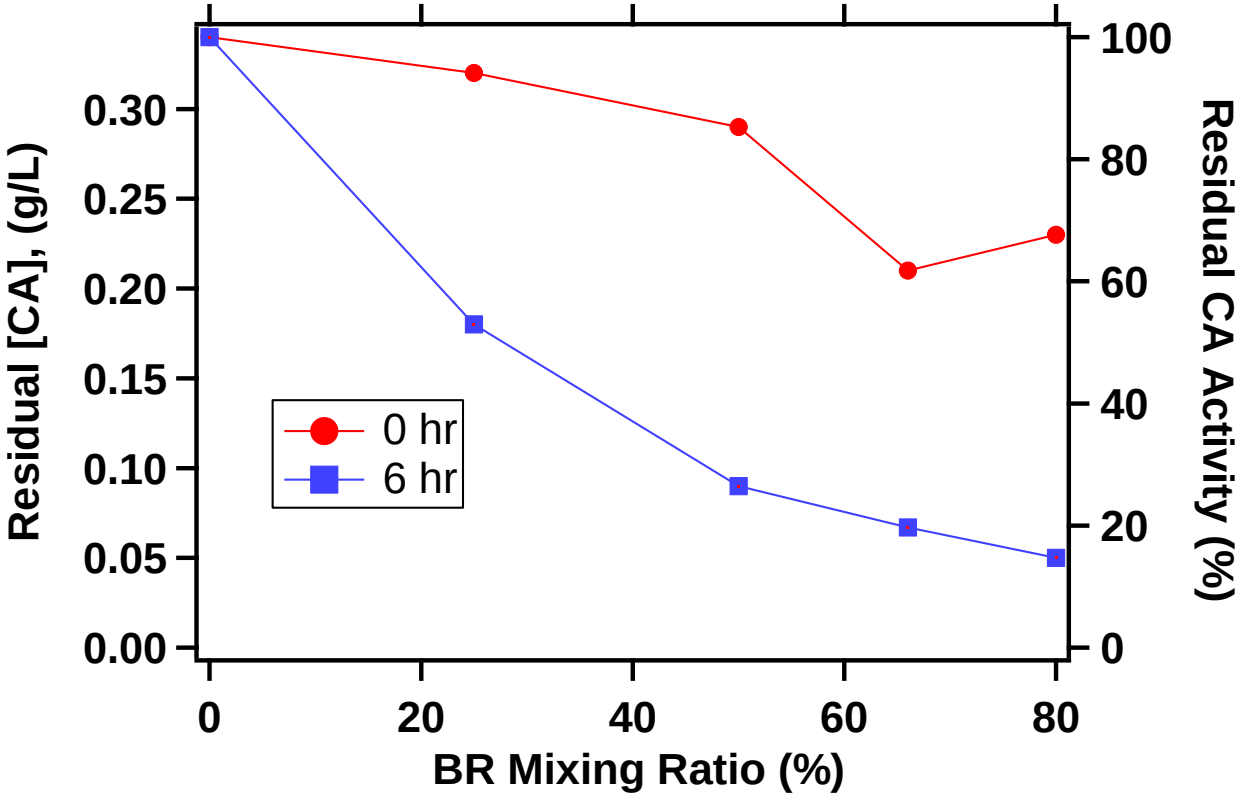

Figure 37: Residual CA activity (Wilbur-Anderson assay) as a function of mixing ratio with bauxite residue immediately after (red curve) and 6 hrs upon mixing.

3.2 Investigation of alternative alkaline industrial wastes as sequestration agents

Thirty-one alkaline wastes representing a wide range of industrial processes were acquired and screened for potential application in an aqueous carbon sequestration process. The wastes were evaluated for their potential to leach carbonate reactive cations, especially Ca^{2+}, and base species. Based on observed reactivity, measured chemical compositions, and estimated carbon sequestration capacities, a subset of samples was chosen for more in-depth analysis. Samples were mixed with a model aqueous carbon dioxide scrubber blowdown and the slurry pH was monitored. After mixing, supernatant samples were titrated to determine alkalinity and solid phases were examined for mineral phase and total carbon. These measured data were used to develop a geochemical equilibrium model to determine the mineral phases and aqueous reactions responsible for the observed behavior. Experimental results indicate that the best performing

samples are capable of sequestering between 2.30 - 2.93 mol CO_2 / kg dry solid. These samples were cement kiln dust, spray drier absorber ash, and circulating dry scrubber ash. Modeling of the supernatant solutions indicated that precipitation of carbonate solids may be inhibited by high levels of complexation. Equilibrium modeling of reaction mechanisms was inconclusive based on the current data set. However, the equilibrium modeling approach allowed for assessment of the validity of experimental results, particularly XRD data.

3.2.1 Introduction

The sequestration of carbon dioxide (CO_2) captured in aqueous scrubber solutions can be achieved by precipitation of stable carbonate minerals which can then be land filled. Alkaline industrial wastes are potential sources of carbonate reactive cations that can react with aqueous carbonate and precipitate carbonate minerals. In addition to the carbon sequestration achieved, this process repurposes abundant and potentially hazardous industrial wastes.

Interest in aqueous mineral carbonation as a large scale option for carbon sequestration arose from observations of natural silicate weathering and abundance of thermodynamically suitable raw materials (Seifritz, 1990). However, carbonation of calcium and magnesium silicate ores require high pressure and temperature to overcome slow CO_2 hydration and mineral dissolution kinetics. This involves relatively high energy expenditure as well as mining of raw materials (Gerdemann et al., 2007; Huijgen and Comans, 2004; Lackner et al., 1995).

Mined ores can be replaced by readily available alkaline industrial residuals as sources of carbonate-reactive calcium and magnesium with limited losses in sequestration efficiency (Fauth et al., 2002; Huijgen et al., 2006). Fly ash, fluidized bed combustion ash, iron/steel making slag, cement kiln dust, flue gas desulfurization spray dryer absorber ash, alumina refining waste (red mud), and waste concrete are some alkaline materials that have been studied with respect to carbonation reactions (Back et al., 2008; Dilmore et al., 2009; Fauth et al., 2002; Huijgen et al., 2005; Huntzinger et al., 2009; Iizuka et al., 2004). However, these experiments have typically employed temperatures and CO_2 pressures similar to those used in studies of silicate carbonation.

This work examines the performance of a wide range of industrial residuals for use in a two-stage system, consisting of an aqueous CO_2 scrubber and separate mineral sequestration process, rather than a single-step process which has been most studied. Studies which have examined systems similar to that discussed herein typically have employed brines as the carbonate reactive cation source with limited work assessing the potential role for alkaline industrial wastes (Liu et al., 2005; Mirjafari et al., 2007; Rawlins, 2008).

The goal of this study was to investigate mechanisms and efficiencies of aqueous alkaline industrial residual reaction with a sodium carbonate solution approximating an aqueous CO_2 scrubber blowdown. This work sought to estimate the relative potential aqueous carbon sequestration capacities of various alkaline residual solids, estimate the reaction time necessary to reach short-term pseudo-equilibrium, estimate the alkalinity generating capacities of the test solids, and determine the underlying geochemical mechanisms of these responses.

3.2.2 Materials and methods

3.2.2.1 Industrial residuals

Materials investigated in this study were obtained based on reported mineral compositions and related prior work. Table 2 highlights some results of prior studies using alkaline industrial residuals to sequester CO_2. The outcome of many of these studies is reported as a sequestration capacity or efficiency. However, due to the variety of process configurations and experimental conditions, the literature lacks uniformity in reporting these estimates. Table 2 illustrates that sequestration capacity is not an intrinsic property of a material, but rather is highly process specific. As a result it becomes difficult to extrapolate lab scale results to assess large scale potential for CO_2 sequestration by this method.

Table 2: Reported literature values of sequestration capacity for various materials under a range of experimental conditions. BR is bauxite residue, FA is fly ash, and SS is steel slag.

Material	Reported capacity	mol CO_2/ kg dry solids	pCO_2 (atm)	Time	Reactor	Solids
BR1	8.5 mg CO_2/kg slurry	0.48	1	30 d	Batch	40% m
BR2	9.5 g CO_2/L slurry	0.13	6.8	30 min	Batch	36% v
FA1	0.23 kg CO_2/kg ash	5.23	0.2	4.5 hr	Flow	7% m
FA2	26 kg CO_2/ ton ash	0.59	29.6	2 hr	Batch	9% m
SS1	0.247 mg CO_2/g slag	5.61	0.15	72 hr	Flow	9% m
SS2	74% Carbonation	4.19	18.8	30 min	Batch	33% m

BR1: (Khaitan et al., 2009b) BR2: (Dilmore et al., 2009)
FA1: (Back et al., 2008) FA2: (Montes-Hernandez et al., 2008)
SS1: (Bonenfant et al., 2008) SS2: (Huijgen et al., 2005)

For this study, thirty-one samples representing several distinct industrial operations were acquired. The test samples included: fly ash (FA), spray dyer absorber ash (SDA), circulating dry scrubber ash (CDS), cement kiln dust (CKD), blast furnace slag (BFS), basic oxygen furnace slag (BOFS), electric arc furnace dust (EAFD), and wet flue gas desulfurization gypsum (GYP). Additionally, two benchmark samples that were previously studied - fly ash and spray drier absorber ash - were obtained from the National Energy Technology Laboratory (NETL) of the U.S. Department of Energy, courtesy of Dr. Yee Soong (Dilmore et al., 2009). Table 3 presents property and source information for the test samples, with more detailed material classifications where available. All SDA and CDS samples came from operations without fly ash pre-collection and thus represent a blend of combustion fly ash and desulfurization solids.

Table 3: Matrix of samples acquired for study.

Sample ID	Sample type	Boiler type	Fuel Type
FAL1	FA	Pulverized coal (PC)	Lignite
FAL2	FA	Cyclone	Lignite
FAL3	FA	PC	Lignite
FAL4	FA	Cyclone	Lignite
FALG	FA	Gassifier	Lignite
FALST1	FA	Spreader stoker	Lignite
FALFB2	FA	FB	Lignite
FAS1	FA	Cyclone	Subbituminous
FAS2	FA	PC	Subbituminous
FAS3	FA	PC	Subbituminous
FAS4	FA	PC	Subbituminous
DOEFA	FA		
FABS	FA	PC	S/B Blend
FALSD1	SDA	PC	Lignite
FALSD3	SDA	Cyclone	Lignite
FASSD1	SDA	PC	Subbituminous
FASSD2	SDA	PC	Subbituminous
FASSD3	SDA	PC	Subbituminous
FASSD4	SDA	PC	Subbituminous
DOESDA	SDA		
FABSD	SDA		Bituminous
CDOR1	CDS	Industrial	
CDB	CDS		Bituminous
CKD1	CKD	N/A	N/A
CKD2	CKD	N/A	N/A
CKD3	CKD	N/A	N/A
BOF1	BOFS	N/A	N/A
BFS1	BFS	N/A	N/A
EAF1	EAFD	N/A	N/A
EAF2	EAFD	N/A	N/A
GYP1	GYP		

3.2.2.2 Preliminary solid composition characterization

3.2.2.2.1 Elemental analysis by X-ray fluorescence

The bulk chemical composition of all samples, reported as percent oxides, was determined using x-ray fluorescence (XRF) spectrometry. Solids were analyzed for aluminum, barium, calcium, chloride, chromium, iron, magnesium, phosphorus, potassium, silicon, sodium, strontium, sulfur, titanium, and zinc. Two XRF techniques (fused pellet and pressed pellet) were employed for the analyses of the samples. ASTM D4326-04 and ASTM D3174 were used for the fused and pressed pellet techniques respectively (ASTM, 2004a; ASTM, 2011).

Fused pellet samples were analyzed on a Philips AXS, wavelength dispersive XRF spectrometer. Each sample report was from a single-run analysis. The instrument is used to determine elemental constituents above 10 ppm (0.001%) and will quantitate concentration levels to better than ±5% of the amount present, provided appropriate standards are available. Analysis of pressed pellet samples was performed using a Rigaku ZSX Primus II wavelength x-ray spectrometer with a detection limit of 0.001%.

3.2.2.2.2 Moisture content and LOI

The moisture content and loss on ignition (LOI) is determined on the samples separate from the XRF analyses (ASTM, 2004b). The study results are reported with the LOI value added to the XRF results and renormalized to 100% as in Equation 3.1 where x_i represents the mass fraction of element i.

$$x_{i,total} = \frac{x_{i,XRF}}{\sum_{i=1}^{n} x_{i,XRF} + LOI} \quad (3.1)$$

3.2.2.3 Screening tests for selection of most promising solids

To focus detailed testing and analysis on the best performing samples, preliminary screening tests, consisting of leach tests in distilled water and a sodium biocarbonate solution, were conducted on the entire suite of solids.

Prior to testing, the samples were ground, if necessary, so that 80% of the sample mass passed through a 1mm screen. Twenty grams of sample were mixed with 120 mL of 0.5 M $NaHCO_3$ solution for 24 hours (in duplicate). The sodium bicarbonate solution was prepared using distilled water which had not been purged with nitrogen gas. Similar tests were conducted with distilled water (specific conductivity < 20 μmhos/cm) as the extraction agent.

Calibration of pH meters was performed using standard buffer solutions at pH 7, pH 10, and pH 12. Measurements of pH were taken of the stirred slurry after 15 seconds, 5 minutes, 1 hour, 2 hours, 4 hours, 7 hours, and 24 hours. After 24 hours of contact, the slurry was allowed to briefly settle; the supernatant was decanted, centrifuged, and then filtered at 0.45 μm; finally 5 grams of the filtrate was titrated to endpoints of pH 8.3 and 4.5 with 1.0 N HCl to determine alkalinity. Each test sample, two in bicarbonate solution and one in water, was titrated in duplicate for a total of six titrations.
Based on reactivity and apparent sequestration capacity, the best performing solids were selected for more detailed investigation. Additionally, at least one sample from each material class was

retained to maintain a broad sample matrix while samples with similar observed behavior within a sample class were excluded to avoid redundancy. In total, 13 of the 31 samples were selected for additional testing.

3.2.2.4 Alkalinity leaching and carbonate precipitation tests

Testing on the narrowed set of samples was performed in the same manner as the screening tests: stirred batch leaching tests with two leach solutions. However, the leach test in distilled water was conducted for only one hour, and the tests in 0.5 M $NaHCO_3$ were conducted for one and four hours. As before, pH was measured and the slurry was separated at the end of the test period with a filtered supernatant sample titrated to determine alkalinity. Supernatants and solids were reserved for further analysis with the solids being dried at 42 - 48 ˚C.

3.2.2.5 Solution chemistry analysis

Supernatant samples were analyzed by inductively coupled plasma-atomic emission spectroscopy (ICP-AES) for (detection limits in parenthesis) Al (2 mg/L), B (2 mg/L), Ca (1.5 mg/L), Fe (0.2 mg/L), Mg (0.2 mg/L), K (5 mg/L), Si (2 mg/L), Na (1 mg/L), S (2 mg/L) and by ion chromatography (IC) for Br^- (0.01 mg/L), Cl^- (0.01 mg/L), CO_3^{2-} (1 mg/L), F^- (0.01 mg/L), NO_3^- (0.01 mg/L), NO_2^- (0.01 mg/L), PO_4^{3-} (0.01 mg/L), SO_4^{2-} (1 mg/L).

3.2.2.6 Solids analysis

Pretest solids and post-test solids from the 4 hr bicarbonate leach test were analyzed for total carbon and for mineral phases. X-ray diffraction (XRD) was used for mineral identification and was performed on a Bruker AXS D8 Advance XRD system. A CHN analyzer was used to determine the total carbon in the as-received samples and the dried samples following the 4-hr bicarbonate screening test. The analyses were performed on a CE 440 Elemental Analyzer modified and sold by Exeter Analytical. It is a modified CHN instrument based on a Perkin-Elmer platform. Total carbon in the as-received samples was also analyzed using a LECO Total Carbon Analyzer for comparison, however post-test solids were not evaluated by this method.

3.2.2.7 Sequestration capacity calculations

Sequestration capacity was estimated using two approaches: (1) alkalinity measured by acid titration, and (2) changes in total carbon measured by CHN analysis. The alkalinity based approach allowed for estimation of sequestration capacity for all 31 test solids and aided in the selection of the samples for more detailed analysis. Comparisons of the total carbon measurements on solids before and after reaction allowed direct assessment of the precipitate sequestration of carbonate in the reactions.

Alkalinity in these systems was assumed to be carbonate dominated (Equation 3.2). A subscript, alk, has been applied to the carbonate species to indicate that these values include aqueous complexes, such as $CaCO_3^0$, which contribute to alkalinity but were not directly measured. Thus, aqueous carbonate speciation was calculated using the measured pH values, alkalinity, and carbonic acid dissociation constants (Equation 3.3). Carbon sequestration, occurring over a test period of time τ, was estimated by a mass balance on total dissolved carbon species (as estimated from titration data) in the system before and after reaction with 0.5 M $NaHCO_3$ (Equation 3.4).

Carbon sequestration capacities were calculated based on test conditions of 120 mL solution and 20 g of solid (Equation 3.5).

$$Alk = -[H^+] + [OH^-] + [HCO_3{}^-]_{alk} + 2 \cdot \left[CO_3{}^{2-}\right]_{alk} [=] \frac{eq}{L} \quad (3.2)$$

$$\left[CO_3{}^{2-}\right]_{alk} = K_{a2} \cdot [HCO_3{}^-]_{alk} \cdot [H^+]^{-1} [=] M \quad (3.3)$$

$$\Delta C_{alk} = \sum[C]_{t=0} - \sum[C]_{t=\tau} [=] M \quad (3.4)$$

$$\mathbb{C}_{alk} = \Delta C_{alk} \cdot V_{test} \cdot m_{t=0}{}^{-1} [=] \frac{mol\ CO_2}{kg\ dry\ solid} \quad (3.5)$$

For the subset of samples receiving additional testing, a solid phase carbon mass balance, determined by CHN analysis before and after reaction with 0.5 M $NaHCO_3$, was used to estimate carbon sequestration. Changes in carbon content, reported as a percentage of total mass, were converted to changes in carbon mass based on the mass of the total sample before and after exposure to 0.5 M $NaHCO_3$ for time τ (Equation 3.6). The molecular weight of carbon, stoichiometry of CO_2, and the initial test sample mass were used to yield a sequestration capacity in the same units produced by the alkalinity estimation method (Equation 3.7).

$$\Delta C_{solid} = (\%C_{t=\tau} \cdot m_{t=\tau}) - (\%C_{t=0} \cdot m_{t=0}) [=] g\ C \quad (3.6)$$

$$\mathbb{C}_{solid} = \Delta C_{solid} \cdot MW_C{}^{-1} \cdot m_{t=0}{}^{-1} [=] \frac{mol\ CO_2}{kg\ dry\ solid} \quad (3.7)$$

3.2.2.8 Geochemical modeling

Chemical equilibrium modeling, performed using PHREEQC, followed methodologies set forth by Meima and Comans (1997) and Khaitan et al. (2009a) (Parkhurst and Appelo, 1999). Post reaction solution chemistries were evaluated to determine the speciation of ions and the critical aqueous interactions governing this speciation while suppressing solids precipitation (Meima and Comans, 1997). Supernatant data simulations also served to evaluate the benefits of using Pitzer equation corrections to ion activity in high ionic strength solutions. Given that the Pitzer database used by PHREEQC does not allow for inclusion of Si or Al, primary elemental components of many of the mineral phases of interest, it was deemed that the errors occurring by use of the standard database and Davies equation activity corrections could be tolerated. Ultimately, the standard database and Davies equation corrections proved comparable to the Pitzer equation corrections even in the higher ionic strength, 0.5 M $NaHCO_3$ leach test cases, validating the use of the more inclusive standard database.

Solid composition data (from XRF, XRD, and CHN measurements) were used to simulate the dissolution and precipitation reactions and assess which minerals and aqueous complexes may be governing solution compositions (Khaitan et al., 2009a; Meima and Comans, 1997); for the sequestration reactions simulated by sample reaction with 0.5 M $NaHCO_3$, only the 4 hour leach data was used as it was assumed to be closer to equilibrium. This was accomplished by converting solid composition to a total aqueous concentration based on experimental conditions (20 g solid in 120 mL of solution) for input into the equilibrium model (Khaitan et al., 2009a; Meima and Comans, 1997). Total carbon measurements, by CHN analysis, were used to represent the C(4) elemental concentration in PHREEQC under the preliminary the assumption

that all measured carbon was inorganic. Solution pH was fixed at the measured value in all cases.

Minerals detected by XRD were included in the model as dissolved solids capable of precipitating. However, many of the mineral phases detected in the test solids are not found in the thermodynamic database used by PHREEQC. To address this issue, an effort was made to enter into the database solubility relationships from the literature for all carbonate minerals that were detected by XRD as well as any other phase where a significant difference was observed between the pre- and post-test XRD analysis.

3.2.3 Results and discussion

3.2.3.1 Preliminary sample characterization

XRF and LOI analyses are summarized for each material class initially screened in Table 4. As expected, the materials obtained for this study generally contained a high fraction of calcium, which has been shown to be more effective than magnesium for sequestration reactions at ambient conditions (Back et al., 2011). For the entire sample population the average calcium composition was 27.3% with a maximum value of 45.1%. In general, the material classes with the highest content were the FGD ashes (SDA and CDS), the cement kiln dusts, and two of the iron/steel slag varietals (BFS/BOFS). Only the electric arc furnace dust samples had lower calcium content than anticipated.

Table 4: Mean (μ), standard deviation (σ), and detection frequency (*n*) of elemental compositions for material classes tested. Number in parentheses is number of samples within sample class obtained for this study. Mean and standard deviation are in units of weight percent. Values that were not reported or below the detection limit are marked BDL. Dashes represent incalculable standard deviation based on the sample size.

Analyte	CDS (2)			CKD (3)			EAFD (2)			FA (13)			FS (2)			GYP (1)			SDA (8)		
	μ	σ	*n*	μ	σ	*n*	μ	σ	*n*	μ	Σ	*n*	μ	σ	*n*	μ	σ	*n*	μ	σ	*n*
CaO	29.2	13.4	2	38.8	1.5	3	6.5	1.0	2	23.1	4.8	13	39.2	2.2	2	35.4	-	1	30.7	7.4	8
MgO	1.0	0.6	2	1.0	0.0	3	2.2	0.1	2	5.6	1.2	13	6.1	2.3	2	0.4	-	1	2.7	1.4	8
SiO_2	10.7	8.9	2	16.0	1.2	3	4.6	0.3	2	32.5	10.5	13	29.6	12.5	2	1.2	-	1	22.9	6.1	8
Al_2O_3	5.0	4.5	2	3.8	0.8	3	0.8	0.1	2	13.7	4.8	13	4.8	2.0	2	0.2	-	1	10.3	3.3	8
Fe_2O_3	2.7	2.0	2	1.8	0.0	3	35.3	1.4	2	6.1	2.0	13	9.9	9.1	2	0.3	-	1	4.3	0.6	8
TiO_2	0.3	0.2	2	0.2	0.0	3	0.2	0.1	2	0.8	0.4	13	0.3	0.0	2	BDL	-	0	0.6	0.2	8
P_2O_5	0.1	-	1	0.2	0.0	3	0.2	0.1	2	0.6	0.5	13	0.7	-	1	BDL	-	0	0.4	0.3	8
Na_2O	0.2	0.1	2	0.1	0.0	3	3.7	0.3	2	3.3	2.1	13	0.3	-	1	BDL	-	0	2.0	1.5	8
K_2O	1.0	-	1	1.6	1.3	3	1.0	0.2	2	1.1	1.1	13	0.5	-	1	BDL	-	0	0.6	0.3	8
SO_3	22.8	10.6	2	1.8	2.3	3	1.1	0.1	2	3.2	2.4	13	1.1	0.5	2	39.2	-	1	15.4	5.1	8
MnO	BDL	-	0	0.1	-	1	3.7	0.7	2	0.1	0.0	5	1.7	1.2	2	BDL	-	0	0.1	0.0	5
BaO	0.1	-	1	0.1	0.0	2	BDL	-	0	0.6	0.2	13	BDL	-	0	BDL	-	0	0.4	0.2	8
SrO	0.1	-	1	BDL	-	0	BDL	-	0	0.4	0.2	13	0.1	-	1	0.1	-	1	0.3	0.1	8
Unknown	14.1	2.2	2	6.7	1.1	3	32.2	0.8	2	8.9	6.0	6	6.6	4.8	2	20.8	-	1	8.6	4.2	4
Cl	0.9	0.7	2	BDL	-	0	2.5	0.1	2	BDL	-	0	BDL	-	0	BDL	-	0	1.2	0.9	2
Cr	BDL	-	0	BDL	-	0	0.3	0.0	2	BDL	-	0	0.2	-	1	BDL	-	0	BDL	-	0
Zn	BDL	-	0	BDL	-	0	3.9	0.0	2	BDL	-	0	BDL	-	0	BDL	-	0	BDL	-	0
LOI	12.7	5.5	2	27.8	6.0	3	2.3	1.1	2	4.8	8.6	13	0.2	0.1	2	2.3	-	1	4.9	2.7	8

High variation for many analytes within the fly ash materials were observed and can be attributed to two samples with compositions highly different from the other fly ashes: FALST1 from a spreader stoker boiler using lignitic coal and FALFB2 from a fluidized bed combustion (FBC) process using lignitic coal. The FBC ash might be expected to have a composition similar to that of the dry FGD materials, SDA and CDS, more than the fly ashes especially with regards to sulfates/sulfites in the mineralogy as a product of desulfurization (U.S.D.O.E., 2009).

3.2.3.2 Screening tests

The pH vs. time data provided information about the rates of leaching of base species from the solids. Asymptotical behavior of the pH vs. time data was observed for the solids, rapidly in most cases, and suggested pseudo-equilibrium had been reached in the system. Huntzinger et al. (2009) attributed plateauing of reaction extent during carbonation of cement kiln dusts to the coating of reactive surfaces by carbonate precipitates leading to slower, diffusion controlled reaction kinetics. The samples that most rapidly reach pseudo-equilibrium likely exhibited the most rapid short-term solids dissolution and could potentially require a shorter retention time for sequestration reactions.

Figure 38 presents the pH vs. time results for two cement kiln dusts in the two test solvents. Based on the pH vs. time profile, CKD1 would not be expected to serve as a suitable sequestrant as it appears to remain nearly inert in water. Within the applicable range, the increased ionic strength of the leach solution would increase mineral solubilities by decreasing ion activities (Stumm and Morgan, 1996); this effect likely explains why an increase in pH, corresponding to alkaline mineral dissolution, is observed during reaction with 0.5 M $NaHCO_3$ but not with distilled water. CKD2 reacts rapidly to reach high pH in both solvents indicating that in the 0.5 M $NaHCO_3$, enough base had been liberated to overcome the pH buffering of the leach solution. Since the goal of the sequestration process is to precipitate carbonates, this release of base is critical as it converts bicarbonate to carbonate and implies liberation of alkaline cations, which are expected to be chiefly calcium.

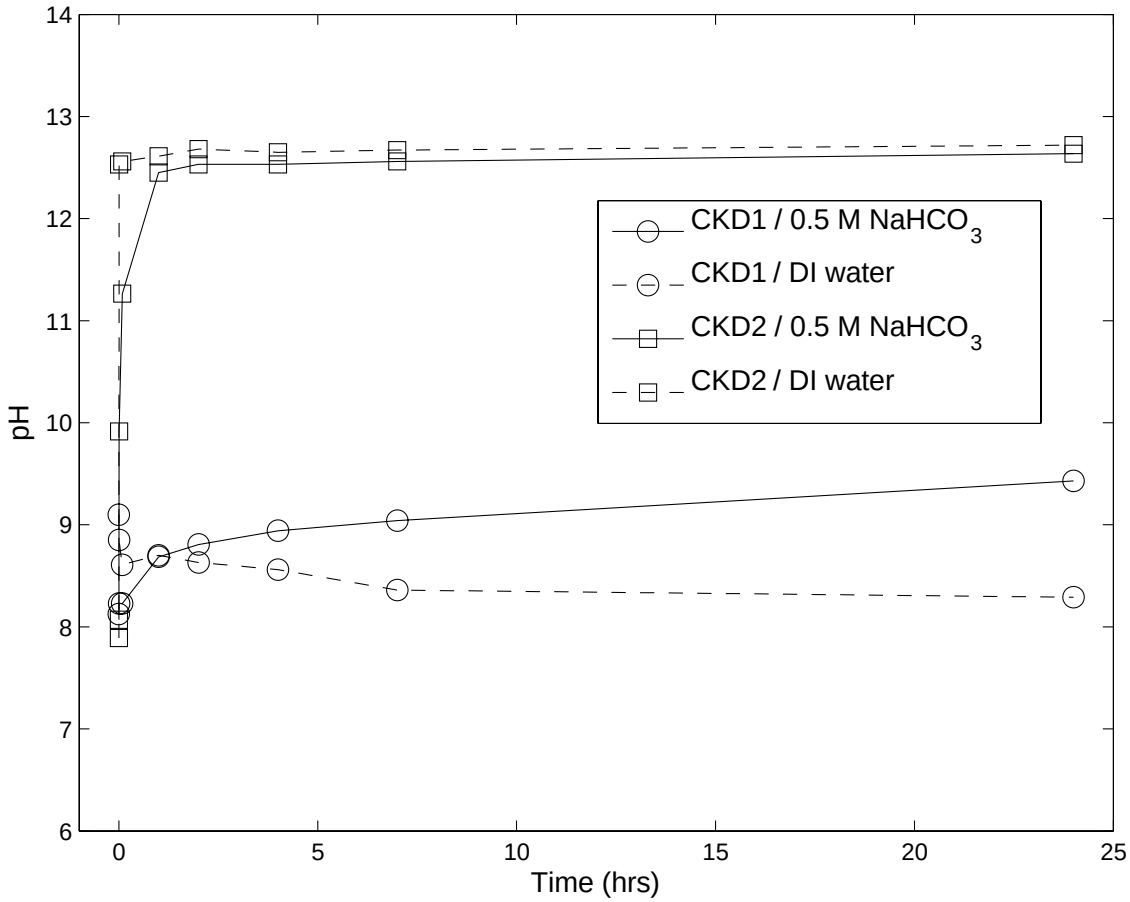

Figure 38: pH test results for two cement kiln dust samples in distilled water and bicarbonate solutions at 6:1 liquid to solid ratios. Values with 0.5 M $NaHCO_3$ as the extraction solution represent averages from duplicate tests. Lines are visual aids, not fitted curves.

Of the 31 samples included in this study, nine achieved 24 hr pH values greater than 10.3 during reaction with 0.5 M $NaHCO_3$ solution (Table 5). These represent the samples where at least 50% of the initial bicarbonate has been dissociated to carbonate and potentially precipitated. These samples were: BOF1, CKD2, CKD3, CDOR1, DOESDA, FALG, FALFB2, FALST1, and FASSD3. All material classes investigated except for EAFD are represented by these nine samples.

Table 5: Selected pH vs. time measurements for samples mixed with 0.5 M $NaHCO_3$. H+ activities were averaged from duplicate tests to yield pH values presented here.

Sample ID	Time of measurement (hrs)		
	1	4	24
FAL1	8.69	8.92	9.28
FASSD3	12.03	12.43	12.52
FALSD3	8.94	9.23	9.16
CKD1	8.67	8.94	9.43
EAF1	8.82	9.06	9.30
FAS2	9.14	9.39	9.70
FAL2	9.10	9.33	9.72
FAL4	8.62	8.89	9.22
BOF1	9.74	9.93	10.58
FAL3	8.61	8.97	9.35
BFS1	8.52	8.84	9.28
FALFB2	9.71	10.67	12.16
FALG	9.30	10.13	11.09
FALSD1	8.33	8.80	9.11
FALST1	9.60	10.11	12.73
EAF2	8.84	9.12	9.46
CKD3	10.01	10.34	12.57
FAS3	9.12	9.42	10.00
CDOR1	12.39	12.46	12.47
FASSD2	8.77	9.23	9.33
FAS4	8.92	9.20	9.60
CKD2	12.45	12.53	12.63
FASSD4	8.09	8.60	8.88
FASSD1	9.11	9.46	9.56
FAS1	9.06	9.40	10.21
DOEFA	9.27	9.53	9.90
GYP1	6.99	7.36	8.20
FABS	9.07	9.40	9.95
FABSD	8.07	8.50	8.51
CDB	8.18	8.54	8.48
DOESDA	13.07	13.12	13.27

Leach tests using 0.5 M $NaHCO_3$ as a model scrubber blowdown were used to simulate the use of the alkaline industrial residuals in a sequestration reactor. As previously described, alkalinity measurements were used as a proxy for dissolved inorganic carbon and used to estimate relative aqueous carbon sequestration capacity through mass balance calculations. Unlike the other results from leach testing, sequestration capacity shows clear trends within sample types as a function of pH. This is likely due to the similar mineral phase composition within the distinct sample types.

Figure 39 presents the estimation of sequestration capacity as a function of pH at 24 hrs for the 31 solids evaluated. The optimal solids for are found in the top right corner of the plot. Calculated sequestration capacity did not show consistent or significant trends as a function of any other measured variables, such as total solid calcium composition, of this test program.

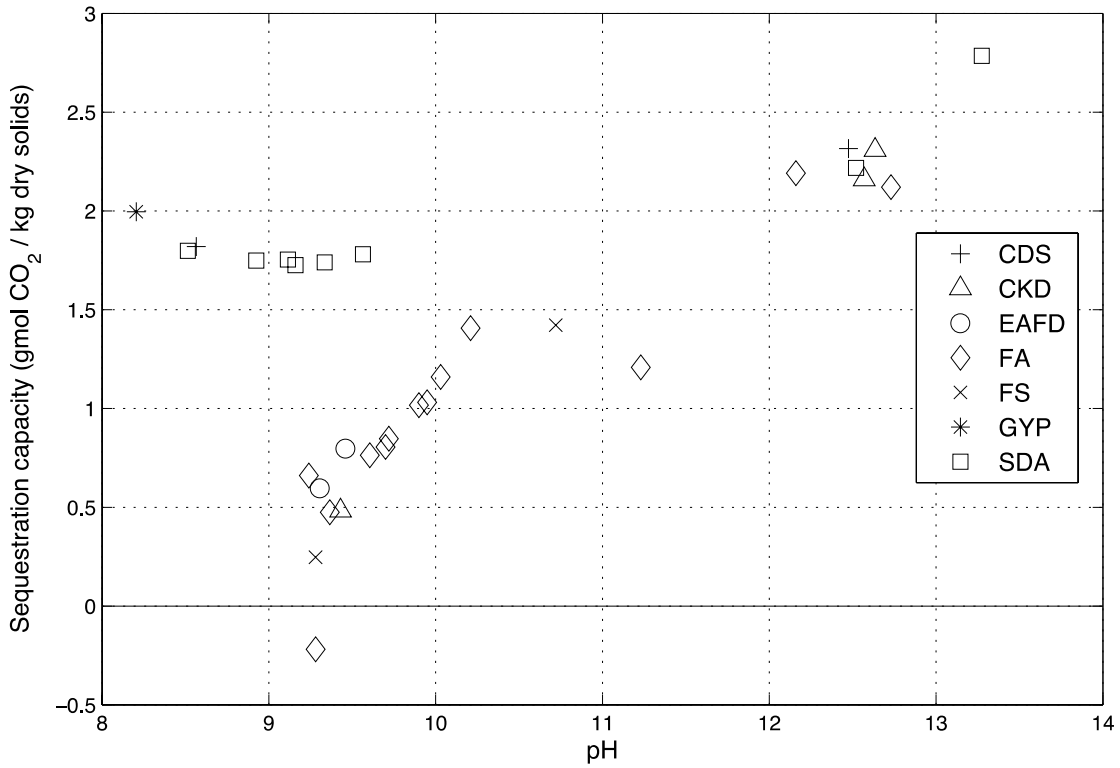

Figure 39: Apparent aqueous carbon sequestration capacity, calculated from alkalinity data, vs. final measured pH for 24 hour exposure of 20 g solids to 120 mL 0.5 M $NaHCO_3$.

To identify the subset of samples for detailed testing and modeling, consideration was given to identifying the most promising carbon sequestration candidates while also ensuring that samples from each of the material types were included, with highly similar samples being excluded to avoid redundancy. The 13 most promising candidates were selected based on carbonate reactive metal content, observed rates of reaction with the 0.5 M $NaHCO_3$, and apparent sequestration capacity calculated from alkalinity titration data. The subset of samples included: BOF1, CDB, CDOR1, CKD2, DOESDA, EAF1, FABS, FABSD, FALFB2, FALG, FAS1, FAS4, and FASSD3.

3.2.3.3 Detailed Tests: Alkalinity leaching and carbonate precipitation tests

More detailed testing was performed to characterize and quantify the reactive behavior of selected solids when mixed with both distilled water and 0.5 M $NaHCO_3$. This was accomplished by the analysis of solution and solid phase chemistries outlined earlier. Tables 6-8 present solution chemistry data (ICP-AES, IC, pH, and alkalinity) for the 4 hour distilled water leach test, 1 hour 0.5 M $NaHCO_3$ leach test, and the 4 hour 0.5 M $NaHCO_3$ leach test respectively. The solid phase chemistry results for these tests are provided in Table 9 (semi-quantitative XRD results for the solids before leach testing), Table 10 (XRD results for mineralogy of the samples after 4 hour reaction with 0.5 M $NaHCO_3$), and Table 11 (pre- and post-test total carbon results obtained by CHN analysis of test sample masses).

Table 6: Summary of solution chemistry for 4 hour DI water leach of select alkaline industrial wastes. BDL is "below detection limit" and varies depending on the element or compound; detection limit values can be found in the methods section.

		FALFB2	FALG	FAS4	FAS1	FASSD3	DOESDA	FABSD	CDOR1	CDB	EAF1	CKD2	BOF1	FABS
Total analytical concentration (M)	Al	4.1E-04	4.6E-02	2.4E-02	8.3E-02	2.5E-04	BDL	BDL	BDL	BDL	BDL	BDL	BDL	6.0E-03
	B	5.4E-04	1.3E-03	3.8E-04	4.3E-04	3.7E-04	4.8E-04	BDL	5.9E-04	3.0E-04	3.1E-04	3.5E-04	4.6E-04	BDL
	Ca	2.6E-02	1.2E-04	4.3E-03	5.3E-04	4.9E-02	4.7E-02	2.9E-02	5.7E-02	4.9E-02	1.0E-02	5.6E-02	2.9E-02	1.3E-03
	Fe	BDL	BDL	BDL	BDL	BDL	BDL	BDL	BDL	BDL	BDL	BDL	BDL	BDL
	Mg	BDL	BDL	BDL	BDL	BDL	BDL	BDL	BDL	BDL	BDL	BDL	BDL	BDL
	K	5.2E-03	3.4E-03	1.7E-04	4.6E-03	1.9E-03	1.4E-03	6.1E-04	1.5E-03	BDL	4.3E-02	4.6E-02	2.5E-04	5.6E-04
	Si	1.3E-04	3.6E-04	BDL	BDL	1.2E-04	BDL	BDL	1.2E-04	BDL	BDL	BDL	1.2E-04	BDL
	Na	1.1E-01	1.2E-01	5.9E-03	4.7E-02	3.8E-02	1.1E-02	1.8E-03	1.3E-02	9.6E-04	6.9E-02	1.4E-02	3.4E-03	1.3E-02
	S	4.3E-02	3.5E-02	1.0E-04	9.4E-04	2.7E-02	1.9E-02	9.5E-03	1.9E-02	1.8E-02	2.6E-02	2.1E-02	1.8E-03	2.0E-03
Total analytical concentration (M)	Br^-	1.7E-05	1.1E-04	BDL	BDL	BDL	5.0E-05	2.4E-04	1.5E-05	1.7E-04	6.1E-04	3.7E-05	BDL	8.3E-05
	Cl^-	7.2E-04	9.9E-04	1.3E-04	2.6E-04	3.8E-04	4.7E-03	4.4E-02	3.4E-03	3.2E-02	6.8E-02	6.6E-03	1.5E-04	1.3E-04
	CO_3^{2-}	2.7E-02	1.8E-02	3.5E-03	1.4E-02	2.0E-02	2.1E-02	5.3E-03	2.1E-02	1.4E-02	9.3E-03	2.6E-02	2.0E-02	5.1E-03
	F^-	1.5E-04	2.8E-04	1.9E-04	4.5E-04	5.6E-05	BDL	2.0E-04	3.7E-05	1.7E-04	4.2E-04	7.7E-05	BDL	6.5E-05
	NO_3^-	4.6E-05	BDL	BDL	7.4E-05	6.9E-03	BDL	1.6E-05	1.1E-04	1.7E-05	7.7E-05	BDL	BDL	BDL
	NO_2^-	BDL	BDL	BDL	BDL	1.7E-03	BDL	3.2E-05	5.1E-04	BDL	5.2E-05	BDL	2.1E-05	BDL
	PO_4^{3-}	BDL	BDL	BDL	BDL	BDL	BDL	BDL	BDL	BDL	BDL	BDL	BDL	BDL
	SO_4^{2-}	4.5E-02	3.6E-02	3.4E-05	6.8E-04	2.5E-02	2.0E-02	8.4E-03	1.7E-02	1.8E-02	2.7E-02	2.3E-02	3.4E-04	1.8E-03
pH		12.41	12.14	11.65	12.19	12.46	12.65	11.18	12.56	11.40	11.98	12.89	11.96	11.48
Alk. (eq/L)		0.250	0.233	0.227	0.234	0.239	0.240	0.214	0.240	0.234	0.225	0.245	0.241	0.224

Table 7: Summary of solution chemistry for 1 hour 0.5 M $NaHCO_3$ leach of select alkaline industrial wastes.

		FALFB2	FALG	FAS4	FAS1	FASSD3	DOESDA	FABSD	CDOR1	CDB	EAF1	CKD2	BOF1	FABS
Total analytical concentration (M)	Al	BDL	BDL	2.0E-04	1.4E-04	1.1E-04	BDL	BDL	3.0E-04	BDL	BDL	2.3E-03	7.4E-05	BDL
	B	5.8E-03	5.0E-03	2.0E-03	2.9E-03	7.8E-04	1.4E-03	1.0E-03	4.7E-04	9.2E-04	6.4E-04	6.5E-04	5.6E-04	2.7E-03
	Ca	7.0E-04	6.7E-04	4.4E-04	3.6E-04	2.0E-04	1.5E-02	4.9E-04	2.1E-02	5.1E-04	6.9E-04	3.8E-04	2.4E-04	4.7E-04
	Fe	BDL	5.4E-06	5.1E-05	1.3E-05	BDL	BDL	BDL	BDL	BDL	2.5E-05	BDL	2.1E-05	5.3E-05
	Mg	7.3E-03	4.8E-03	2.9E-03	1.4E-03	1.3E-04	BDL	BDL	BDL	1.1E-03	2.9E-03	BDL	1.4E-03	2.2E-03
	K	5.6E-03	2.5E-03	3.3E-04	4.3E-03	2.5E-03	2.6E-03	7.9E-04	1.9E-03	5.1E-04	3.8E-02	3.8E-02	5.9E-04	6.4E-04
	Si	3.2E-03	4.6E-03	4.6E-03	4.8E-03	1.5E-03	1.1E-04	2.6E-04	3.6E-04	2.7E-04	3.6E-03	2.7E-02	5.7E-03	2.7E-03
	Na	5.9E-01	5.9E-01	5.1E-01	5.5E-01	5.5E-01	5.1E-01	5.2E-01	5.4E-01	5.2E-01	5.7E-01	4.9E-01	5.0E-01	5.3E-01
	S	1.4E-01	2.9E-02	2.1E-02	7.9E-02	1.5E-01	1.6E-01	6.7E-02	2.4E-01	8.9E-02	2.4E-02	9.6E-02	4.6E-03	3.0E-02
Total analytical concentration (M)	Br^-	1.9E-05	1.3E-04	BDL	2.6E-05	BDL	5.0E-05	2.6E-04	2.4E-05	1.5E-04	5.3E-04	3.5E-05	BDL	1.4E-04
	Cl^-	7.6E-04	7.7E-04	1.5E-04	2.8E-04	4.1E-04	5.1E-03	3.2E-02	3.9E-03	3.3E-02	6.7E-02	6.9E-03	3.2E-04	1.6E-04
	CO_3^{2-}	6.6E-02	8.9E-02	9.4E-02	7.9E-02	5.1E-02	3.8E-02	7.1E-02	2.4E-02	6.4E-02	9.4E-02	5.0E-02	1.2E-01	8.8E-02
	F^-	4.2E-05	9.3E-05	4.1E-04	5.0E-04	1.3E-04	1.0E-04	3.6E-04	2.4E-05	2.3E-04	1.9E-03	7.8E-04	8.8E-05	1.6E-04
	NO_3^-	8.9E-05	BDL	2.2E-05	8.5E-05	6.2E-03	2.4E-05	2.3E-05	1.6E-04	2.0E-05	6.7E-05	BDL	BDL	BDL
	NO_2^-	BDL	BDL	1.9E-05	BDL	1.6E-03	BDL	4.7E-05	5.7E-04	BDL	BDL	BDL	BDL	BDL
	PO_4^{3-}	BDL	BDL	BDL	1.6E-03	BDL	BDL	BDL	BDL	BDL	BDL	BDL	BDL	1.4E-03
	SO_4^{2-}	1.6E-01	3.0E-02	2.2E-02	8.7E-02	1.4E-01	1.7E-01	5.7E-02	2.5E-01	7.9E-02	2.5E-02	1.0E-01	1.8E-03	2.9E-02
pH		10.00	9.51	8.96	9.20	10.25	12.56	7.98	12.44	8.14	8.94	12.78	9.66	9.15
Alk. (eq/L)		0.26	0.56	0.42	0.39	0.25	0.26	0.39	0.26	0.33	0.42	0.31	0.44	0.42

Table 8: Summary of solution chemistry for 4 hour 0.5 M $NaHCO_3$ leach of select alkaline industrial wastes.

		FALFB2	FALG	FAS4	FAS1	FASSD3	DOESDA	FABSD	CDOR1	CDB	EAF1	CKD2	BOF1	FABS
Total analytical concentration (M)	Al	9.7E-02	BDL	BDL	BDL	1.1E-01	BDL	BDL	3.6E-04	BDL	BDL	BDL	BDL	BDL
	B	8.9E-03	9.3E-03	2.5E-03	3.2E-03	1.8E-03	1.1E-03	1.4E-03	4.5E-04	1.2E-03	7.5E-04	6.9E-04	4.9E-04	2.8E-03
	Ca	4.5E-05	4.1E-04	5.4E-04	5.8E-04	8.0E-05	1.8E-02	4.0E-04	2.2E-02	3.8E-04	5.2E-04	1.1E-02	1.9E-04	3.7E-04
	Fe	BDL	BDL	8.6E-05	9.0E-06	9.8E-06	BDL	BDL	BDL	BDL	2.1E-05	BDL	1.8E-05	1.2E-04
	Mg	BDL	2.2E-03	1.5E-02	1.0E-02	BDL	BDL	2.1E-04	BDL	2.3E-04	3.6E-03	BDL	3.6E-03	7.4E-03
	K	5.0E-03	2.9E-03	5.6E-04	6.2E-03	2.6E-03	2.4E-03	7.9E-04	2.2E-03	6.4E-04	4.1E-02	4.3E-02	5.1E-04	6.6E-04
	Si	BDL	5.9E-03	2.5E-03	4.2E-03	1.8E-03	9.6E-05	BDL	4.6E-04	BDL	2.8E-03	2.4E-04	4.2E-03	7.1E-04
	Na	6.0E-01	6.0E-01	5.1E-01	5.5E-01	5.6E-01	5.2E-01	5.2E-01	5.4E-01	5.2E-01	5.9E-01	5.1E-01	5.3E-01	5.1E-01
	S	1.5E-01	3.2E-02	2.2E-02	8.1E-02	1.5E-01	1.9E-01	1.3E-01	2.5E-01	1.4E-01	2.9E-02	1.4E-01	4.7E-03	2.7E-02
Total analytical concentration (M)	Br^-	1.6E-05	1.1E-04	BDL	9.5E-05	BDL	5.4E-05	2.6E-04	3.7E-05	1.7E-04	5.7E-04	4.4E-05	BDL	8.4E-05
	Cl^-	8.4E-04	9.3E-04	1.4E-04	2.9E-04	4.5E-04	5.5E-03	4.9E-02	4.2E-03	3.8E-02	7.0E-02	7.6E-03	3.1E-04	1.8E-04
	CO_3^{2-}	5.6E-02	8.4E-02	9.2E-02	7.5E-02	4.4E-02	3.4E-02	5.0E-02	2.1E-02	4.9E-02	9.1E-02	3.7E-02	1.1E-01	8.8E-02
	F^-	3.2E-04	1.6E-04	3.1E-04	2.3E-04	7.8E-04	6.8E-05	5.3E-04	2.7E-05	3.0E-04	3.8E-03	2.6E-04	8.1E-05	1.7E-04
	NO_3^-	1.1E-04	BDL	BDL	1.2E-04	6.6E-03	2.4E-05	2.2E-05	1.8E-04	3.3E-05	8.9E-05	BDL	BDL	BDL
	NO_2^-	BDL	BDL	BDL	BDL	1.7E-03	BDL	2.8E-05	6.6E-04	4.3E-05	BDL	BDL	BDL	BDL
	PO_4^{3-}	BDL	BDL	BDL	BDL	BDL	BDL	BDL	BDL	BDL	BDL	BDL	BDL	1.1E-03
	SO_4^{2-}	1.7E-01	3.3E-02	2.2E-02	9.0E-02	1.4E-01	2.0E-01	1.2E-01	2.5E-01	1.4E-01	2.9E-02	1.5E-01	1.9E-03	2.9E-02
pH		10.70	9.92	9.26	9.57	12.47	12.54	8.48	12.32	8.50	9.23	12.79	9.90	9.32
Alk. (eq/L)		0.26	0.53	0.42	0.39	0.27	0.26	0.22	0.25	0.22	0.42	0.27	0.43	0.42

Table 9: As-received semi-quantitative XRD results. Values are approximate mass percentages that are not corrected for amorphous content.

Mineral name and formula		FALFB2	FALG	FAS4	FAS1	FASSD3	DOESDA	FABSD	CDOR1	CDB	EAF1	CKD2	BOF1	FABS
Akermanite, magnesian, syn	$Ca_2(Mg_{0.75}Al_{0.25})(Si_{1.75}Al_{0.25}O_7)$		13.1											
Anhydrite III, syn	$CaSO_4$			14.1	11.7			4.3	6.3				5.2	
Bassanite	$Ca(SO_4)\cdot 0.5H_2O$					16.7			10.3					
Bredigite	$Ca_{13.5}Ba_{.3}Mg_{1.8}Mn_{.4}Si_9O_{32}$		10.2											
Brownmillerite	$FeAlO_3(CaO)_2$							3						
Brownmillerite, ferrian, syn	$Ca_2((Fe_{0.741}Al_{1.259})O_5)$								4.5	2.5				
Buchwaldite, syn	$NaCaPO_4$												20	
Calcite, syn	$CaCO_3$		5			12.5	6.7		7.7			9.4		
Calcium Aluminum Oxide	$Ca_3Al_2O_6$	12.1		23	19.1		9.2	7		6		9	8.4	
Calcium Aluminum Oxide Sulfite Hydrate	$Ca_6Al_2O_6(SO_3)_3\cdot 32H_2O$												14.9	
Calcium Phosphate Hydrate	$Ca_2(P_4O_{12})\cdot 4H_2O$													
Calcium Silicate	Ca_2SiO_4													13.2

Table 9 cont.

Mineral name and formula		FALFB2	FALG	FAS4	FAS1	FASSD3	DOESDA	FABSD	CDOR1	CDB	EAF1	CKD2	BOF1	FABS
Calcium Sulfate	$CaSO_4$	12.4	1.7				9.4	7.1		6.1		9.2		
Copper Iron Phosphate	$Cu_2Fe_5(PO_4)_6$												11	
Ettringite	$Ca_6Al_2(SO_4)_3(OH)_{12}26H_2O$													
Franklinite, syn	$Zn_{1.1}Fe_{1.9}O_4$										34.7			
Gehlenite	$Ca_2Al_2SiO_7$			9.9	8.2								3.6	
Gehlenite, syn	$Ca_2Al(Al_{1.22}Si_{0.78}O_{6.78})(OH)_{0.22}$		8.5											
Gypsum	$Ca(SO_4)2H_2O$				9.3				5	2.9				10.5
Hannebachite, syn	$CaSO_3 \cdot 0.5H_2O$						10.4	31.6	11.7	13.6			12.8	
Hatrurite, syn	$Ca_3(SiO_4)O$						19.1	14.5				18.8		
Hauyne	$Na_6Ca_2(Al_6Si_6O_{24})(SO_4)_2$									2.7				
Hematite, syn	Fe_2O_3													4
Hematite	Fe_2O_3	1.3		2.4	2		1			0.6	1	1		
Heulandite	$Ca_{3.6}K_{0.8}Al_{8.8}Se_{27.4}O_{72} \cdot 26.1H_2O$									7.4				

Table 9 cont.

Mineral name and formula		FALFB2	FALG	FAS4	FAS1	FASSD3	DOESDA	FABSD	CDOR1	CDB	EAF1	CKD2	BOF1	FABS
Hydroxylapatite, syn	$Ca_{10}(PO_4)_6(OH)_2$													
Lime, syn	CaO	42.5					32.2		36.2	21		31.7		
Magnesioferrite	$Mg_{0.64}Fe_{2.36}O_4$										7.6			
Magnetite, syn	$Fe_{2.9}O_4$													
Mayenite, syn	$Ca_{12}Al_{14}O_{33}$		5.3		6.4				2.8					
Merwinite, syn	$Ca_3Mg(SiO_4)_2$	12.5	13.9	23.7	19.7			7.1	10.6			9.3	8.7	12.4
Monohydrocalcite, syn	$CaCO_3 \cdot H_2O$		8.2											
Mullite	$Al_{4.64}Si_{1.36}O_{9.68}$							5.6						
Natrite	$Na_2(CO_3)$									2.7				
Natrolite	$Na_2(Al_2Si_3O_{10}) \cdot 2H_2O$													
Periclase	MgO	3.6	4.6	10.7	8.8	5		2.1		1.8	4.2	2.7		
Portlandite, syn	$Ca(OH)_2$	5.8				38.8	4.4	6.5	4.9	5.6		4.3		4.4
Potassium alum, syn	$KAl(SO_4)_2 \cdot 12H_2O$													
Potassium Aluminum Sulfate	$K_2Al(SO_4)_3$													23.8
Potassium Carbonate	$K_2(CO_3)$				3.3					1				

Table 9 cont.

Mineral name and formula		FALFB2	FALG	FAS4	FAS1	FASSD3	DOESDA	FABSD	CDOR1	CDB	EAF1	CKD2	BOF1	FABS
Potassium Iron Oxide	$K_4(Fe_2O_5)$												4.5	
Quartz, low, syn	SiO_2	8.9	9.9	13.8	11.5	24.6	6.8	10.2		8.8	5.5	4	5.1	25
Rostite	$Al(SO_4)(OH)$ $\cdot 5H_2O$		19.5											
Rutile	TiO_2	0.9		2.4		2.4	0.7	1		0.9		0.6	0.9	
Silicon Oxide	SiO_2													6.6
Smithsonite	$Zn(CO_3)$													
Sodium Carbonate Hydrate	$Na_2(CO_3)$ $\cdot 10H_2O$									16.6				
Thaumasite	$Ca_3Si(OH)_6(SO_4)(CO_3)$ 12H2O													
Trona, syn	$Na_3H(CO_3)_2$ $\cdot 2H_2O$													
Zinc Iron Oxide	$Zn_{0.945}$ $Fe_{1.78}O_{3.71}$												4.9	
Zincite, syn	ZnO										47			

Table 10: Mineral phase content approximated by XRD analysis for solids after 4 hour reaction with 0.5 M $NaHCO_3$. Values are approximate mass percentages that are not corrected for amorphous content.

Mineral name and formula		FALFB2	FALG	FAS4	FAS1	FASSD3	DOESDA	FABSD	CDOR1	CDB	EAF1	CKD2	BOF1	FABS
Akermanite, magnesian, syn	$Ca_2(Mg_{0.75}Al_{0.25})(Si_{1.75}Al_{0.25}O_7)$		7.2											
Anhydrite III, syn	$CaSO_4$			8	6.8				4.7	2.2			3.7	
Bassanite	$Ca(SO_4)·0.5H_2O$								7.6	3.5				
Bredigite	$Ca_{13.5}Ba_{.3}Mg_{1.8}Mn_{.4}Si_9O_{32}$		5.6											
Brownmillerite	$FeAlO_3(CaO)_2$							2.5						
Brownmillerite, ferrian, syn	$Ca_2((Fe_{0.741}Al_{1.259})O_5)$								3.3	1.5				
Buchwaldite, syn	$NaCaPO_4$												8.3	
Calcite, syn	$CaCO_3$	12	2.7			62.5	4.6	39.7	5.7	24.7		7		
Calcium Aluminum Oxide	$Ca_3Al_2O_6$	8		13.1	11.1	8.9	6.1	5.7		3.5		6.7	6	
Calcium Aluminum Oxide Sulfite Hydrate	$Ca_6Al_2O_6(SO_3)_3·32H_2O$												10.6	
Calcium Phosphate Hydrate	$Ca_2(P_4O_{12})·4H_2O$													11

Table 10 cont.

Mineral name and formula		FALFB2	FALG	FAS4	FAS1	FASSD3	DOESDA	FABSD	CDOR1	CDB	EAF1	CKD2	BOF1	FABS
Calcium Silicate	Ca_2SiO_4													6.9
Calcium Sulfate	$CaSO_4$	8.2	1				6.3	5.8		3.6		6.9		
Copper Iron Phosphate	$Cu_2Fe_5(PO_4)_6$												7.8	
Ettringite	$Ca_6Al_2(SO_4)_3(OH)_{12}$ $\cdot 26H_2O$						11.6			6.6				
Franklinite, syn	$Zn_{1.1}Fe_{1.9}O_4$										33.9			
Gehlenite	$Ca_2Al_2SiO_7$			5.6	4.8								2.6	
Gehlenite, syn	$Ca_2Al(Al_{1.22}Si_{0.78}O_{6.78})(OH)_{0.22}$		4.6											
Gypsum	$Ca(SO_4)2H_2O$				5.4				3.7	1.7				5.4
Hannebachite, syn	$CaSO_3 \cdot 0.5H_2O$						7	6.4	8.6				6.8	
Hatrurite, syn	$Ca_3(SiO_4)O$						12.7					14		
Hauyne	Na_6Ca_2 $(Al_6Si_6O_{24})(SO_4)_2$									1.6				
Hematite, syn	Fe_2O_3													2.1
Hematite	Fe_2O_3	0.8		1.4	1.2		0.6	0.6		0.4	0.9	0.7	0.6	

Table 10 cont.

Mineral name and formula		FALFB2	FALG	FAS4	FAS1	FASSD3	DOESDA	FABSD	CDOR1	CDB	EAF1	CKD2	BOF1	FABS
Heulandite	$Ca_{3.6}K_{0.8}Al_{8.8}Se_{27.4}O_{72}\cdot 26.1H_2O$									4.3				
Hydroxylapatite, syn	$Ca_{10}(PO_4)_6(OH)_2$									6.5			11.1	
Lime, syn	CaO	28					21.5		26.7	12.3		23.7		
Magnesioferrite	$Mg_{0.64}Fe_{2.36}O_4$										7.4			
Magnetite, syn	$Fe_{2.9}O_4$												1.2	
Mayenite, syn	$Ca_{12}Al_{14}O_{33}$		2.9		3.7				2	1.6				
Merwinite, syn	$Ca_3Mg(SiO_4)_2$	8.2	7.6	13.5	11.5			5.8	7.8			6.9	6.2	6.5
Monohydrocalcite, syn	$CaCO_3\cdot H_2O$		4.5											
Mullite	$Al_{4.64}Si_{1.36}O_{9.68}$							8.6						
Natrite	$Na_2(CO_3)$		4.1	5.3	4.5					1.6	3.6	2.7		
Natrolite	$Na_2(Al_2Si_3O_{10})\cdot 2H_2O$					4.6				1.8				
Periclase	MgO	2.4	2.5		5.2	2.7				1.1		2	1.8	
Portlandite, syn	$Ca(OH)_2$	3.8				8.3	2.9	5.3	3.6	3.3		3.2		2.3
Potassium alum, syn	$KAl(SO_4)_2\cdot 12H_2O$													6.9

Table 10 cont.

Mineral name and formula		FALFB2	FALG	FAS4	FAS1	FASSD3	DOESDA	FABSD	CDOR1	CDB	EAF1	CKD2	BOF1	FABS
Potassium Aluminum Sulfate	$K_2Al(SO_4)_3$													12.3
Potassium Carbonate	$K_2(CO_3)$				1.9					0.6				
Potassium Iron Oxide	$K_4(Fe_2O_5)$												3.2	
Quartz, low, syn	SiO_2	5.9	5.5	7.9	6.7	13.1	4.5	8.3		5.2		3	3.6	13
Rostite	$Al(SO_4)(OH)·5H_2O$		10.7											
Rutile	TiO_2	0.6		1.4			0.4			0.5		0.5	0.6	
Silicon Dioxide	SiO_2													3.4
Smithsonite	$Zn(CO_3)$										8.4			
Sodium Carbonate Hydrate	$Na_2(CO_3)·10H_2O$	22.2	28.1	33.6	28.6		17		21.1	9.7		17.3	15.4	30.2
Thaumasite	$Ca_3Si(OH)_6(SO_4)(CO_3)·12H2O$							11.4						
Trona, syn	$Na_3H(CO_3)_2·2H_2O$		12.9	10.2	8.7		4.8		5.2	2.4		5.3	6.8	
Zinc Iron Oxide	$Zn_{0.945}Fe_{1.78}O_{3.71}$												3.5	
Zincite, syn	ZnO										45.8			

Table 11: Total carbon results for raw materials and 4 hr bicarbonate leach post test solids by CHN analysis and LECO Total Carbon analysis with mass differential.

Sample Group	Sample ID	Solid Sample	C fraction, % (CHN / LECO)	Sample mass, g
CDS	CDOR1	As-Received	1.0 / 1.0	20.00
		4-Hr Bicarbonate Post Test	4.2	21.43
	CDB	As-Received	16.2 / 17.0	20.00
		4-Hr Bicarbonate Post Test	18.5	18.65
CKD	CKD2	As-Received	1.8 / 1.6	20.00
		4-Hr Bicarbonate Post Test	4.4	23.63
EAFD	EAF1	As-Received	1.5 / 0.8	20.00
		4-Hr Bicarbonate Post Test	1.5	16.16
FA	FALFB2	As-Received	26.4 / 32.0	20.00
		4-Hr Bicarbonate Post Test	26.3	20.36
	FALG	As-Received	1.2 / 1.5	20.00
		4-Hr Bicarbonate Post Test	3.0	17.81
	FAS4	As-Received	0.2 / 0.2	20.00
		4-Hr Bicarbonate Post Test	1.0	19.68
	FAS1	As-Received	0.4 / 0.7	20.00
		4-Hr Bicarbonate Post Test	2.4	19.62
	FABS	As-Received	4.2 / 3.7	20.00
		4-Hr Bicarbonate Post Test	5.0	18.68
FS	BOF1	As-Received	0.4 / 0.2	20.00
		4-Hr Bicarbonate Post Test	1.4	19.15
SDA	FASSD3	As-Received	1.4 / 1.5	20.00
		4-Hr Bicarbonate Post Test	4.9	18.86
	DOESDA	As-Received	1.9 / 1.9	20.00
		4-Hr Bicarbonate Post Test	4.9	22.10
	FABSD	As-Received	7.7 / 7.6	20.00
		4-Hr Bicarbonate Post Test	9.5	18.20

3.2.3.3.1 Distilled water leach test solution chemistry

The test solids yielded significant amounts of calcium, as well as other alkaline cations such as sodium and potassium, upon exposure to distilled water. Somewhat surprising was the undetectable liberation of magnesium in all distilled water leach tests. The acid-base balance in a water sample is commonly calculated from the equivalent sum of strong acid tracer anions having negative equivalents in the sum and strong base tracer cations having positive equivalents in the sum (Stumm and Morgan, 1996); for these waters the strong acid tracers include Br^-, Cl^-, F^-, and SO_4^{2-} while the strong base tracers are Ca^{2+}, K^+, and Na^+. Figure 40 presents the relationship between pH and the acid-base balance equivalents in the distilled water leach tests; as expected a positive relationship was observed. This relationship confirms that significant amounts of the alkaline cations were both present and accessible by solution in an oxide or hydroxide form. However, as the correlation indicates, a linear relationship to the sum of these species does not fully explain the variance in pH of the solutions.

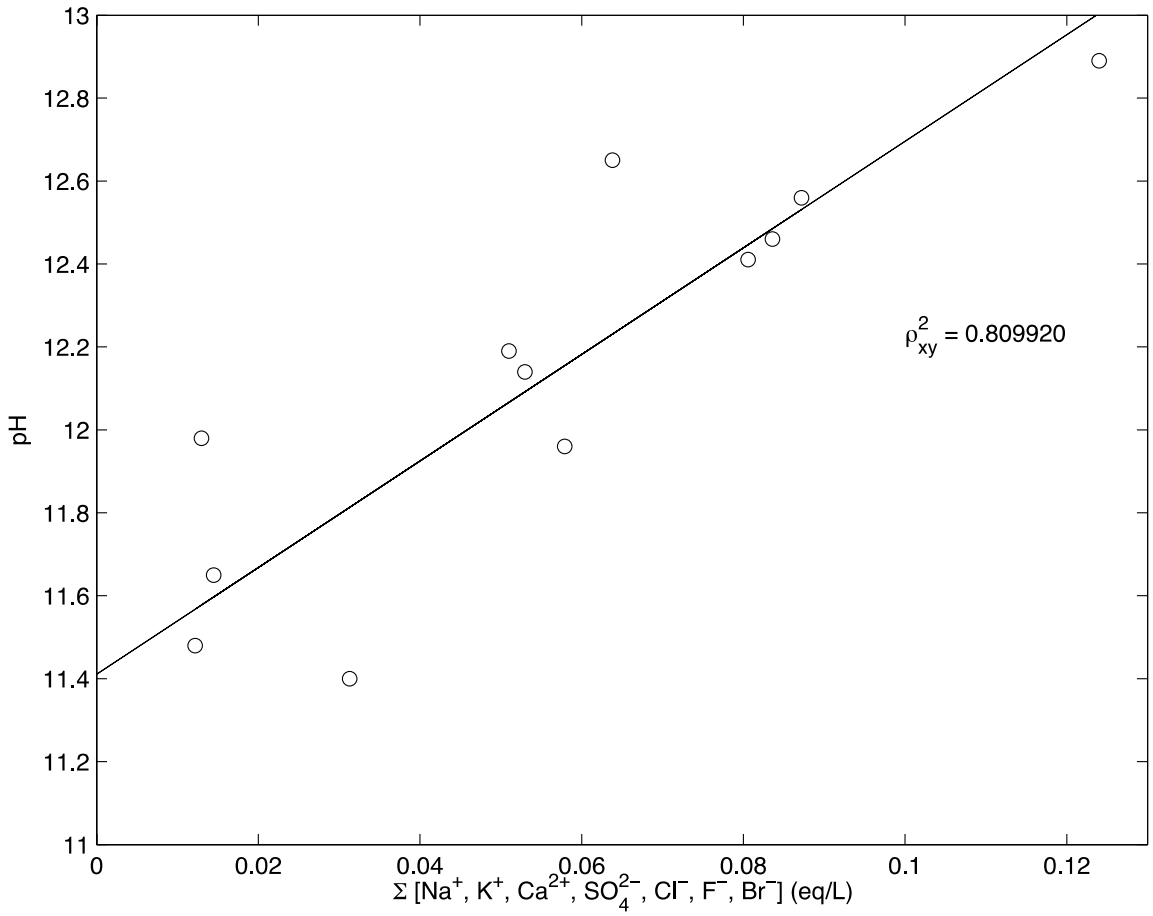

Figure 40: Observed dependence of measured pH on acid-base balance (quantified by ICP-AES and IC) for solids in contact with distilled water for 4 hours. Magnesium concentrations were below detection limits for all test samples and thus have not been included in the sum. Similarly, nitrate concentrations were too low to have a significant effect on the sum and were not included. The solid line represents the linear least squares fit of the data.

For BOF1, FAS1, and FAS4 in distilled water, total carbonate, calculated from alkalinity titration results, exceeded the expected maximum concentration that would arise from dissolution of the measured solid carbon content. Further analysis and modeling show that dissolved aluminum contributes significantly to the alkalinity measured for sample FAS1. However this more rigorous estimation of dissolved inorganic carbon still exceeds the maximum theoretical value established by measured carbon content for BOF1 and FAS4 by a factor of two for both samples. Based on solution pH for these samples, this effect may be explained by absorption of atmospheric CO_2 into solution during testing. Duchene and Reardon (1998) examined aqueous CKD systems closed to the atmosphere at the same liquid to solid ratio with similar sample elemental composition and observed higher pH values and lower alkalinity, which would be expected without exchange with the atmosphere. This imbibition effect makes accurately assessing the carbonate alkalinity generated directly by solid dissolution difficult under these test conditions.

3.2.3.3.2 Sodium bicarbonate leach test solution chemistry

As was done for the 24 hr leach test samples, alkalinity measurements were used to calculate a sequestration capacity for the leach test samples from one and four hour contact with the bicarbonate solution. These data combined with the 24 hour data permitted an examination of reaction kinetics, similar to the approach used by Huntzinger et al. (2009) based on the kinetic model of Lee (2004). Lee (2004) proposed a model for carbonation of CaO to $CaCO_3$ assuming a conversion ratio that decreases as the extent of conversion increases. The defining equations are as follows:

$$\frac{dX}{dt} = k\left(1 - \frac{X}{X_u}\right)^n \tag{3.8}$$

where X represents the conversion of CaO to $CaCO_3$, k is the initial rate of conversion, X_u is the maximum achievable conversion, and n will take values of either 1 or 2 (Lee, 2004). For n=1 and n=2 respectively, the differential equation can be integrated to obtain:

$$X = X_u\left[1 - exp\left(-\frac{k}{X_u}t\right)\right] \tag{3.9}$$

$$X = \frac{X_u t}{(X_u/k)+t} \tag{3.10}$$

For the solids in this study, the extent of conversion, X, is replaced by the estimated sequestration capacity at each time step, which will allow for fitting of an initial sequestration rate, k, and a maximum achievable sequestration capacity, X_u. Table 12 summarizes the results of kinetic modeling of the data obtained for the 13 test samples including: best performing model (with respect to n), model accuracy (by root mean square error), and the fitted parameters. These parameters provide an additional tool for comparing the performance of the large group of study solids. This analysis identifies the best performing samples, both in terms of maximum potential and kinetic response, as CDOR1, CKD2, DOESDA, FALFB2, and FASSD3. Other samples, CDB and FABSD, have high maximum sequestration capacities but slower reaction kinetics, indicating feasible deployment of these solids for aqueous carbon sequestration may require longer reaction times or some form of preprocessing to improve kinetics.

Table 12: Results of kinetic model parameter estimation based on equations of Lee (2004). The order of the differential equation used in the model which best fit the data is denoted by *n*. RMSE is the root mean square error of the model fit. X_u is the maximum achievable sequestration capacity for a given solid and *k* is the initial rate of sequestration.

Sample ID	*n*	RMSE	X_u (mol CO_2/kg solid)	*k* (mol CO_2/kg solid hr)
CDB	1	0.013	1.807	1.466
CDOR1	1	0.008	2.310	27.404
CKD2	2	0.043	2.341	111.467
EAF1	1	0.029	0.635	1.844
FABS	2	0.099	0.972	1.506
FALFB2	2	0.012	2.197	10.446
FALG	1	0.063	1.317	0.139
FAS1	2	0.124	1.366	1.479
FAS4	2	0.022	0.749	2.211
BOF1	2	0.107	1.396	1.398
DOESDA	2	0.155	2.655	14.830
FABSD	1	0.065	1.844	0.972
FASSD3	1	0.021	2.245	4.800

In addition to the measured alkalinity, the metals chemistry of the supernatants is important in evaluating the reactions during leaching tests. The solution chemistry from the 1 and 4 hour 0.5 M $NaHCO_3$ leach tests shows increased concentrations of iron and magnesium from the distilled water leach tests in which neither were detected for any sample. In the carbonate precipitation sequestration process, the sequestration of CO_2 is accomplished by precipitation of various carbonate minerals of which calcite is expected to predominate. Numerous factors, both physical and chemical, are known to inhibit calcite growth and are commonly exploited in processes seeking to minimize calcite precipitation. Inorganic ions can strongly retard calcite crystal growth rates or lead to unproductive precipitation of carbonate reactive cations, e.g. calcium sulfate polymorphs (Meyer, 1984; Sudmalis and Sheikholeslami, 2000).

While other ions have been shown to slow calcite growth significantly, iron (especially ferric iron) can completely inhibit calcite growth at concentrations orders of magnitude lower than calcium and carbonate by adsorption of ions or colloidal solids blocking growth sites (Katz et al., 1993). The alkaline wastes of this study contain iron in significant amounts, and any iron leached will oxidize rapidly at high pH (Sung and Morgan, 1980), suggesting that ferric iron will dominate the soluble iron species.

The complexity of the systems being studied herein may significantly distort the effects seen under well-controlled reagent conditions. As Matty and Tomson (1988) note, calcite growth inhibitors behave additively and the studied leachates are expected to contain other growth inhibitors such as magnesium, aluminum, and phosphate. Similarly, Katz et al. (1993) showed that the inhibitory effect of iron was amplified with increasing alkalinity; however it was also shown that this inhibitory effect was diminished with increasing supersaturation and pH (Katz et al., 1993).

Several studies of alkaline wastes in water show significant supersaturation of calcite even after long exposure times, likely due to the leaching of inhibitors (Bhattacharyya et al., 2011; Duchesne and Reardon, 1998; Huijgen and Comans, 2006; Roy and Griffin, 1984). The presence of these, and other inhibitors, may explain, in part, the supersaturation of calcite, which is seen upon equilibrium modeling of the supernatants.

3.2.3.3.3 Solid mineral phase chemistry

It was expected that a significant amount of the total calcium would be available for reaction as an oxide or hydroxide for these material classes (Dilmore et al., 2009; Huijgen et al., 2005; Huntzinger et al., 2009; Mattigod et al., 1990). Neither the fly ash samples nor the iron and steel residuals (EAFD and BOFS) met this expectation, with the crystalline calcium content of these materials occurring primarily as mixed metal silicates or oxides. Other common dissolving calcium minerals include various sulfate/sulfite polymorphs.

Of the 13 samples, only four were found to have gained a substantial calcite mineral phase. However, significant amorphous phases were identified, though not quantified, which could include calcium or magnesium carbonates. More commonly, various sodium carbonate polymorphs were observed as precipitating including natrite (Na_2CO_3), natron ($Na_2CO_3 \cdot 10\ H_2O$), and trona ($NaHCO_3 \cdot Na_2CO_3 \cdot 2\ H_2O$). It is unclear whether these minerals precipitated during reaction or were the result of the evaporation of pore water during sample drying.

3.2.3.3.4 Carbon sequestration measurements

Measurement of total carbon in the solid phase before and after reaction with 0.5 M $NaHCO_3$ was used to calculate the mass of carbonate truly sequestered as a solid. If the assumptions made about alkalinity titration data are accurate, then a 1:1 correlation would be expected between these two measurements. As can be seen in Figure 41, there is poor agreement between the two estimation methods. However, the samples EAF1 and FALFB2 account for a combined 51% of the total square error between these estimates indicating that these data points may represent outliers as a result of experimental or calculation error.

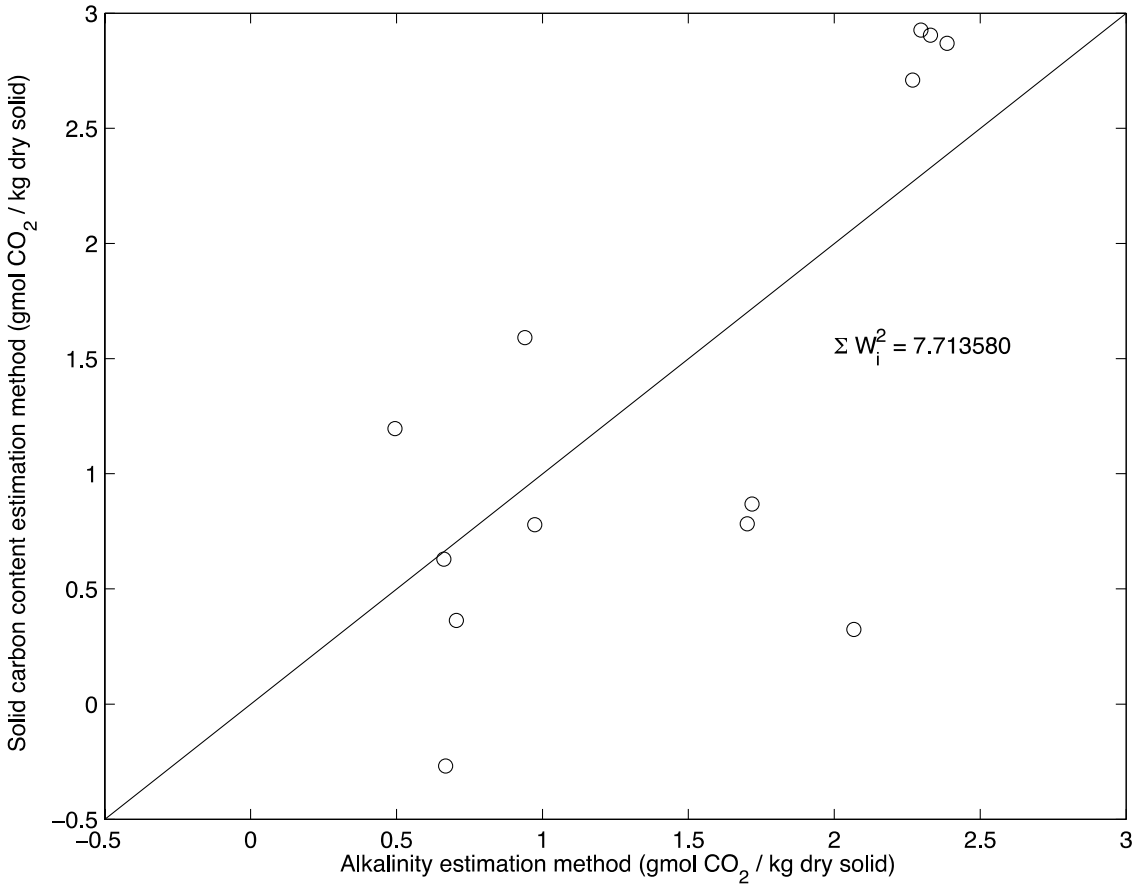

Figure 41: Sequestration capacity estimation method comparison using data from 4 hr reaction of 20 g solid with 120 mL 0.5 M $NaHCO_3$. Abscissa values are calculated through a mass balance on dissolved carbonate, estimated from titration data. Ordinate values are calculated through a mass balance on solid phase carbon mass, estimated from CHN analysis and change in sample mass. The solid line represents a 1:1 relationship.

For values where the total carbon measurement predicts a greater capacity than the alkalinity, it is possible that experimental artifacts have introduced the error. Because the slurries were stirred with a magnetic bar, some mass may not have been recovered following reaction; a smaller post reaction mass would result in an elevated sequestration capacity estimate. Some contribution to the increased solid carbon sequestration estimate can be explained by the moisture content of the centrifuged solids contributing extra carbonate solids through evaporation during drying of the samples. As the moisture content of the solids was not explicitly measured, it is not possible to correct for porewater contribution quantitatively.

Another possible explanation would be that the assumption that carbonate species dominate the alkalinity could be false. For example, the solution chemistry for sample FASSD3 indicates high levels of dissolved aluminum, which at high pH becomes highly hydroxylated and would contribute significantly to alkalinity (Stumm and Morgan, 1996); Under the assumption of carbonate dominated alkalinity, the estimate of dissolved inorganic carbon would be artificially high yielding a lower estimate of sequestration.

Finally, suspended, colloidal carbonate minerals may have artificially elevated the measured alkalinity, which would lead to lower estimates of sequestration capacity by the alkalinity method. It is known that in solutions of high supersaturation, such as those studied here, amorphous calcium carbonate can rapidly form as spheres with diameters between 50 and 400 nm, which would pass through the 450 nm filter used to separate the slurry (Brečević and Nielsen, 1989).

The opposite case, where the alkalinity method yields a higher estimation than the solid carbon method, may be explained by inaccurate measurements of solid phase carbon content. CHN analysis and LECO Total Carbon analysis yielded a 22% average absolute difference in estimation of as-received total carbon for the 13 sample test group. While post-test solids were not analyzed by the LECO technique, this disparity indicates the potential for inaccurate results by either method.

3.2.3.4 Chemical equilibrium modeling

3.2.3.4.1 Supernatant speciation and saturation calculations

Modeling of the solution chemistry for the distilled water and bicarbonate solution leach tests, with suppression of solid formation, was performed with the chemical equilibrium model PHREEQC to examine the speciation of the major ions in solution and the saturation indices of minerals of interest. In particular, saturation indices of carbonate minerals in the supernatants of the bicarbonate leach tests gave some indication of which mineral phases were governing the sequestration observed in solid phase carbon measurements. The chemical equilibrium modeling also enabled calculation of sequestration capacity with accounting for solution density, ionic strength, and non-carbonate contributions to alkalinity. A summary of results for modeling of supernatant solution chemistries is presented in Table 13.

Table 13: Summary of PHREEQC modeling of supernatant solution chemistry for 1 hr distilled water (D.W.), 1 hr bicarbonate solution (B.C.), and 4 hr bicarbonate solution leach tests. Sequestration capacity (Seq. Cap.) was calculated with Equation 3.5. Saturation indices were calculated with Equation 3.12.

Sample ID	Test condition	Complexed CO_3 (%)	Seq. Cap. (mol CO_2/kg solid)		Saturation Index			
			Alkalinity	Model	Calcite	$amCaCO_3$	Natron	Trona
FALFB2	1 hr D.W.	43.72	N/A		3.62	1.54	-3.47	-8.31
	1 hr B.C.	54.60	1.82	2.12	1.97	-0.11	-2.26	-4.18
	4 hr B.C.	65.06	2.07	2.68	0.61	-1.48	-2.56	-5.51
FALG	1 hr D.W.	40.24	N/A		1.00	-1.09	-4.01	-9.27
	1 hr B.C.	40.01	0.03	0.72	2.05	-0.03	-2.05	-3.22
	4 hr B.C.	50.97	0.49	1.11	1.87	-0.22	-1.99	-3.51
FAS4	1 hr D.W.	8.66	N/A		2.87	0.79	-5.88	-11.14
	1 hr B.C.	1.09	0.57	0.63	1.76	-0.33	-6.30	-9.18
	4 hr B.C.	33.59	0.66	1.12	1.89	-0.19	-2.31	-3.48
FAS1	1 hr D.W.	27.38	N/A		1.84	-0.25	-4.55	-10.04
	1 hr B.C.	30.06	0.80	1.21	1.67	-0.41	-2.32	-3.45
	4 hr B.C.	42.21	0.94	1.44	1.94	-0.14	-2.21	-3.60
FASSD3	1 hr D.W.	49.74	N/A		3.89	1.81	-4.38	-9.74
	1 hr B.C.	56.08	1.98	2.18	1.70	-0.38	-2.29	-4.45
	4 hr B.C.	66.39	2.27	2.80	0.72	-1.36	-2.78	-7.70
DOESDA	1 hr D.W.	46.77	N/A		3.87	1.79	-5.46	-11.55
	1 hr B.C.	64.24	2.31	2.36	3.28	1.19	-2.42	-6.98
	4 hr B.C.	64.78	2.33	2.37	3.34	1.26	-2.42	-6.98
FABSD	1 hr D.W.	25.47	N/A		3.70	1.62	-6.92	-12.19
	1 hr B.C.	13.29	0.69	0.62	1.15	-0.93	-3.22	-4.02
	4 hr B.C.	17.84	1.70	1.75	1.38	-0.70	-2.95	-4.06
CDOR1	1 hr D.W.	50.34	N/A		3.96	1.88	-5.29	-11.20
	1 hr B.C.	64.21	2.31	2.35	3.40	1.32	-2.40	-6.83
	4 hr B.C.	64.25	2.30	2.31	3.43	1.35	-2.38	-6.68
CDB	1 hr D.W.	37.07	N/A		3.93	1.84	-7.48	-13.26
	1 hr B.C.	13.72	1.01	0.98	1.25	-0.83	-3.13	-4.02
	4 hr B.C.	16.02	1.72	1.76	1.23	-0.85	-3.02	-4.15
EAF1	1 hr D.W.	25.90	N/A		3.24	1.16	-3.81	-8.32
	1 hr B.C.	25.31	0.60	0.90	1.92	-0.16	-2.38	-3.32
	4 hr B.C.	33.42	0.67	1.12	1.87	-0.21	-2.22	-3.31
CKD2	1 hr D.W.	60.24	N/A		3.88	1.79	-5.43	-11.88
	1 hr B.C.	62.25	2.26	2.49	1.67	-0.41	-2.48	-7.33
	4 hr B.C.	64.89	2.39	2.48	3.10	1.02	-2.49	-7.36
BOF1	1 hr D.W.	24.73	N/A		3.71	1.63	-6.33	-12.06
	1 hr B.C.	42.20	0.78	1.30	1.61	-0.47	-2.19	-3.61
	4 hr B.C.	50.36	0.97	1.45	1.52	-0.56	-2.11	-3.73
FABS	1 hr D.W.	5.82	N/A		2.36	0.28	-5.17	-9.82
	1 hr B.C.	29.67	0.65	1.06	1.81	-0.27	-2.31	-3.39
	4 hr B.C.	33.77	0.70	1.18	1.73	-0.35	-2.29	-3.49

For the 1 and 4 hour bicarbonate leach test, modeling of supernatant chemistry for all samples revealed high levels of carbonate complexation, primarily with sodium. This may limit the availability of carbonate for precipitation and slow the sequestration process. Unfortunately, given that the capture solution simulated here is high in sodium, and would remain so in a steady state situation, this is an effect that cannot be avoided.

For three samples, FAS1 in distilled water and FASSD3 and FALFB2 in bicarbonate for 4 hours, the measured total aluminum concentration would theoretically yield an alkalinity greater than what was measured because of a four equivalent per mole contribution of the species $Al(OH)_4^-$, which becomes the dominant dissolved aluminum phase at pH above 7 (Stumm and Morgan, 1996). Based on the complexity of an ICP measurement versus an alkalinity titration, it was assumed that the measured alkalinity value was correct rather than the ICP quantification of aluminum.

In order to obtain useful output from the model for these samples, the total aluminum was adjusted based on Equation 3.11 assuming all appreciable aluminum is present as $Al(OH)_4^-$ at the high pH values of the leach tests.

$$[Al]_{TOT} = \frac{1}{4}\left(Alk - 2 \cdot \left[{CO_3}^{2-}\right] - [OH]\right) \qquad (3.11)$$

The IC results for carbonate were used for the value of $[CO_3^{2-}]$ in this expression. This approximation resulted in input total aluminum values of 0.046, 0.045, and 0.037 mol/kg solution for samples FAS1, FASSD3, and FALFB2 respectively; all estimates of total aluminum by this method represent deviations from the measured values far outside the reported instrument accuracy likely indicating faulty assumptions or experimental error.

For the 1 hour bicarbonate leach test, calculation of sequestration capacity using model results for total dissolved inorganic carbon resulted in increased estimates for 11 of the 13 samples. The estimation for sample FALG using modeled results was nearly 28 times higher than the estimate calculated from titration data alone, representing a clear outlier from the group. The source of this anomaly has not yet been identified. For the 4 hour bicarbonate leach test, modeling results yielded increased sequestration capacity estimates for all 13 samples, with an average increase of 38% for the entire sample group.

These new estimates of sequestration capacity deviated, based on residual sum of squares, even more from the sequestration capacity values calculated from total carbon analysis of the solids than did the estimates from the original alkalinity method, i.e. Figure 41. Figure 42 presents the comparison of sequestration capacity estimation methods using alkalinity estimates from modeling. However, the new estimates more closely aligned with the solid carbon calculation for all samples where the solid carbon estimate was higher than the original alkalinity method estimation. This change seems to indicate that for samples where solid carbon estimates exceeded alkalinity based estimates, contributions of non-carbonate alkalinity leading to over estimated dissolved inorganic carbon concentrations were the primary factor in the disparity. As before, samples EAF1 and FALFB2 contribute disproportionately to the residual sum of squares error compared to measurements, a combined 66%. When these samples were omitted from the

data set in both circumstances, the new model-based alkalinity estimates provided a better fit to the solid carbon content data than the original estimate.

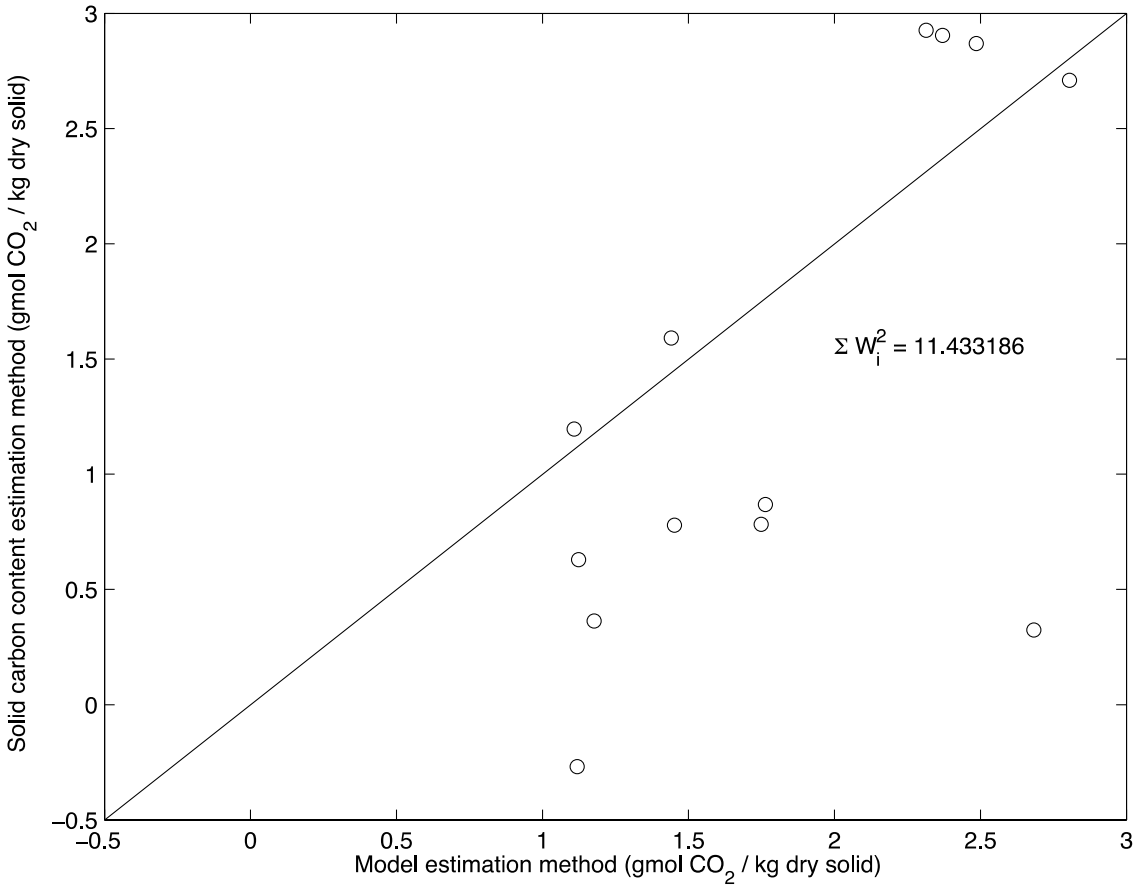

Figure 42: Sequestration capacity estimation method comparison using data from 4 hr reaction of 20 g solid with 120 mL 0.5 M $NaHCO_3$. Abscissa values are calculated through a mass balance on dissolved carbonate, estimated from PHREEQC model outputs. Ordinate values are calculated through a mass balance on solid phase carbon mass, estimated from CHN analysis and change in sample mass. The solid line represents a 1:1 relationship.

Saturation indices for important minerals were calculated using Equation 3.12 where IAP is the ion activity product and K_{sp} is the solubility product of the mineral of interest.

$$SI = \log(IAP) - \log(K_{sp}) \qquad (3.12)$$

In the distilled water supernatant speciation, all samples were supersaturated with calcite with SI ranging from 1.00 to 3.96. In the 1 and 4 hour bicarbonate leach tests the SI range from 1.15–3.40 and 0.61–3.43 respectively. The cases where the SI was very high (≥ 1.00) may be a result of leached growth inhibitors mentioned previously and discussed by Katz et al. (1993) and Matty and Tompson (1988). Alternatively, it has been suggested that incorporation of other ions - such as Na^+, Mg^{2+}, or SO_4^{2-} - in the calcite crystal lattice may enhance solubility, though not likely to the extent observed (Akin and Lagerwerff, 1965; He and Morse, 1993).

Meima and Comans (1997) considered any minerals where the SI approached zero to be potential controlling phases. For calcite, only 4 hour bicarbonate leach samples FALFB2 and FASSD3 met this criterion with SI values of 0.61 and 0.72 respectively; these were also two of the four minerals where an appreciable increase in solid phase calcite was observed by XRD. For amorphous $CaCO_3$, after the 1 hour bicarbonate leach test all samples except for DOESDA and CDOR1 were in the SI range -1 to 1, while after 4 hours the SI for sample CKD2 exceeded 1. Amorphous $CaCO_3$ is a metastable predecessor of calcite which will naturally undergo dissolution and recrystallization to maximize thermodynamic stability (Brečević and Nielsen, 1989).

Experimental results indicate that sodium carbonate polymorphs made up the majority of crystalline carbonate phases which saw significant increases during reaction (see Tables 9 and 10). Based on the modeling it would appear unlikely that either natron ($Na_2CO_3 \cdot 10\ H_2O$) or trona ($NaHCO_3 \cdot Na_2CO_3 \cdot 2\ H_2O$) precipitated during reaction. Rather, given the calculated SI values for both minerals in both bicarbonate leach tests were -1.98 or lower and that less hydrated sodium carbonate polymorphs (e.g. Na_2CO_3) have higher solubility (Monnin and Schott, 1984), these minerals probably formed as a result of evaporation during sample drying. This had been postulated as one potential mechanism artificially inflating sequestration capacity estimates from solid carbon phase measurements. However, this was shown to be at most secondary to contributions of variable solution density and non-carbonate alkalinity.

3.2.3.4.2 Leach test simulations

Simulations of leach tests (4 hour distilled water and 4 hour bicarbonate only) were performed in a method similar to other studies involving modeling of alkaline waste aqueous reactivity (Khaitan et al., 2009a; Meima and Comans, 1997). Because of the number, variety, and complexity of the samples evaluated in this study only the solids with the highest sequestration capacity estimates were considered for this phase of chemical modeling. Based upon reactivity and sequestration capacity quantified by total carbon analysis, the solids chosen for modeling were CDOR1, CKD2, and FASSD3. Another top performing solid, DOESDA, was excluded from modeling because the sample was collected for a previous study and was likely no longer representative of the fresh material.

Solids not found in the PHREEQC thermodynamic database were included based on cited values for Gibb's free energy of formation which were used to calculate solubility products for theorized dissolution reactions. Table 13 presents thermodynamic data for all minerals which were added to the model database. For the dissolution of hannebachite ($CaSO_3 \cdot 0.5\ H_2O$), it was assumed that sulfite would oxidize rapidly upon dissolution and could be approximated by sulfate (Avrahami and Golding, 1968).

Table 14: Thermodynamic data compiled from literature studies for minerals observed by XRD analysis (either pre- or post-reaction with 0.5 M $NaHCO_3$ for 4 hrs) and considered for inclusion in equilibrium modeling at 298 K. Amorphous $CaCO_3$ was not observed but is believed to be an important mineral phase given the short length of testing.

Mineral name	Formula	ΔG_f^0 (kJ/mol)	Source
Akermanite	$Ca_2MgSi_2O_7$	-3663.786	(Berman, 1988)
Amorphous $CaCO_3$	$CaCO_3$	-1067.71	(Brečević and Nielsen, 1989)
Bassanite	$Ca(SO_4) \cdot ½ H_2O$	-1431.65	(Amathieu and Boistelle, 1988)
Calcium Silicate	Ca_2SiO_4	-2316.534	(Haas Jr. et al., 1981)
Ettringite	$Ca_6Al_2(SO_4)_3(OH)_{12} \cdot 26 H_2O$	-15204.7	(Myneni et al., 1998)
Gehlenite	$Ca_2Al_2SiO_7$	-3981.707	(Haas Jr. et al., 1981)
Hannebachite	$CaSO_3 \cdot ½ H_2O$	-1195.9	(Rai et al., 1991)
Hatrurite	$Ca_3(SiO_4)O$	-2787.747	(Haas Jr. et al., 1981)
Lime	CaO	-603.38	(Berman, 1988)
Merwinite	$Ca_3Mg(SiO_4)_2$	-4309.707	(Berman, 1988)
Natrolite	$Na_2(Al_2Si_3O_{10}) \cdot 2 H_2O$	-5316.6	(Johnson et al., 1983)
Natron	$Na_2(CO_3) \cdot 10 H_2O$	-3427.661	(Harvie et al., 1984)
Periclase	MgO	-569.209	(Berman, 1988)
Thaumasite	$Ca_3Si(OH)_6(SO_4)(CO_3) \cdot 12 H_2O$	-15128.46	(Schmidt et al., 2008)
Tricalcium Aluminate	$Ca_3Al_2O_6$	-3643.343	(Khaitan et al., 2009a)
Trona	$Na_3H(CO_3)_2 \cdot 2 H_2O$	-2360.608	(Harvie et al., 1984)

Without mineral phase confirmation by XRD inclusion of other minerals to control dissolution and aqueous phase speciation of elements would have been purely speculative. In the short testing period employed it is possible that unidentified amorphous minerals controlled the solution composition. However, there was not adequate information available to confirm which phases may be present or to develop accurate solubility expressions from thermodynamics for these phases.

Speciation of supernatant samples for FASSD3, CDOR1, and CKD2 suggested a number of potential minerals to consider for inclusion in the solid reaction model. However, a good agreement between observed and modeled results for several trial sets of minerals was not obtained. In particular, minerals could not be identified which adequately controlled solution compositions of aluminum, carbonate, magnesium, and silicon. At high pH and in the absence of calcite, portlandite was found to provide reasonable control over dissolved calcium, consistent with the findings of other studies (Meima and Comans, 1997). Mineral phases which were detected as forming but that provided poor control over solution chemistry include tricalcium aluminate and the various calcium sulfate polymorphs detected by XRD.

The inability to achieve convergence between observed and model results likely arises as a result of kinetic- and surface-reaction-related deviations from equilibrium conditions. The lack of agreement between observed and modeled results indicates that the equilibrium assumption for all reactions was likely invalid, and the systems are still evolving chemically after 4 hours. A kinetic model incorporating diffuse- and surface-reaction-controlled time scales could provide more insight into system behavior, but the current data set does not contain the information necessary to generate or evaluate this type of model.

3.2.4 Summary and conclusions

The objective of the leaching study was to identify alkaline industrial wastes which could serve as sources of carbonate reactive cations in an aqueous carbon sequestration process. This was accomplished by examining the reaction of several industrial solid residues with a simulated aqueous CO_2 scrubber blowdown for varying time periods in a mixed batch reactor followed by analysis of solution and solid phase chemistries and equilibrium modeling of the results.

This work has demonstrated the feasibility of using select alkaline industrial wastes as sources of carbonate reactive cations in an aqueous carbon sequestration scheme. Experimental results indicate the best performing solids may sequester between 2.30 and 2.93 moles of CO_2 per kg of dry material depending upon estimation method. These samples were a cement kiln dust, a spray drier absorber ash, and a circulating dry scrubber ash. However, screening of a number of samples in each material class indicated that there was high variability in sequestration performance within each class, likely due to operating conditions within the process generating the waste.

Estimates of sequestration capacity can be made through use of a chemical equilibrium model. Modeling suggests that the controlling carbonate mineral phase in aqueous waste leaching reactions is primarily amorphous $CaCO_3$, which evolves over time to form more stable calcite. Given the complexity of the solids and the time scale of the studies, it was not possible to

determine the reaction mechanisms at work. However, experimentation and modeling gave no indication that the pathway would deviate from that which has been generally hypothesized whereby calcium is liberated from a glassy matrix and precipitated with carbonate.
Future work should focus on understanding and modeling the kinetic processes which dominate these systems as well as optimizing process variables to achieve maximum sequestration. Additionally, the performance variability within sample classes could be thoroughly characterized through more testing, and the feasibility for wide spread deployment of this technology could be understood through statistical simulations.

3.2.5 References

Akin G.W., Lagerwerff J.V. (1965) Calcium carbonate equilibrium in solutions open to the air. II. Enhanced solubility of $CaCO_3$ in the presence of Mg^{2+} and SO_4^{2-}. Geochimica et Cosmochimica Acta 29:353-360.

Amathieu L., Boistelle R. (1988) Crystallization kinetics of gypsum from dense suspension of hemihydrate in water. Journal of Crystal Growth 88:183-192.

ASTM. (2004a) Standard Test Method for Major and Minor Elements in Coal and Coke Ash By X-Ray Fluorescence.

ASTM. (2004b) Standard Test Methods for Sampling and Testing Fly Ash or Natural Pozzolans for Use in Portland-Cement Concrete.

ASTM. (2011) Standard Test Method for Ash in the Analysis Sample of Coal and Coke from Coal.

Avrahami M., Golding R.M. (1968) The oxidation of the sulphide ion at very low concentrations in aqueous solutions. Journal of the Chemical Society A: Inorganic, Physical, Theoretical:647-651.

Back M., Bauer M., Stanjek H., Peiffer S. (2011) Sequestration of carbon dioxide after reaction with alkaline earth metal oxides CaO and MgO. Applied Geochemistry 26:1097-1107. DOI: 10.1016/j.apgeochem.2011.03.125.

Back M., Kuehn M., Stanjek H., Peiffer S. (2008) Reactivity of alkaline lignite fly ash towards carbon dioxide in water. Environmental Science and Technology 42:4520-4526. DOI: 10.1021/es702760v.

Berman R.G. (1988) Internally-consistent thermodynamic data for minerals in the system Na_2O-K_2O-CaO-MgO-FeO-Fe_2O_3-Al_2O_3-SiO_2-TiO_2-H_2O-CO_2. Journal of Petrology 29:445-522.

Bhattacharyya P., Reddy K.J., Attili V. (2011) Solubility and Fractionation of Different Metals in Fly Ash of Powder River Basin Coal. Water Air and Soil Pollution 220:327-337. DOI: 10.1007/S11270-011-0757-1.

Bonenfant D., Kharoune L., Sauvé S., Hausler R., Niquette P., Mimeault M., Kharoune M. (2008) Carbon dioxide sequestration potential of steel slags at ambient pressure and temperature. Industrial & Engineering Chemical Research 47:7610-7616. DOI: 10.1021/ie701721j.

Brečević L., Nielsen A.E. (1989) Solubility of amorphous calcium carbonate. Journal of Crystal Growth 98:504-510.

Dilmore R., Howard B., Soong Y., Griffith C., Hedges S., DeGalbo A., Morreale B., Baltrus J., Allen D., Fu J. (2009) Sequestration of carbon dioxide in mixtures of caustic byproduct and saline waste water. Environmental Engineering Science 26:1325-1333. DOI: 10.1089/ees.2008.0395.

Duchesne J., Reardon E.J. (1998) Determining controls on element concentrations in cement kiln dust leachate. Waste Management 18:339-350.

Fauth D.J., Soong Y., White C.M. (2002) Carbon sequestration utilizing industrial solid residues. Abstracts of Papers of the American Chemical Society 223:U565-U565.

Gerdemann S., O'Connor W., Dahlin D., Penner L., Rush H. (2007) Ex situ aqueous mineral carbonation. Environmental Science and Technology 41:2587-2593. DOI: 10.1021/es0619253.

Haas Jr. J.L., Robinson Jr. G.R., Hemingway B.S. (1981) Thermodynamic tabulations for selected phases in the system $CaO-Al_2O_3-SiO_2-H_2O$ at 101.324 kPa (1 atm) between 273.15 and 1800 K. Journal of Physical and Chemical Reference Data 10.

Harvie C.E., Møller N., Weare J.H. (1984) The prediction of mineral solubilities in natural waters: The $Na-K-Mg-Ca-H-Cl-SO_4-OH-HCO_3-CO_3-CO_2-H_2O$ system to high ionic strengths at 25˚C. Geochimica et Cosmochimica Acta 48:723-751.

He S., Morse J.W. (1993) The carbonic acid system and calcite solubility in aqueous $Na-K-Ca-Mg-Cl-SO_4$ solutions from 0 to 90˚C. Geochimica et Cosmochimica Acta 57.

Huijgen W.J.J., Comans R.N.J. (2004) Carbon dioxide sequestration by mineral carbonation: Literature review update 2003-2004, Energy research Center of the Netherlands.

Huijgen W.J.J., Comans R.N.J. (2006) Carbonation of steel slag for carbon dioxide sequestration: Leaching of products and reaction mechanisms. Environmental Science and Technology 40:2790-2796. DOI: 10.1021/es052534b.

Huijgen W.J.J., Ruijg G.J., Comans R.N.J., Witkamp G.-J. (2006) Energy consumption and net CO2 sequestration of aqueous mineral carbonation. Industrial & Engineering Chemical Research 45:9184-9194. DOI: 10.1021/ie060636k.

Huijgen W.J.J., Witkamp G.-J., Comans R.N.J. (2005) Mineral carbon dioxide sequestration by steel slag carbonation. Environmental Science and Technology 39:9676-9682. DOI: 10.1021/es050795f.

Huntzinger D., Dierke J., Kawatra S.K., Eisele T., Sutter L. (2009) Carbon dioxide sequestration in cement kiln dust through mineral carbonation. Environmental Science and Technology 43:1986-1992. DOI: 10.1021/es802910z.

Iizuka A., Fujii M., Yamasaki A., Yanagisawa Y. (2004) Development of a new CO2 Sequestration process utilizing the carbonation of waste cement. Industrial & Engineering Chemical Research 43:7880-7887. DOI: 10.1021/ie0496176.

Johnson G.K., Flotow H.E., O'Hare P.A.G., Wise W.S. (1983) Thermodynamic studies of zeolites: natrolite, mesolite, and scolecite. American Mineralogist 68:1134-1145.

Katz J., Reick M., Herzog R., Parsiegla K. (1993) Calcite growth inhibition by iron. Langmuir 9:1423-1430.

Khaitan S., Dzombak D.A., Lowry G.V. (2009a) Chemistry of the acid neutralization capacity of bauxite residue. Environmental Engineering Science 26:873-882. DOI: 10.1089/ees.2007.0228.

Khaitan S., Dzombak D.A., Lowry G.V. (2009b) Mechanisms of bauxite neutralization of bauxite residue by carbon dioxide. Journal of Environmental Engineering 135:433-438. DOI: 10.1061/(ASCE)EE.1943-7870.0000010.

Lackner K.S., Wendt C.H., Butt D.P., Joyce Jr. E.L., Sharp D.H. (1995) Carbon dioxide disposal in carbonate minerals. Energy 20:1153-1170.

Lee D.K. (2004) An apparent kinetic model for the carbonation of calcium oxide by carbon dioxide. Chemical Engineering Journal 100:71-77.

Liu N., Bond G.M., Abel A., McPherson B.J., Stringer J. (2005) Biomimetic sequestration of CO2 in carbonate form: Role of produced waters and other brines. Fuel Processing Technology 86:1615-1625. DOI: 10.1016/j.fuproc.2005.01.008.

Mattigod S.V., Rai D., Eary L.E., Ainsworth C.C. (1990) Geochemical factors controlling the mobilization of inorganic constituents from fossil fuel combustion residues: I. Review of major elements. Journal of Environmental Quality 19:188-201.

Matty J., Tomson M. (1988) Effect of multiple precipitation inhibitors on calcium carbonate nucleation. Applied Geochemistry 3:549-556.

Meima J.A., Comans R.N.J. (1997) Geochemical modeling of weathering reactions in municipal solid waste incinerator bottom ash. Environmental Science & Technology 31:1269-1276. DOI: 10.1021/es9603158.

Meyer H.J. (1984) The influence of impurities on the growth rate of calcite. Journal of Crystal Growth 66:639-646.

Mirjafari P., Asghari K., Mahinpey N. (2007) Investigating the application of enzyme carbonic anhydrase for carbon dioxide sequestration purposes. Industrial & Engineering Chemical Research 46:921-926. DOI: 10.1021/ie060287u.

Monnin C., Schott J. (1984) Determination of the solubility products of sodium carbonate minerals and an application to trona deposition in Lake Magadi (Kenya). Geochimica et Cosmochimica Acta 48:571-581. DOI: 10.1016/0016-7037(84)90285-0.

Montes-Hernandez G., Pérez-López R., Renard F., Nieto J.M., Charlet L. (2008) Mineral sequestration of carbon dioxide by aqueous carbonation of coal combustion fly-ash. Journal of Hazardous Materials 161:1347-1354. DOI: 10.1016/j.jhazmat.2008.04.104.

Myneni S.C.B., Traina S.J., Logan T.J. (1998) Ettringite solubility and geochemistry of the $Ca(OH)_2$-$Al_2(SO_4)_3$-H_2O system at 1 atm pressure and 298 K. Chemical Geology 148:1-19.

Parkhurst D.L., Appelo C.A.J. (1999) PHREEQC, U.S. Geological Survey.

Rai D., Felmy A.R., Fulton R.W., Moore D.A. (1991) An aqeuous thermodynamic model for Ca^{2+} - SO_3^{2-} ion interactions and the solubility product of crystalline $CaSO_3$ - 0.5 H_20. Journal of Solution Chemistry 20:623-632.

Rawlins C. (2008) Geological sequestration of carbon dioxide by hydrous carbonate formation in steelmaking slag, Metallurgical Engineering, Missouri University of Science and Technology, Rolla, MO.

Roy W., Griffin R. (1984) Illinois Basin coal fly ashes. 2. Equilibria relationships and qualitative modeling of ash-water reactions. Environmental Science and Technology 18:739-742.

Schmidt T., Lothenbach B., Romer M., Scrivener K., Rentsch D., Figi R. (2008) A thermodynamic and experimental study of the conditions of thaumasite formation. Cement and Concrete Research 38:337-349. DOI: 10.1016/j.cemconres.2007.11.003.

Seifritz. (1990) Carbon dioxide disposal by means of silicates. Nature 345:486.

Stumm W., Morgan J. (1996) Aquatic Chemistry. 3rd ed. John Wiley & Sons, Inc., New York.

Sudmalis M., Sheikholeslami R. (2000) Copreipication of calcium carbonate and calcium sulfate. The Canadian Journal of Chemical Engineering 78:21-31.

Sung W., Morgan J. (1980) Kinetics and product of ferrous iron oxygenation in aqueous systems. Environmental Science & Technology 14:561-568.

U.S.D.O.E. (2009) Fluidized bed technology - Overview, U.S. Department of Energy.

4.0 Techno-economic analysis

A techno-economic analysis was performed to evaluate the commercial viability of the proposed carbon capture and sequestration process in full-scale at an aluminum smelter and a refinery location. Compared to techno-economic evaluation performed as part of Phase I project, more refined assumptions have been used to develop this assessment. The rest of this section describes in detail the critical flow and sequestration capacity assumptions, the cost tables and the annualized cost information as it pertains to control of 50% CO_2 capture from a typical aluminum smelter producing 260,000 MTPY of aluminum and ~5% CO_2 from boiler exhausts at a aluminum refinery, enough to neutralize the entire stream of alkaline clay media generated by the refinery for the entire year.

4.1 Smelter Application

For the smelter application, two separate processes were investigated: (i) using in-duct scrubber (IDS) technology to capture 50% CO_2 from a typical smelter with 260,000 MTPY capacity followed by sequestration of the bi-carbonate rich blowdown stream using cement kiln dust/blast furnace slag type of material with high sequestration potential; (ii) using traditional amine based CO_2 capture and concentration process followed by geological storage.

The following assumptions are used to develop the techno-economic analysis around an aluminum smelter for comparing the annualized cost $/ton CO_2 between the in-duct scrubber aided carbon capture/sequestration process and traditional amine based carbon capture, concentration followed by geologic storage method.

- Typical Aluminum Smelter with a production rate ~260,000 Metric Tons of Al per year
- Air Flow Rate of 2.06 Million Nm^3/h
- CO_2 Concentration of 0.8 vol%
- CO_2 capture rate of 50%
- Total CO_2 removed = 137,400 tons per year (using an operating factor of 97%)

The capture process includes two horizontal induct scrubbers, operated in parallel, each capable of treating 710,000 Am3/h of flue gas. Each scrubber is equipped with a cross-flow section with a dimension of 6.8 m × 6.8 m × 30 m (Height × Width × Length) and an ID fan capable of processing 750,000 of inlet Am^3/h. The exhaust from each fan will lead to a 12 m (dia) × 40 m (height) wet stack equipped with a top convergent cone & internal condensate drainage ribbons.
The sequestration process entails processing of the bi-carbonate rich scrubber blowdown slurry into a sequestration system that includes reaction of the bi-carbonate stream with waste alkaline solids such as, lime kiln dust and/or lignitic fly ash type material for conversion of bi-carbonate into calcium carbonate and recovery of the alkalinity for processing back in the scrubber circuit.

Table 15 shows a summary of sequestration capacities for different materials screened in this work. The upper limit of 3 gmole/kg material for the range of measured sequestration capacities was used in this techno-economic evaluation.

As part of the flue gas treatment for CO_2 removal via Na based scrubbing, SO_2 will also be automatically removed because of the chemistry of the scrubbing liquor. Because SO_2 levels in smelter off-gases are about $1/100^{th}$ the concentration of CO_2, some gypsum (~2% of the total weight of the solid) will be formed in the sequestered solids. This is an inherent advantage of the Na based scrubbing system over a traditional amine based CO_2 capture system, where the SO_2 levels of the flue gas needs to be reduced from ~100 ppm down to ~10 ppm for the amine system to properly capture the CO_2.

Table 15: List of Screened Sequestration Agents with Measured Sequestration Capacities

Sample Type	Sequestration Capacity (gmol CO_2 / kg dry solid)		
	1 hr	4 hr	24 hr
CDS	2.31	2.30	2.32
CKD	2.23	2.39	2.31
EAFD	0.60	0.67	0.80
FA	1.82	2.07	2.19
FS	0.78	0.97	1.42
SDA	2.31	2.33	2.79
BR	**0.3 gmol CO_2/kg dry solid (supernatant only)**		

The other critical assumptions based on consultation with the enzyme producers (Codexis and CO_2 Solutions) are the optimal concentration, stability and cost of the soluble enzyme once it is ready for commercial-scale production in the next two to three years. These parameters are as follows:

- Projected Enzyme concentration = 500 mg/L
- Projected Enzyme cost = $100/ kg
- Projected Enzyme Survival = 2 months with minimal foaming loss

Table 16 provides the cost details to estimate the annual operating cost with and without capital recovery for treating 50% CO_2 from a typical aluminum smelter with generation of beneficial residuals. As a conservative estimate, $10/ton is used for disposition of the residuals created from the sequestration process, which could change depending on the proximal presence of a beneficial use product recycler/broker dealing with the distribution of agriculture amendment, construction fill, or soil stabilization material.

Table 16: Detailed Cost Breakdown for Estimating Capital Recovery (2011 BY$) for Smelter Application of IDS aided Carbon Capture/Sequestration Process

Smelter FS In-Duct CCS OPEX - Soluble Enzyme						**12-Jan-12**
	Assumptions:	• Smelter offgas treated	2,058,000	NCuM/h		
		• 50% CO_2 removal	137,400	tonnes CO_2/year		
		• Operation hours per year	**8,500**			
		• 12-hour shifts				
		• Soluble enzyme conc'n	500			
		Units	**Price (USD)**	**Quantity**	**Cost**	
	Utilities					
	Power	Mwh	35	27,400	959,000	
	Water	CuM	1	901,800	901,800	
	Total Utilities				**1,860,800**	
	Chemicals					
	Sequestrant Dry Solids	tonnes	5	1,040,700	5,203,500	
	Caustic 50%	tonnes	250	8,600	2,150,000	
	Enzyme Powder	kg	100	6,200	620,000	
	Defoamer 30% Solution	kg	2	156,000	312,000	
	Total Chemicals				**8,285,500**	
	Waste Disposition					
	Sequestered Solids - Cake	tonnes	10	1,371,400	13,714,000	
	Enzyme	tonnes	0	0	0	
	Total Waste Disposition				**13,714,000**	
	Operating Labor					
	Supervision	h	60	8,800	528,000	
	Operating Labor	h	45	39,400	1,773,000	
	Trcuk Coordinators	h	30	35,040	1,051,200	
	Safety Coordinators	h	45	8,400	378,000	
	Technical Support	h	60	6,240	374,400	
	Environmental Support	h	50	3,120	156,000	
	Analytical Support	Lot	50,000	1	50,000	
	Total Labor				**4,310,600**	
	Maintenance					
	Supervision	h	60	8,800	528,000	
	Planner	h	45	13,100	590,000	
	Craft Labor	h	30	42,500	1,275,000	
	Spare Parts	% of Eq't	3.0%	34,059,000	1,022,000	
	Total Maintenance				**3,415,000**	
	General & Administrative	% of O&M	8.0%	31,585,900	**2,527,000**	
	Total Annual Operating Cost without Capital Recovery				**31,585,900**	
	Capital Recovery	% of CAPEX	10.0%	163,279,000	**16,328,000**	
	Total Annual Operating Cost with Capital Recovery				**47,913,900**	
	Total Cost / tonne CO_2 Removed - No Capital Recovery				**230**	
	Total Cost / tonne CO_2 Removed - With Capital Recovery				**349**	

4.1.1 Amine Based Carbon Capture, Concentration and Geological Sequestration Process

To estimate the cost of a traditional amine based carbon capture and sequestration process, the NETL/CMU developed Integrated Environmental Control Systems Model (IECM)[1] was employed to design a full scale MEA based carbon capture and sequestration process for a typical Al smelter with a production rate of 260,000 MTPY. The IECM model simulates an advanced MEA system, based on the Fluor Econamine FG Plus process. A general schematic of the advanced MEA system with vertical absorber and stripper is shown in Figure 43.

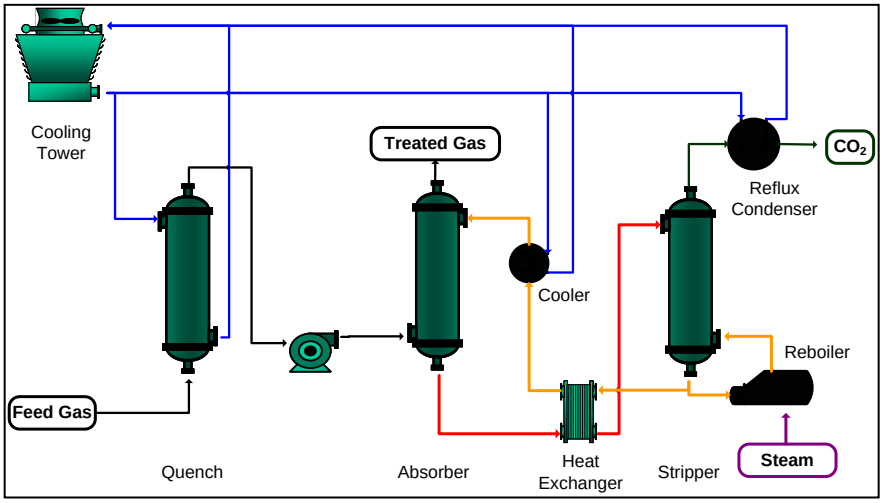

Figure 43: Conventional Amine Based CO_2 Capture and Concentration Process.

The output from the IECM simulation model has been coupled with cost for adequate piping and compression cost, as part of a geologic sequestration process, in order to develop an annualized cost for the amine process. Table 17 provides the detailed cost breakdown to estimate the capital cost for the amine process. It is important to note that the total CAPEX for the amine process also includes the cost of a flue gas desulfurization (FGD) system utilizing a conventional Limestone Forced Oxidation (LSFO) system for SO_2 control prior to the CO_2 capture by the amine process. Table 18 provides the detail breakdown for the operating cost of the amine and FGD process including the capital recovery to arrive at a value for net $/ton of CO_2 removed.

4.1.1.2 Cost Comparison for Smelter Application

Table 19 summarizes the cost comparison between the two technologies: (i) Advanced amine based CO_2 capture, concentration followed by geologic sequestration and (ii) in-duct scrubbing of CO_2 followed by mineral carbonation. In the latter case, both preliminary Phase I and a more refined Phase II cost comparison is given. The primary difference between the two estimates

[1] Rao, A.B., Rubin, E.S., and M.B. Berkenpas, 2004: *An integrated modeling framework for carbon management technologies*, Final report to DOE/NETL (Contract number DE-FC26-00NT40935), from Center for Energy and Environmental Studies, Carnegie Mellon University, Pittsburgh, PA, USA.

(Phase I and Phase II) is in enzyme concentration (100 mg/L vs. 500 mg/L) and cost ($10/kg vs. $100/kg).

As shown in Table 19, a 44% reduction in annual cost could be realized by applying the Na-based scrubbing of the flue gas using the in-duct scrubber technology compared to an amine-based CCS process.

Table 17: Detailed Cost Breakdown for Estimating Capital Cost (2010 BY$) for Smelter Application of MEA process for Carbon Capture, Concentration and Geological Sequestration

Amine CCS CAPEX ($M)		
Capture and Compression		
Direct + Infdirect Costs		
Direct Contact Cooler	40.42	
Fan	7.42	
Absorber Vessel	104.82	
Heat Exchangers	2.53	
Pumps	4.69	
Sorbent Regenerator	12.50	
Reboiler	2.01	
Sorbent Reclaimer	0.13	
Sorbent Processing	0.17	
Drying and Compression Unit	4.11	
NG Boiler	3.70	
Process Facilities		182.5
Process Royalty		0.9
Process Contingency		9.2
Total Process Facilties		192.6
General Facilities		18.2
Sitework - Allowance		6.0
Ducting/Dampers/Supports		11.3
Stacks		3.4
Utilities Supply		5.8
Total Facilities		237.3
Other Indirects		
Engineering and Home Office		23.7
Project Contingency		78.3
AFUDC		0.0
Training, Startup & Working Inventory		3.6
Subtotal - Capture and Compresssion		**343.0**
Transport and Storage		
Process Facilities		39.2
General Facilities		3.9
Sitework - Allowance		10.0
Engineering andf Home Office		3.7
Project Contingency		17.0
AFUDC		0.0
Training, Startup & Working Inventory		1.3
Subtotal - Transport and Storage		**75.2**
Total Amine CCS CAPEX ($M)		**418.1**
$/kw Equivalent		**804**
FGD CAPEX		
Total FGD CAPEX ($M)		**192.6**
$/kw Equivalent		**370**
Total Project CAPEX ($M)		**610.8**
$/kw Equivalent		**1,175**

Table 18: Detailed Cost Breakdown for Estimating Capital Recovery (2010 BY$) for Smelter Application of MEA process for Carbon Capture, Concentration and Geological Sequestration

Amine CCS OPEX ($)	**CO_2 Capture Capacity (tonnes/d)**	**390**
Capture and Compression System		
Utilities		
Power		7,058,000
Natural Gas		3,831,000
Water		890,000
Chemicals and Supplies		
Caustic		27,000
Sorbent		51,000
Carbon		51,000
Waste Disposal		13,000
Operating Labor		1,621,000
Maintenance		
Labor		1,669,000
Materials		2,497,000
General & Administrative		1,062,000
Subtotal - Capture and Compresssion		**18,770,000**
Transport and Storage System		
Utilities		---
Chemicals and Supplies		---
Operating Labor		---
Maintenance		---
General & Administrative		---
Subtotal - Transport and Storage		**620,000**
Total Amine W/O Capital Recovery		**19,390,000**
FGD OPEX ($)		
Total FGD W/O Capital Recovery		**5,239,000**
Total Project OPEX W/O Capital Recovery		
Total Project OPEX ($)		**24,629,000**
$/tonne CO_2		**180**
Capital Recovery		**61,075,000**
Total Project OPEX ($)		**85,704,000**
$/tonne CO_2		**626**

Table 19: Cost Comparison between Amine and IDS Technologies for Smelter Application

Smelter CCS
2.06 M Nm^3/h - 50% CO_2 Capture
137,000 Annual tonnes CO_2

	Advanced Amine	Alcoa IDS Phase I	Alcoa IDS Phase II	Delta
CAPEX ($M)				
FGD	192.6	0.0	0.0	
CCS	418.1	177.5	163.3	
Total	**610.7**	**177.5**	**163.3**	
$/kw eq	**1,175**	**342**	**315**	
OPEX ($M)				
O&M - FGD	5.2	0.0	0.0	
O&M - CCS	19.4	23.3	31.6	
Capital Recovery	61.1	17.8	16.3	
Total	**85.7**	**41.0**	**47.9**	
$/tonne CO_2	**627**	**299**	**349**	**-44%**
$/tonne Al	**398**	**189**	**221**	

4.2 Refinery Application

For the aluminum refinery application, two different approaches have been evaluated: (i) an integrated carbon capture process using in-duct scrubber with red mud neutralization and (ii) an amine based carbon capture and concentration step followed by high pressure residue carbonation. To develop the cost details for these two technology approaches, Alcoa's Point Comfort refinery has been chosen as the template for calculating the amount of CO_2 required to completely neutralize ~1.24 million MT of dry red mud (43% solids) per year from the last stage washer underflow. Based on the measured bauxite residue sequestration capacity, it has been estimated that ~ 50% CO_2 removal is required on a slip stream of 45,000 Nm^3/hour from one of the high pressure boilers used at the Point Comfort refinery power house. This amounts to less than 5% of the total CO_2 footprint of the refinery. However, the biggest benefit of this process is the complete neutralization of the bauxite residue and conversion of an industrial waste product to a beneficial use media. A lower cost residue neutralization via carbonation could render red mud "non-hazardous" with numerous benefits:

- Enable neutralized bauxite residue back to mine approach
- Enable re-use applications for neutralized bauxite residue
- Enable potential savings in refinery caustic use
- Potential savings in bauxite residue management

The rest of the section provides all the information regarding the benefits of the integrated carbon capture approach via in-duct scrubber along with cost details and cost comparison with traditional MEA based carbon capture, concentration and direct carbonation process.

4.2.1 Integrated Carbon Capture with Red Mud Neutralization

This process allows the capture of CO_2 from a slip stream of the boiler flue gas using carbonic anhydrase (CA) enzyme aided sodium carbonate liquor solution in the in-duct scrubber followed by reaction of the concentrated bi-carbonate solution in the scrubber blowdown with bauxite residue slurry from the refinery's last stage washer underflow to form stable mineral carbonates with a final pH of the neutralized product in the vicinity of 10.5. The neutralization reaction also regenerates the sodium carbonate alkalinity for recycle back in the scrubber to aid in the capture process.

When the carbon capture process is integrated with the refining operation, the inherent benefits are many:

- Soda recovery based on reduced Dawsonite formation
- Lime Savings
- Lime-CO_2 footprint elimination
- Fuel Saving from Powerhouse
- CO_2 removed from mud, not counting CO_2 reduction from boiler Powerhouse
- Powerhouse CO_2 emission reduction
- Production increase (99 MT/Day)
- Beneficial use of residue resulting in no pH "spring back"
- Beneficial use of by-product calcite

Table 20 provides the detailed cost breakdown for estimation of capital cost for the in-duct scrubber carbon capture and residue neutralization process when integrated with the refining circuit. As shown in Table 10, the equipment and material cost for the in-duct scrubber for carbon capture followed by residue sequestration process is about 15.5 million USD whereas the cost for the lime neutralization system is around 3.4 million USD to a total equipment and material cost of 19.32 million USD. The total installed project cost including outside the boundary limit allowance, engineering, procurement, construction management and contingency amounts to 37.4 million USD. Table 21 provides the detail breakdown for the operating cost of the integrated carbon capture and residue neutralization process including the capital recovery to arrive at a value for net \$/ton of CO_2 removed.

Table 20: Capital Cost breakdown for the Integrated Carbon Capture and Residue Neutralization Process.

Point Comfort In-Duct CCS CAPEX - Soluble Enzyme						**12-Jan-12**
Assumptions:	• Flue gas treated - 45,000 Nm^3/h capacity					
	• 50% CO_2 removal - 30,000 tonnes/year capacity					
	• \$2011 BY Estimate					
Cost Component (\$)	**Equipment & Material**	**Structural Steel [1]**	**Foundations**	**Freight**	**Erection & Installation [2]**	**Total**
ISBL						
Absorber and Fan	649,000	194,000	113,000	34,000	572,000	1,562,000
Tanks & Skids [3]	2,039,000	606,000	572,000	106,000	2,080,000	5,403,000
Pumps & Piping	2,288,000	688,000	481,000	119,000	1,600,000	5,176,000
Buildings & Enclosures						550,000
Electrical & Controls	1,487,000			59,000	1,643,000	3,189,000
Lime Neutralization System						3,439,565
Subtotal - ISBL	**6,463,000**	**1,488,000**	**1,166,000**	**318,000**	**5,895,000**	**19,319,565**
OSBL Allowances						
Sitework						1,800,000
Ducting/Dampers/Supports						1,500,000
Stack						400,000
Utility Connections/Controls						1,600,000
Subtotal - OSBL						**5,300,000**
EPCm						3,690,000
Contingency						8,490,000
Startup Support & Training						600,000
Total Project						**37,400,000**
[1]	Includes support steel, platforms and staircases					
[2]	Includes painting, insulation and lagging					
[3]	Includes agitators and supports					

Table 21: Detailed Cost Breakdown for Estimating Capital Recovery (2010 BY$) for Refinery Application of Integrated Carbon Capture using In-Duct Scrubber and Residue Neutralization process.

Point Comfort In-Duct CCS OPEX - Soluble Enzyme							**12-Jan-12**
	Assumptions:	• Flue gas treated		45,000	NCuM/h		
		• 50% CO_2 removal		30,000	tonnes CO_2/year		
		• Operation per year		8,500	hrs		
		• 12-hour shifts					
		• Free enzyme concentratio		500	mg/L		
			Units	**Price (USD)**	**Quantity**	**Cost**	
	Utilities						
	Power		Mwh	35	5,300	186,000	
	Water		CuM	1	14,000	14,000	
		Total Utilities				**200,000**	
	Chemicals						
	Red Mud	~43% Slurry	dry tonnes	0	1,241,000	0	
	Caustic	50%	tonnes	250	0	0	
	Enzyme	Powder	kg	100	657,300	65,730,000	
	Flocculant	30% Solution	kg	2	72,000	144,000	
	Defoamer	30% Solution	kg	2	72,000	144,000	
		Total Chemicals				**66,018,000**	
	Waste Disposition						
	Sequestered Solids		dry tonnes	0	1,275,000	0	
	Enzyme		tonnes	0	0	0	
		Total Waste Disposition				**0**	
	Operating Labor						
	Supervision		h	60	2,200	132,000	
	Operating Labor		h	45	11,000	495,000	
	Technical Support		h	60	1,000	60,000	
	Analytical Support		Lot	20,000	1	20,000	
		Total Labor				**707,000**	
	Maintenance						
	Supervision		h	50	3,300	165,000	
	Craft Labor		h	30	17,000	510,000	
	Materials		% of Eq't	3.0%	10,527,259	316,000	
		Total Maintenance				**991,000**	
	G&A					**5,433,280**	
	Total Annual Operating Cost without Capital Recovery					**73,349,280**	
	Capital Recovery		% of CAPEX	10.0%	37,400,000	3,740,000	
	Total Annual Operating Cost with Capital Recovery					**77,089,280**	
	Total Cost / tonne CO_2 Removed - No Capital Recovery					**2,445**	
	Total Cost / tonne CO_2 Removed - With Capital Recovery					**2,570**	

4.2.2 Amine Based CO_2 Capture, Concentration and Direct Residue Carbonation

To estimate the cost of a traditional amine based carbon capture and concentration process, the NETL/CMU developed Integrated Environmental Control Systems Model (IECM)[1] was again employed to design a full scale MEA based carbon capture and concentration process for Point Comfort with a net CO_2 removal of 30,000 MTPY from a 45,000 Nm3/h of natural gas fired boiler flue gas slip stream. The IECM model simulates an advanced MEA system and is based on the Fluor Econamine FG Plus process. A general schematic of the advanced MEA system with vertical absorber and stripper is shown in Figure 43. The downstream of the MEA process can then be coupled with direct residue carbonation process by reacting the concentration CO2 gas stream from the amine process with the residue underflow slurry in a series of carbonation reactors as depicted in Figure 44.

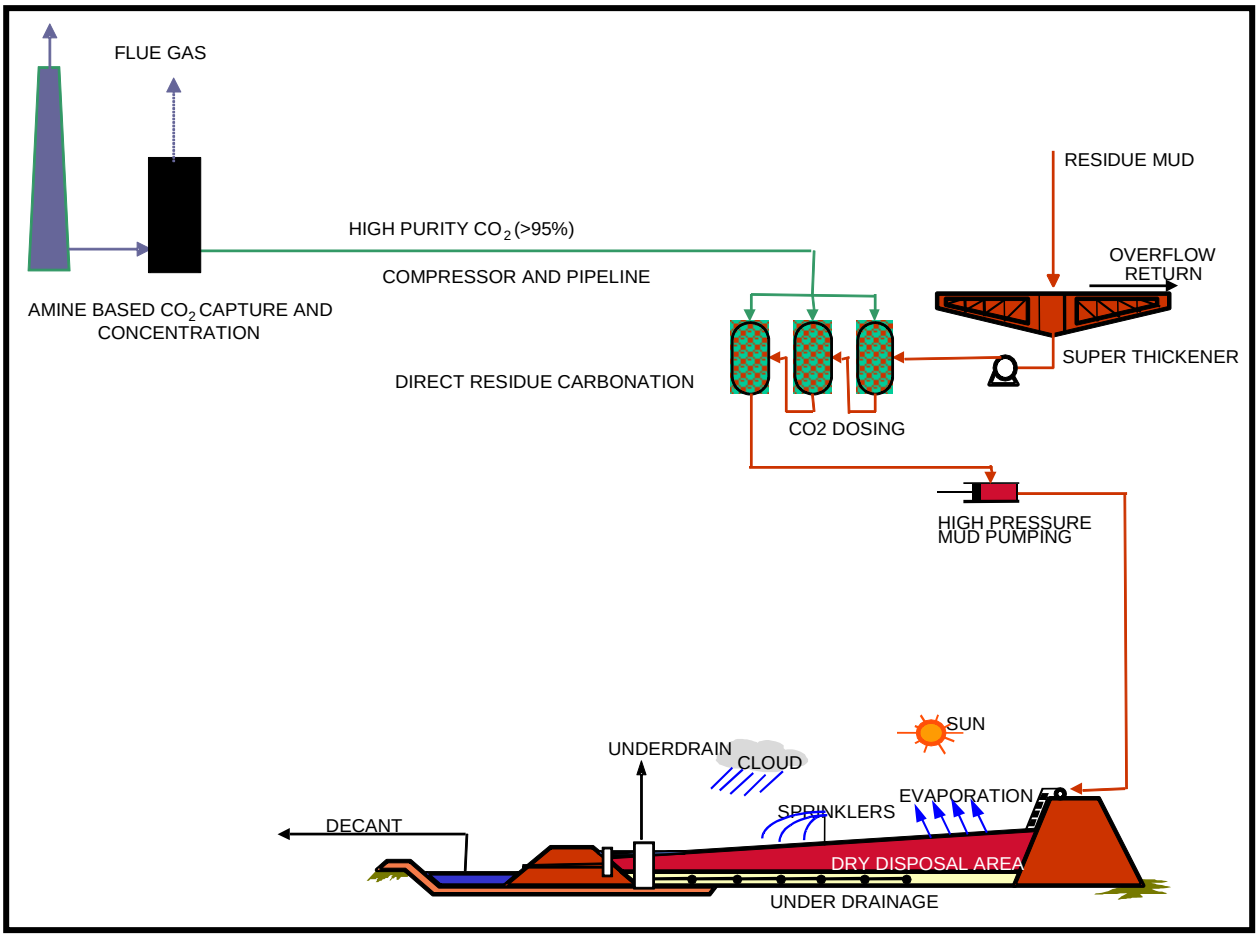

Figure 44: Direct Residue Carbonation process at a Refinery using Concentrated CO_2 stream from a MEA aided Carbon Capture and Concentration Process.

Table 22 provides the detailed cost breakdown for estimation of capital cost for the MEA process for the Point Comfort application. As shown in Table 22, the total CAPEX for the amine system including the CO_2 carbonation equipment amounts to $48.7 million. Table 23 provides the detailed breakdown for the operating cost of the MEA process for the Point Comfort application including the capital recovery to arrive at a value for net $/ton of CO_2 removed.

Table 22: Capital Cost breakdown for the Amine aided Carbon Capture and Residue Carbonation process at Point Comfort

CAPEX ($M)		
Base Year Cost	**2010 BY$**	
CAPEX Cost Index	**1.125**	
Operating Factor	**91.3%**	
Amine CCS CAPEX ($M)		
Capture and Compression		
Direct + Infdirect Costs		
Direct Contact Cooler	2.48	
Fan	0.45	
Absorber Vessel	6.43	
Heat Exchangers	0.25	
Pumps	0.53	
Sorbent Regenerator	1.97	
Reboiler	0.11	
Sorbent Reclaimer	0.05	
Sorbent Processing	0.09	
Drying and Compression Unit	1.89	
NG Boiler	0.29	
Process Facilities		14.5
Process Royalty		0.1
Process Contingency		0.7
Total Process Facilties		15.3
General Facilities		2.3
Total Facilities		17.6
Other Indirects		
Engineering and Home Office		2.6
Project Contingency		6.1
AFUDC		0.0
Training, Startup & Working Inventory		0.9
Subtotal - Capture and Compresssion		**27.3**
Sequestration + OSBL		
Sitework - Allowance		1.8
Ducting/Dampers/Supports		1.5
Stack		0.4
Gas Pipeline and Compressor		1.7
Carbonation Reactors		2.0
Causticizer and Pipeline		4.2
Utilities Supply and Controls		2.4
Engineering and Home Office		2.1
Project Contingency		4.8
Training, Startup & Working Inventory		0.5
Subtotal - Transport and Storage		**21.5**
Total Amine CCS CAPEX ($M)		**48.7**
$/kw Equivalent		**3,214**

Table 23: Detailed Cost Breakdown for Estimating Capital Recovery (2010 BY$) for Refinery Application of Amine aided Carbon Capture and Residue Carbonation process at Point Comfort

OPEX ($)		**Alcoa Adjusted**
Base Year Cost		**2010 BY$**
OPEX Cost Index		**1.000**
Operating Factor		**97.0%**
Capture and Compression System	**CO_2 Capture Capacity (tonnes/d)**	**113**
Utilities		
Power - MEA + Compression		68,500
Power - Compression		55,500
Power - Sequestration		50,400
Natural Gas		838,800
Water		207,000
Chemicals and Supplies		
Caustic		6,000
Sorbent		11,300
Carbon		11,300
Waste Disposal		2,000
Operating Labor		788,000
Maintenance		
Labor		512,000
Materials		688,000
General & Administrative		259,000
Subtotal - Capture and Compresssion		**3,497,800**
Transport and Storage System		
Utilities		0
Chemicals and Supplies		0
Operating Labor		0
Maintenance		0
General & Administrative		0
Subtotal - Transport and Storage		**0**
Total Project OPEX W/O Capital Recovery		**3,497,800**
$/tonne CO_2		**87**
Capital Recovery		**4,873,000**
Total Project OPEX ($)		**8,370,800**
$/tonne CO_2		**279**

4.2.3 Cost Comparison for Refinery Application

Table 24 summarizes the cost comparison between the two technologies: (i) Advanced amine based CO_2 capture, concentration followed by direct residue carbonation (ii) integrated refinery CO_2 capture and residue neutralization using in-duct scrubber. For the latter scenario, both Phase I (preliminary) and Phase II (refined) cost estimates are listed. As was noted in Phase I report, a number of assumptions were made in the preliminary assessment, including: (i) sequestration capacity of sequestrants; (ii) beneficial use value of generated residuals; (iii) enzyme performance; (iv) optimal enzyme concentration and longevity; and (v) cost projection for the enzyme. A refined techno-economic analysis based on the results of Phase II measurements has been performed, and results are presented in Table 24.

As shown in Table 24, the Phase II cost estimate is significantly higher than that derived from Phase I work. The principal driver for the cost increase is the increase in projected enzyme cost ($100/kg vs. $10/kg) and working enzyme concentration (500 mg/L vs. 20 mg/L). The current estimated cost is $2570/ton of CO_2 removed.

Table 24: Cost Comparison between Amine and IDS Technologies for Refinery Application

Refinery NG Boiler CCS
45.000 Nm^3/h - 50% CO_2 Capture
30,000 Annual tonnes CO_2

	Advanced Amine	Alcoa IDS (Phase I)	Alcoa IDS (Phase II)	In-Duct Delta
CAPEX ($M)				
FGD	0.0	0.0	0.0	
CCS	48.7	37.4	37.6	
Total	**48.7**	**37.4**	**37.6**	
$/kw eq	**4,286**	**3,289**	**3,307**	
OPEX ($M)				
O&M - FGD	0.0	0.0	0.0	
O&M - CCS	3.5	2.7	73.3	
Capital Recovery	4.9	3.7	3.8	
Total	**8.4**	**6.4**	**77.1**	
$/tonne CO_2	**279**	**215**	**2,570**	**821%**

Figure 45 shows cost sensitivity of the refinery CCS process to the working concentration of CA enzyme for two enzyme cost assumptions: 1) $10/kg (blue line) and 2) $100/kg (red line). As can be seen from Figure 45, the overall cost for the refinery CCS application is quite sensitive to both enzyme cost and concentration. The target cost of ~200$/tn CO_2 removed could be achieved at enzyme concentration of ~20mg/L and enzyme cost of $10/kg. Additionally, it is foreseen that using filtration technology provided by CO_2 Solutions, the enzyme could be filtered from the CO_2 absorbent before sequestration process, and retained in the scrubber, thus dramatically reducing the enzyme consumption in the overall process. However, this technology option was not pursued as additional commercialization time would have been required, pushing operational demonstration of the system beyond the 2014 timeline imposed by DOE under the program.

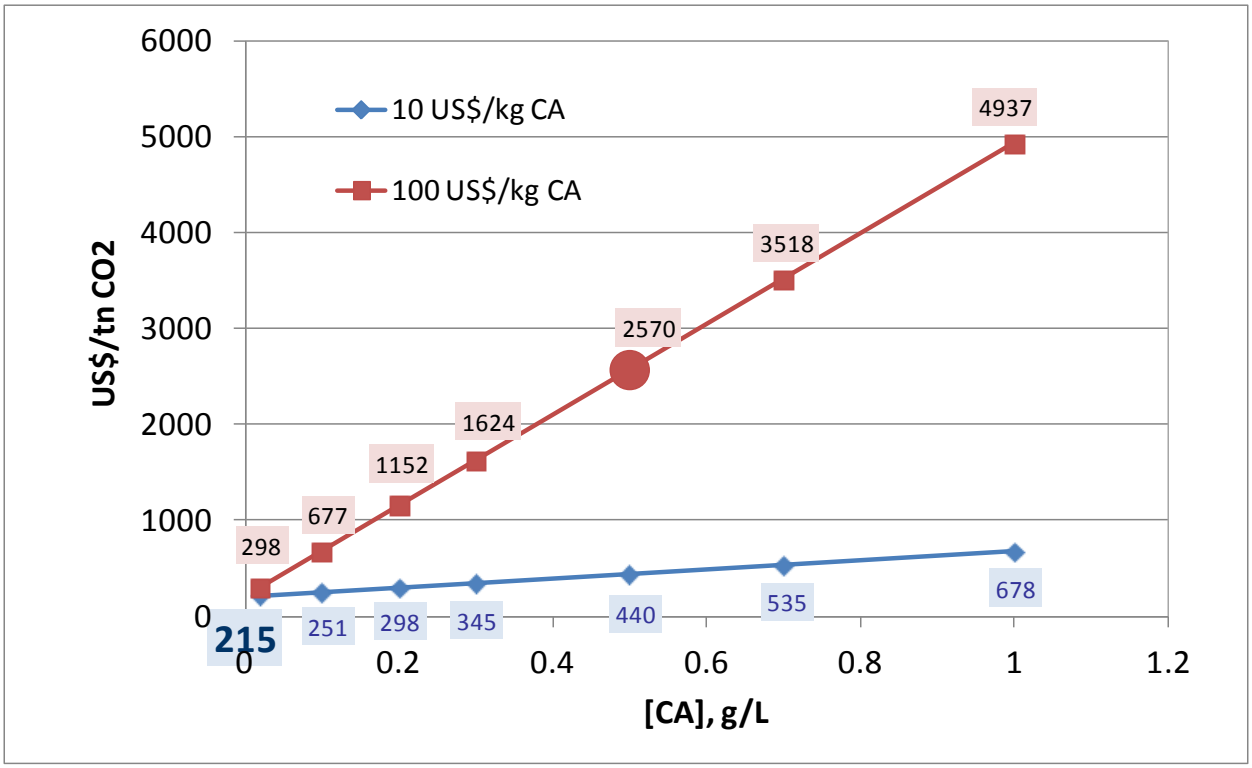

Figure 45: Sensitivity of the refinery CCS application to enzyme concentration and cost.

5.0 Life cycle assessment

A preliminary analysis was performed to estimate the effect of indirect green house gas (GHG) emissions associated with the Alcoa carbon capture and sequestration (CCS) process, including emissions related to both construction and operation, on the overall CO_2 sequestration efficiency of the process. The analysis utilized economic input-output life cycle assessment (LCA) to evaluate indirect emissions. The goal of this preliminary analysis was to obtain an initial estimate of the carbon penalty incurred by the indirect emissions and calculate an effective CO_2 removal including this penalty.

Three applications of the CCS process were examined using economic input-output LCA: aluminum smelter, alumina refinery with onsite waste disposal, and alumina refinery with offsite waste shipment for beneficial reuse. For the aluminum smelter case, the construction and operation of the CCS process emits approximately 46,780 equivalent tons of CO_2 (t CO_2e) annually compared to the 140,000 tons of CO_2 directly sequestered. At the alumina refinery where the wastes are disposed onsite, indirect emissions total 22,795 t CO_2e compared to 30,000 t CO_2 captured. For the alumina refinery where the wastes are shipped offsite for beneficial use, the result is 29,935 tons of indirect emissions, resulting in net CO_2 emissions for this scenario. The simplicity of this model warrants further analysis involving more accurate, process-based life cycle assessment.

5.1 Introduction

The goal of this preliminary analysis was to obtain an initial estimate of indirect GHG emissions associated with the Alcoa CCS process using the public-domain Economic Input-Output Life Cycle Assessment (EIO-LCA) web-based tool developed at Carnegie Mellon (www.eiolca.net). Three scenarios were examined: a smelter application, a refinery application with onsite waste disposal, and a refinery with offsite beneficial use of waste. Conservative assumptions were made in an attempt to generate an upper bound estimate of indirect emissions.

5.2 Approach

The EIO-LCA model developed by the Carnegie Mellon University Green Design Institute was utilized to calculate indirect GHG emissions associated with economic activity in various sectors, such as structural metals and water usage. The emissions, which include CO_2 from fuel combustion, CO_2 not from fuel combustion, N_2O, CH_4, and HFC/PFCs, are normalized to equivalent tons of CO_2 based upon their relative global warming potential (GWP).

Using the most recent techno-economic analysis developed by Alcoa for the CCS process, various process components were identified whose indirect emissions could be readily approximated using the EIO-LCA tool. Figure 46 schematically illustrates the system representation and boundary encompassing the components that could be included in the EIO-LCA calculation.

The components used in the calculation are listed in Table 26 and refer only to the smelter application of the Alcoa CCS process. Aqueous waste management is shown in Figure 46,

however it was not included in the LCA analysis due to a lack of information. A summary of all raw information used in the analysis can be found in Appendix A. A CO_2 sequestration capacity of 3 moles/kg dry solids was assumed for the analysis of the aluminum smelter application. This is a best case scenario regarding sequestration candidate performance.

Table 25: Construction and operation components used in the EIO-LCA indirect GHG emission calculations. "E&M" refers to the equipment and materials associated with individual components while structural steel and foundations represent the total for all combined components.

Construction	Operation
Structural steel	Power
Foundations	Water
Pumps and piping (E&M)	Caustic
Electrical controls (E&M)	Defoamer
Tanks and skids (E&M)	Enzyme
Absorber and fans (E&M)	Sequestrant handling (raw and waste)

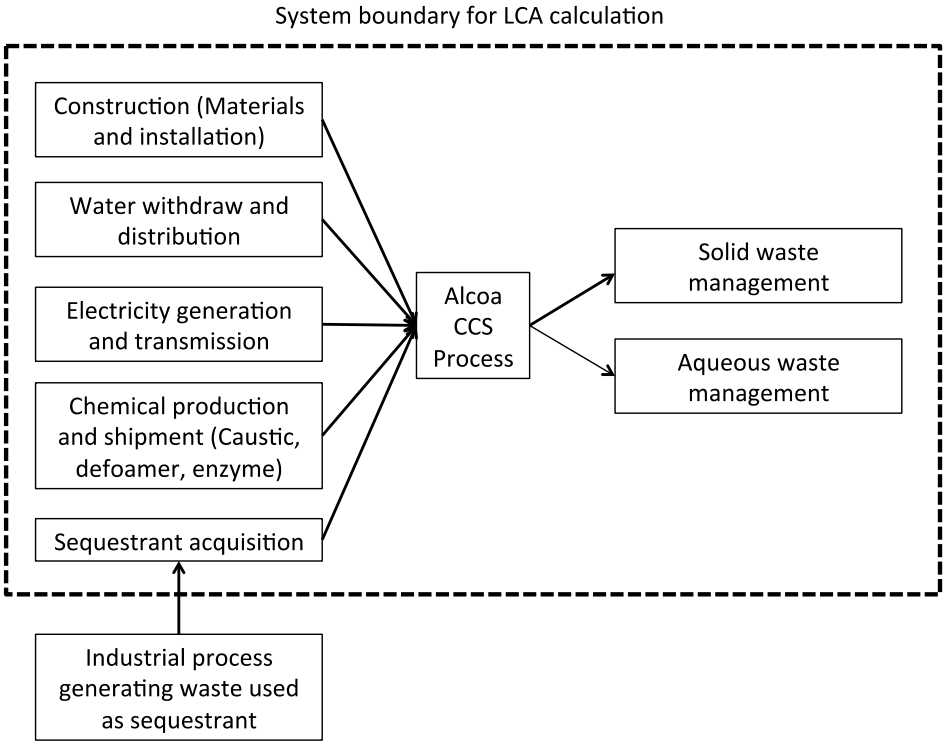

Figure 46: Simplified schematic of CCS process representation for LCA calculations, including system boundary. Boxed units refer to complete life cycle emissions associated with a process. Emissions associated with generation of waste material were not included in calculation; only the acquisition and usage of the material as a sequestrant were considered.

The EIO-LCA tool requires dollar value inputs in 2002 US dollars (USD). The Bureau of Labor Statistics' Consumer and Producer Price Indices (CPI, PPI) were consulted to convert input data (in 2010 USD) to appropriate values. In each case an attempt was made to identify the most appropriate economic sector with available data for each component. Additionally, some components contained multiple appropriate sectors; in these instances, the most conservative indices were chosen to provide a higher estimation of GHG emissions. 2010 USD were converted to 2002 USD by multiplying the given value by the ratio of 2002 PPI to 2010 PPI. Table 28 summarizes the indices used for these calculations.

Table 26: Summary of PPI used to convert given economic information to appropriate input for the EIO-LCA tool. Indices are from the Bureau of Labor Statistics unless otherwise noted. For each commodity a base index of 100 refers to the cost in 1982-1984.

Commodity	Producer Price Index	
	2002	2010
Industrial commodities	132.4	187.0
Electric power	136.8	184.4
Industrial electric power	139.9	193.1
Industrial chemicals	127.3	269.2
Fabricated structural metal	145.0	201.1
Fabricated structural metal (NAICS)	136.9	174.2
Machinery and equipment	122.9	131.1
Overall total	179.9	218.1

Once converted to the appropriate base year, the economic activity in each sector can be used in the EIO-LCA tool to calculate the indirect GHG emissions associated with this activity. As with the PPI, the most appropriate economic sector was chosen for each component with a more conservative option chosen for equally appropriate sectors. With more detailed economic information the components could be further broken down to yield more accurate results. Construction emissions were amortized over a 30-year project life and added to the emissions from regular operation.

In addition to this basic assessment, a sensitivity analysis was conducted for the smelter application on the basis of sequestration capacity. For the sensitivity analysis calculations it was assumed that the sequestration capacity only affected the mass of sequestrant being handled.

Analyses of the two refinery applications followed much the same framework as for the smelter, with only minor changes. First, onsite handling of process waste in residue impoundments was ignored in the calculation, as this operation could remain unchanged by the installation of a CCS process. Secondly, the Alcoa techno-economic analysis lists an additional construction component, "Lime neutralization system," which was modeled with NAICS sector #562.

5.3 Results and Discussion

Table 28 outlines the input values used in the calculation, the economic sector chosen to represent the component, and the resulting total emissions in equivalent tons of CO_2. Table 29 gives a detailed example of emissions associated with power generation. Table 29 highlights the variety of indirect emissions generated by a product from cradle to grave. Other major GHG species emitted have been converted to an equivalent emission of CO_2 based on their relative global warming potential (GWP).

For the smelter case, this analysis yielded a total annual GHG emission of 46,730 t CO_2e per year compared to the designed capture of 140,000 tons. When these indirect emissions are included in the overall CO_2 footprint of the smelter operation, the designed CO_2 removal rate is decreased from 50% of operational CO_2 emissions to 43%. The relative contribution of each component to indirect emissions can be seen in Figure 47.

Table 27: EIO-LCA inputs and results for smelter application of the proposed Alcoa CCS process using 2002 Purchaser model[2]. NAICS sector number definitions can be found in Section 5.6.

Component	Inputs		Results
	NAICS sector #	Activity (Million $)	Emissions (t CO_2e)
Structural steel	33231	6.3	5,870
Foundations	230103	5.2	3,180
Pumps and piping	333911	11.5	6,090
Electrical controls	334513	7.5	2,260
Tanks and skids	33242	10.2	9,630
Absorber and fans	33341A	3.3	2,110
Power	2211	0.7	6,560
Water	2213	0.8	1,420
Caustic	325181	1.0	2,100
Defoamer	32519	0.2	509
Enzyme	325414	0.5	150
Sequestrant acquisition	424	4.3	6,020
Sequestrant disposal	562	11.3	29,000

[2] Carnegie Mellon University Green Design Institute. (2012) Economic Input-Output Life Cycle Assessment (EIO-LCA) US 2002 (428) model [Internet], Available from: <http://www.eiolca.net/>

Table 28: Sample EIO-LCA tool output for 0.7 million 2002 USD economic activity in power generation. Only the top 5 contributing sectors are shown and do not sum to the shown total.

Sector	GHG emissions (t CO_2e)					
	Total	$CO_{2,\ fuel}$	$CO_{2,\ process}$	CH_4	N_2O	HFC/PFCs
Power generation and supply	6170	6080	0	16.7	37.8	39.1
Coal mining	161	18.1	0	143	0	0
Oil and gas extraction	90.3	25.4	16.5	48.3	0	0
Pipeline transportation	47	21.5	0.059	25.4	0	0
Rail transportation	18.2	18.2	0	0	0	0
Total	**6560**	**6210**	**21.9**	**242**	**39.4**	**40.2**

It is readily evident in Figure 47 that the handling of sequestrant material will have a significant impact on the overall sequestration efficiency of the process. For this calculation, expenditure on sequestrant disposal was attributed to "Waste Management and Remediation Services" (NAICS # 562000). Use of this approach to represent sequestrant disposal includes multi-modal transportation as well as general landfilling and upkeep but may also factor in extraneous information. This example highlights the wide variability inherent in using only one economic sector to characterize a process component and underscores the need for more in-depth analysis.

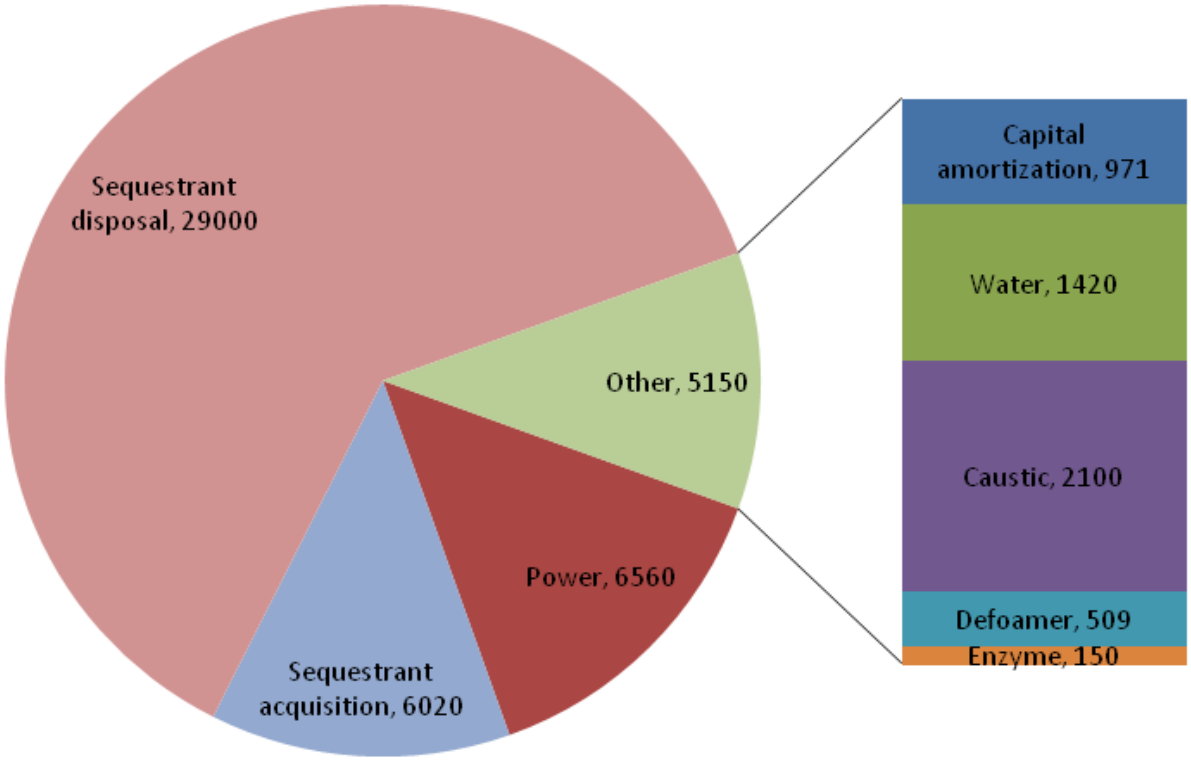

Figure 47: Relative contribution to annual indirect GHG emissions by each sector included in analysis. Total annual emissions have been estimated at 46,780 t CO_2e .

Results of the sensitivity analysis for sequestrant disposal in the smelter case, shown in Figure 48, indicate that above the current best case scenario for sequestration capacity, the reduction of indirect emissions is minimal. This occurs because the contribution of system components not related to sequestrant handling begin to dominate the indirect emissions, and these are essentially fixed. However, as the sequestration capacity decreases, the efficiency of the capture process drops off significantly.

For the refinery cases, LCA analysis results indicate that the carbon sequestration benefits are not practically viable. Figure 49 shows the relative contribution of each process component to the indirect emissions for each refinery case. In the case of onsite disposal, approximately 23,000 t CO_2e are emitted, compared to the 30,000 t CO_2 captured annually. When the waste is shipped (by truck) offsite for beneficial use the indirect emissions rise to approximately 30,000 t CO_2e, effectively creating no net CO_2 benefit. The additional value for the beneficial offsite use scenario was determined by the difference between a $10 per ton disposal fee and the estimated $7.7 million cost of onsite disposal.

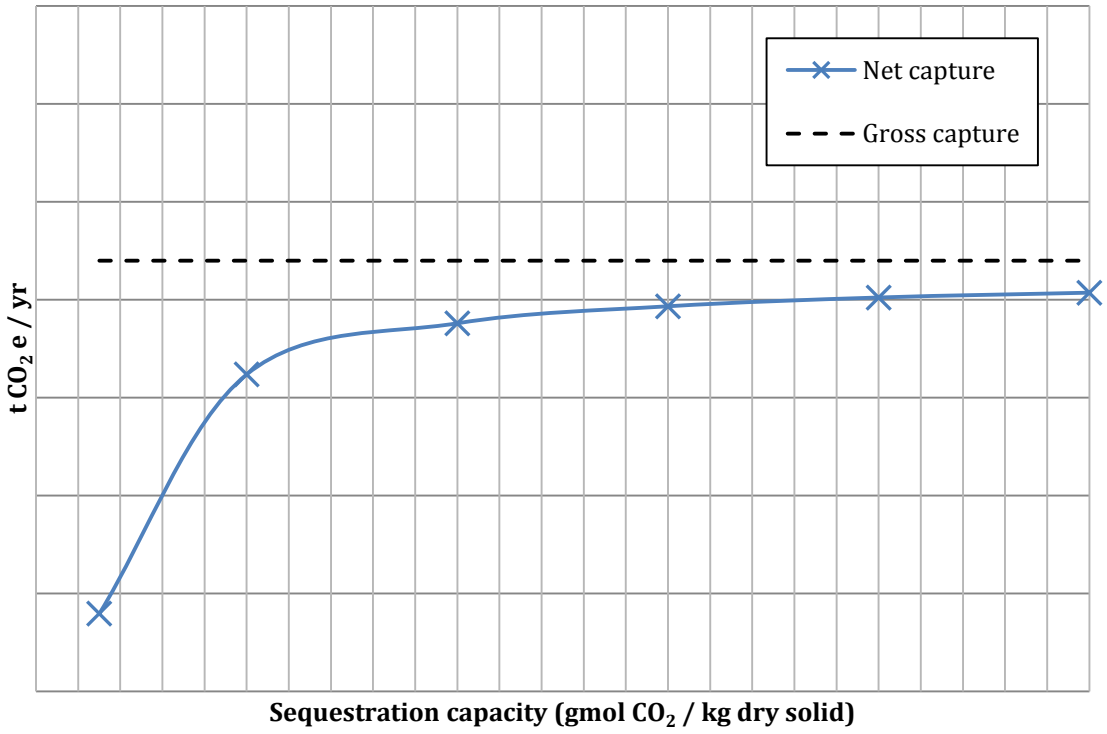

Figure 48: Sensitivity of net CO_2 capture rate to changing sequestration capacity of industrial residuals for the smelter case. Varying sequestration capacity was assumed to only affect the mass of sequestrant needed and the mass of waste disposed. Calculation performed for a smelter application of CCS process assuming capture of 140,000 t CO_2 / yr.

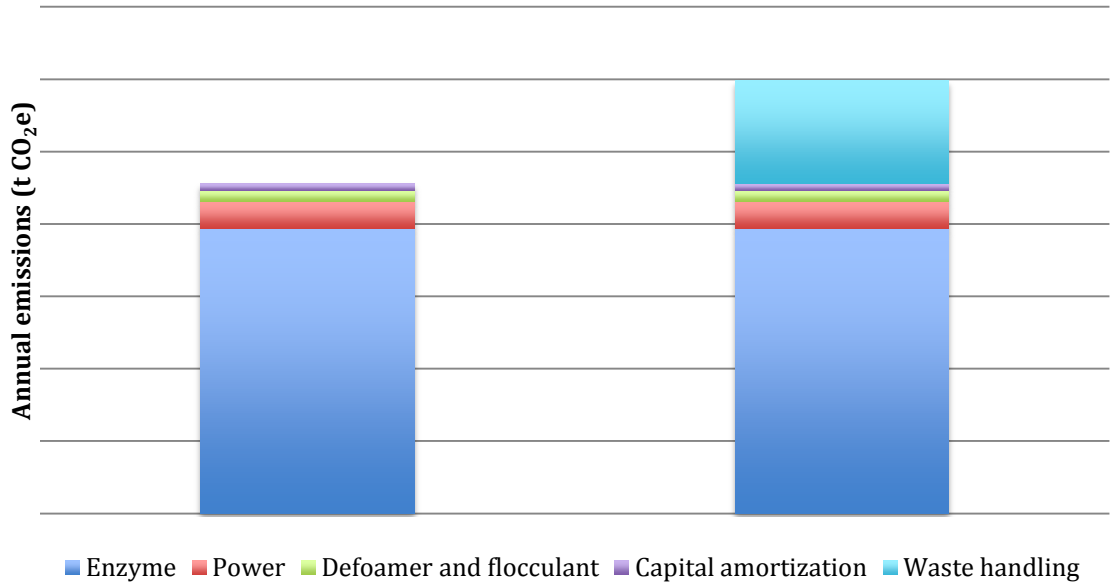

Figure 49: Summary of indirect emissions, by component, associated with two refinery applications of the Alcoa CCS process.

5.4 Summary, conclusions, and recommendations for additional analysis

A preliminary analysis of indirect GHG emissions associated with the Alcoa CCS process was performed for applications of the technology at a smelter and at an alumina refinery. In the latter analysis on-site waste disposal and offsite re-use scenarios were explored. Handling of the sequestrant/process waste was shown to be the largest source of indirect emissions for all applications. By making conservative assumptions, this work could represent an upper bound on the indirect emissions. However, the large number of simplifications made to the system and assumptions made within the EIO-LCA model mean that there is significant uncertainty in these preliminary results. These preliminary analysis revealed that while the indirect GHG emissions associated with the Alcoa CCS process are significant, they do not overwhelm the benefit of designed CO_2 reduction for a smelter application, however the refinery application is of marginal or no net benefit, for onsite waste disposal or offsite re-use scenarios, respectively.

These preliminary analyses using EIO-LCA should be followed with more detailed, process-based analysis using process LCA tools such as Simapro. If continued, future work will seek to yield a more detailed, accurate calculation and identify the process variables that can be most effectively manipulated to increase CO_2 sequestration efficiency. This process based analysis is the ideal method for examining the proposed Alcoa CCS system. Future work should be directed toward disaggregating the components of the system and allow for sensitivity analysis and increased accuracy.

Appendix 5A: Alcoa TEA tables used for EIO-LCA calculations

Smelter FS In-Duct CCS OPEX - Soluble Enzyme						12-Jan-12
Assumptions:	• Smelter offgas treated		2,058,000	NCuM/h		
	• 50% CO_2 removal		137,400	tonnes CO_2/year		
	• Operation hours per year		**8,500**			
	• 12-hour shifts					
	• Soluble enzyme conc'n		500			
		Units	**Price (USD)**	**Quantity**	**Cost**	
Utilities						
Power		Mwh	35	27,400	959,000	
Water		CuM	1	901,800	901,800	
	Total Utilities				**1,860,800**	
Chemicals						
Sequestrant	Dry Solids	tonnes	5	1,040,700	5,203,500	
Caustic	50%	tonnes	250	8,600	2,150,000	
Enzyme	Powder	kg	100	6,200	620,000	
Defoamer	30% Solution	kg	2	156,000	312,000	
	Total Chemicals				**8,285,500**	
Waste Disposition						
Sequestered Solids - Cake		tonnes	10	1,371,400	13,714,000	
Enzyme		tonnes	0	0	0	
	Total Waste Disposition				**13,714,000**	
Operating Labor						
Supervision		h	60	8,800	528,000	
Operating Labor		h	45	39,400	1,773,000	
Trcuk Coordinators		h	30	35,040	1,051,200	
Safety Coordinators		h	45	8,400	378,000	
Technical Support		h	60	6,240	374,400	
Environmental Support		h	50	3,120	156,000	
Analytical Support		Lot	50,000	1	50,000	
	Total Labor				**4,310,600**	
Maintenance						
Supervision		h	60	8,800	528,000	
Planner		h	45	13,100	590,000	
Craft Labor		h	30	42,500	1,275,000	
Spare Parts		% of Eq't	3.0%	34,059,000	1,022,000	
	Total Maintenance				**3,415,000**	
General & Administrative		% of O&M	8.0%	31,585,900	**2,527,000**	
Total Annual Operating Cost without Capital Recovery					**31,585,900**	
Capital Recovery		% of CAPEX	10.0%	163,279,000	**16,328,000**	
Total Annual Operating Cost with Capital Recovery					**47,913,900**	
Total Cost / tonne CO_2 Removed - No Capital Recovery					**230**	
Total Cost / tonne CO_2 Removed - With Capital Recovery					**349**	

Point Comfort In-Duct CCS CAPEX - Soluble Enzyme						**12-Jan-12**
Assumptions:	• Flue gas treated - 45,000 Nm^3/h capacity					
	• 50% CO_2 removal - 30,000 tonnes/year capacity					
	• $2010 BY Estimate					
Cost Component ($)	**Equipment & Material**	**Structural Steel [1]**	**Foundations**	**Freight**	**Erection & Installation [2]**	**Total**
ISBL						
Absorber and Fan	649,000	194,000	113,000	34,000	572,000	1,562,000
Tanks & Skids [3]	2,039,000	606,000	572,000	106,000	2,080,000	5,403,000
Pumps & Piping	2,288,000	688,000	481,000	119,000	1,600,000	5,176,000
Buildings & Enclosures						550,000
Electrical & Controls	1,487,000			59,000	1,643,000	3,189,000
Lime Neutralization System						3,439,565
Subtotal - ISBL	**6,463,000**	**1,488,000**	**1,166,000**	**318,000**	**5,895,000**	**19,319,565**
OSBL Allowances						
Sitework						1,800,000
Ducting/Dampers/Supports						1,500,000
Stack						400,000
Utility Connections/Controls						1,600,000
Subtotal - OSBL						**5,300,000**
EPCm						3,690,000
Contingency						8,490,000
Startup Support & Training						600,000
Total Project						**37,400,000**

Capital expense attributed to each aspect of the smelter application (e.g. Equipment and materials for Tanks and Skids) was calculated using the same percentages used for the refinery application without the lime neutralization process.

Smelter In-Duct CCS CAPEX - Soluble Enzyme							**12-Jan-12**
Assumptions:	• Flue gas treated - 2,040,000 Nm^3/h						
	• 50% CO_2 removal - 140,000 tonnes/year capacity						
	• $2010 BY Estimate						
Cost Component ($M)	**Equipment & Material**	**Structural Steel**	**Foundations**	**Freight**	**Erection & Installation**	**Total**	
ISBL							
Absorber and Fan							
Tanks & Skids							
Pumps & Piping							
Buildings & Enclosures							
Electrical & Controls							
Subtotal - ISBL						**85.1**	
OSBL Allowances							
Sitework						5.3	
Ducting/Dampers/Supports						11.3	
Stacks						3.4	
Utility Connections/Controls						3.2	
Subtotal - OSBL						**23.2**	
EPCm						16.3	
Contingency						37.4	
Startup Support & Training						1.3	
Total Project						**163.3**	

Point Comfort In-Duct CCS OPEX - Soluble Enzyme						12-Jan-12
Assumptions:	• Flue gas treated		45,000	NCuM/h		
	• 50% CO_2 removal		30,000	tonnes CO_2/year		
	• Operation per year		8,500	hrs		
	• 12-hour shifts					
	• Free enzyme concentratio		500	mg/L		
		Units	**Price (USD)**	**Quantity**	**Cost**	
Utilities						
Power		Mwh	35	5,300	186,000	
Water		CuM	1	14,000	14,000	
	Total Utilities				**200,000**	
Chemicals						
Red Mud	~43% Slurry	dry tonnes	0	1,241,000	0	
Caustic	50%	tonnes	250	0	0	
Enzyme	Powder	kg	100	657,300	65,730,000	
Flocculant	30% Solution	kg	2	72,000	144,000	
Defoamer	30% Solution	kg	2	72,000	144,000	
Total Chemicals					**66,018,000**	
Waste Disposition						
Sequestered Solids		dry tonnes	0	1,275,000	0	
Enzyme		tonnes	0	0	0	
Total Waste Disposition					**0**	
Operating Labor						
Supervision		h	60	2,200	132,000	
Operating Labor		h	45	11,000	495,000	
Technical Support		h	60	1,000	60,000	
Analytical Support		Lot	20,000	1	20,000	
	Total Labor				**707,000**	
Maintenance						
Supervision		h	50	3,300	165,000	
Craft Labor		h	30	17,000	510,000	
Materials		% of Eq't	3.0%	10,527,259	316,000	
Total Maintenance					**991,000**	
G&A					**5,433,280**	
Total Annual Operating Cost without Capital Recovery					**73,349,280**	
Capital Recovery		% of CAPEX	10.0%	37,400,000	3,740,000	
Total Annual Operating Cost with Capital Recovery					**77,089,280**	
Total Cost / tonne CO_2 Removed - No Capital Recovery					**2,445**	
Total Cost / tonne CO_2 Removed - With Capital Recovery					**2,570**	

Appendix 5B: NAICS Code Index

All descriptions from 2002 NAICS code database (via Census.gov) except #230103, which was given by the EIO-LCA output but is not found in the 2002 NAICS code database.

33231: Plate Work and Fabricated Structural Product Manufacturing

This industry comprises establishments primarily engaged in manufacturing one or more of the following: (1) prefabricated metal buildings, panels and sections; (2) structural metal products; and (3) metal plate work products.

230103: Other Nonresidential Structures

333911: Pump and Pumping Equipment Manufacturing

This U.S. industry comprises establishments primarily engaged in manufacturing general purpose pumps and pumping equipment (except fluid power pumps and motors), such as reciprocating pumps, turbine pumps, centrifugal pumps, rotary pumps, diaphragm pumps, domestic water system pumps, oil well and oil field pumps and sump pumps.

334513: Instruments and Related Products Manufacturing for Measuring, Displaying, and Controlling Industrial Process Variables

This U.S. industry comprises establishments primarily engaged in manufacturing instruments and related devices for measuring, displaying, indicating, recording, transmitting, and controlling industrial process variables. These instruments measure, display or control (monitor, analyze, and so forth) industrial process variables, such as temperature, humidity, pressure, vacuum, combustion, flow, level, viscosity, density, acidity, concentration, and rotation.

332420: Metal Tank (Heavy Gauge) Manufacturing

This industry comprises establishments primarily engaged in cutting, forming, and joining heavy gauge metal to manufacture tanks, vessels, and other containers.

333411: Air Purification Equipment Manufacturing

This U.S. industry comprises establishments primarily engaged in manufacturing stationary air purification equipment, such as industrial dust and fume collection equipment, electrostatic precipitation equipment, warm air furnace filters, air washers, and other dust collection equipment.

2211: Electric Power Generation, Transmission and Distribution

This industry group comprises establishments primarily engaged in generating, transmitting, and/or distributing electric power. Establishments in this industry group may perform one or more of the following activities: (1) operate generation facilities that produce electric energy; (2) operate transmission systems that convey the electricity from the generation facility to the distribution system; and (3) operate distribution systems that convey electric power received from the generation facility or the transmission system to the final consumer.

2213: Water, Sewage and Other Systems

325181: Alkalies and Chlorine Manufacturing

This U.S. industry comprises establishments primarily engaged in manufacturing chlorine, sodium hydroxide (i.e., caustic soda), and other alkalies often using an electrolysis process.

32519: Other Basic Organic Chemical Manufacturing

This industry comprises establishments primarily engaged in manufacturing basic organic chemicals (except petrochemicals, industrial gases, and synthetic dyes and pigments).

325414: Biological Product (except Diagnostic) Manufacturing

This U.S. industry comprises establishments primarily engaged in manufacturing vaccines, toxoids, blood fractions, and culture media of plant or animal origin (except diagnostic).

562: Waste Management and Remediation Services

Industries in the Waste Management and Remediation Services subsector group establishments engaged in the collection, treatment, and disposal of waste materials. This includes establishments engaged in local hauling of waste materials; operating materials recovery facilities (i.e., those that sort recyclable materials from the trash stream); providing remediation services (i.e., those that provide for the cleanup of contaminated buildings, mine sites, soil, or ground water); and providing septic pumping and other miscellaneous waste management services. There are three industry groups within the subsector that separate these activities into waste collection, waste treatment and disposal, and remediation and other waste management.

Excluded from this subsector are establishments primarily engaged in collecting, treating, and disposing waste through sewer systems or sewage treatment facilities that are classified in Industry 22132, Sewage Treatment Facilities and establishments primarily engaged in long-distance hauling of waste materials that are classified in Industry 48423, Specialized Freight (except Used Goods) Trucking, Long-Distance. Also, there are some activities that appear to be related to waste management, but that are not included in this subsector. For example, establishments primarily engaged in providing waste management consulting services are classified in Industry 54162, Environmental Consulting Services.

6.0 Conclusions

The overall goal of this DOE Phase 2 project was to further develop and conduct pilot-scale and field testing of a biomimetic in-duct scrubbing system for the capture of gaseous CO_2 coupled with sequestration of captured carbon by carbonation of alkaline industrial wastes. The Phase 2 project, reported on here, combined efforts in enzyme development, scrubber optimization, and sequestrant evaluations to perform an economic feasibility study of technology deployment.

The optimization of carbonic anhydrase (CA) enzyme reactivity and stability are critical steps in deployment of this technology. A variety of CA enzyme variants were evaluated for reactivity and stability in both bench scale and in laboratory pilot scale testing to determine current limits in enzyme performance.

Optimization of scrubber design allowed for improved process economics while maintaining desired capture efficiencies. A range of configurations, materials, and operating conditions were examined at the Alcoa Technical Center on a pilot scale scrubber. This work indicated that a cross current flow utilizing a specialized gas-liquid contactor offered the lowest system operating energy.

Various industrial waste materials were evaluated as sources of alkalinity for the scrubber feed solution and as sources of calcium for precipitation of carbonate. Solids were mixed with a simulated sodium bicarbonate scrubber blowdown to comparatively examine reactivity. Supernatant solutions and post-test solids were analyzed to quantify and model the sequestration reactions. The best performing solids were found to sequester between 2.3 and 2.9 moles of CO_2 per kg of dry solid in 1-4 hours of reaction time. These best performing solids were cement kiln dust, circulating dry scrubber ash, and spray dryer absorber ash.

A techno-economic analysis was performed to evaluate the commercial viability of the proposed carbon capture and sequestration process in full-scale at an aluminum smelter and a refinery location. For both cases the in-duct scrubber technology was compared to traditional amine-based capture. Incorporation of the laboratory results showed that for the application at the aluminum smelter, the in-duct scrubber system is more economical than traditional methods. However, the reverse is true for the refinery case, where the bauxite residue is not effective enough as a sequestrant, combined with challenges related to contaminants in the bauxite residue accumulating in and fouling the scrubber absorbent. Sensitivity analyses showed that the critical variables by which process economics could be improved are enzyme concentration, efficiency, and half-life. It is also noted that CO_2 Solutions proposed an initial solution to reduce process costs through more advanced enzyme management, however, DOE program requirements restricting any technology development extending beyond 2014 as commercial deployment timeline did not allow this solution to be undertaken.

At the end of the first part of the Phase 2 project, a gate review (DOE Decision Zero Gate Point) was conducted to decide on the next stages of the project. The original plan was to follow the pre-testing phase with a detailed design for the field testing. In absence of further time to

optimize the process, unfavorable economics, however, resulted in a decision to conclude the project before moving to field testing.

7.0 PATENTS

No activities.

8.0 GOVERNMENT PROPERTY

No property purchased.

9.0 PUBLICATIONS

No publications issued.

10.0 PRESENTATIONS

"Innovative CO_2 Capture Process Coupled with Alkaline Clay Mineralization," M. Gershenzon, N. Dando, J. Anglin, D. Iwig, L. Nguyen, S. Fradette, G. Versteeg, C. Noack, D. Nakles, D. Dzombak, J. Laumb, L. Heebink, S. Hawthorne, R. Lunt, and R. Ghosh, Eleventh Annual Conference on Carbon Capture, Utilization & Sequestration, Pittsburgh, Pennsylvania 2012, May.

11.0 SPENDING SUMMARY – PHASE 1& 2

Recipient:	Alcoa Inc.		
DOE #:	DE-FE0002415		
Spending Summary			
Object Class Categories	**Approved Budget**	**Project Expenditures**	
Per SF 425	**PHASE I & II**	**This Quarter**	**Cumulative to Date**
a. Personnel	**1,097,638**	**1,371**	**349,885**
b. Fringe Benefits	**1,993,199**	**2982**	**703,915**
c. Travel	**152,160**	**0**	**5,876**
d. Vendors	**5,636,500**	**0**	**2,290,296**
e. Supplies	**32,700**	**0**	**14,145**
f. Contractual	**0**	**34,855**	
g. Construction	**4,134,693**		**265,781**
h. Other	**425,020**		
i.Total Direct Charges (sum a-h)	**13,768,222**	**39,208**	**3,629,898**
j.Total Indirect Charges	**1,855,511**	**11,141**	**660,772**
k. Totals (sum of i and j)	**16,873,433**	**50,349**	**4,290,670**
DOE Share	**13,498,746**	**40,288**	**3,475,324**
Cost Share	**3,374,687**	**10,061**	**865,694**
Calculated Cost Share Percentage	**80%/20%**	**80%/20%**	**80%/20%**

12.0 COST SHARE CONTRIBUTIONS – PHASE 1& 2

Funding Source	Approved Cost Share		This Quarter		Cumulative to Date	
	Cash	In-Kind	Cash	In-Kind	Cash	In-Kind
Alcoa	3,374,687		10,070		865,694	
Total	3,374,687		10,070		865,694	
Cumulative Cost Share Contributions					865,694	

13.0 SPEND PLAN

Quarter	From	To	A. Federal Share of Outlays (a)	Cumulative Federal Share	B. Recipient Share of Outlays (b)	Cumulative Recipient Share
2010 Q1	1/1/10	3/31/10	41,561	41,561	10,258	10,258
2010 Q2	4/1/10	6/30/10	732,512	774,073	182,471	192,729
2010 Q3	7/1/10	9/30/10	176,551	950,624	43,776	236,505
2010 Q4	10/1/10	12/31/10	31,755	982,379	7,840	244,345
2011 Q1	1/1/11	3/31/11	23,329	1,005,708	5,744	250,089
2011 Q2	4/1/11	6/30/11	336,359	1,342,067	83,664	333,753
2011 Q3	7/1/11	9/30/11	1,047,462	2,390,175	261,865	594,972
2011 Q4	10/1/11	12/31/11	1,041,067	3,431,243	259,792	854,763
2012 Q1	1/1/12	3/31/12	3,793	3,435,036	870	855,633
2012 Q2	4/1/12	6/30/12	40,279	3,475,324	10,070	865,694

14.0 MAJOR TASK SCHEDULE – PHASE 1 & 2

Recipient:	Alcoa, Inc.
DOE #:	DE-EE0002415

Major Task Schedule

Task #	Task Description	Task Completion Date				Progress Notes
		Original Planned	Revised Planned	Actual	Percent Complete	
1.0	Project Management and Planning	1,261,888		483,766	38.34%	
2.0	Research and Development	4,861,557		3,772,736	77.60%	
3.0	Conceptual Design	276,824		75,584	27.30%	
4.0	Permitting and NEPA	152,698		8,732	5.72%	
5.0	Preliminary Design	549,073				
6.0	Detailed Design	1,026,487				
7.0	Construction	6,244,454				
8.0	Operations Testing	998,775				
9.0	Decommission and Dismantel	251,977				

RD&E REPORT APPROVAL SHEET

Title: Innovative CO_2 Sequestration from Flue Gas Using Industrial Sources and Innovative Concept for Beneficial CO_2 Use – Phase II

ALCOA PROPRIETARY INFORMATION

Report #: 12-119

Date: 2012-06-01

Reported by: Neal Dando, Rajat Ghosh, Mike Gershenzon, Jim Anglin

Approved by: John R. Smith
J. R. Smith

Date Noted: June 4, 2012